Turbo Coded Pulse Position Modulation for Optical Communications

A THESIS

Presented to

The Academic Faculty

By

Abdallah Said Alahmari

In Partial Fulfillment
of the Requirements for the Degree of
Doctor of Philosophy in Electrical Engineering

School of Electrical and Computer Engineering
Georgia Institute of Technology

January, 2003

Dedication

To My Parents and My Wife

Acknowledgements

I would like to express my gratitude and thanks to Professor John R. Barry for his guidance, support, and encouragement over the past several years. His commitment, continuous advice, and support have been invaluable during these difficult times. I really appreciate all he offered to me as a student and there are not enough words to thank him.

I thank Professors Mary Ann Ingram, Ye (Geoffrey) Li, Douglas Williams and Christopher Heil for agreeing to serve on my final defense committee. I especially thank Professor S. McLaughlin for his help. Many thanks to Dr. Ray, Dr. Web, Dr. Hertling, and Marilou Mycko who helped me in various ways.

I wish to acknowledge the financial support of the KFUPM University during the course of my graduated studies. I offer special thanks to Dr. Ali Badi and Dr. Jamil Makhadmi for their continuous advice and help during the past several years. Thank you to all the members of the Saudi Mission to the USA for their continuous help and support.

I would also like to express my gratitude and thanks to my family, who each helped in uncountable ways. My parents were a constant source of emotional and spiritual support.

Their sacrifices and continuous prayers helped my throughout my life. Thanks to my wife for her support, encouragement, and prayers throughout all the uncertain times. Her sacrifices helped me complete this work. I am grateful for the emotional and spiritual support of my brothers and sisters and for their continuous support and encouragement. Special thanks to my uncles and aunts, who gave me constant support and encouragement.

I would like to express my thanks and appreciation to my friends and colleagues at Georgia Tech for their invaluable friendship. They made the last few years enjoyable. I especially thank Chen-Chu Yeh, Richard Causey, Renato Lopes, Badri Varadarajan, Arvand Nayak, Joon Hyun Sung, Piya Kovintavewat, Deric Waters, Kofi Anim-Appiah, Anh Nguyen, Pornchai Supnithi, Andrew Thangaraj, Estuardo Licona-Nunez, and Sarat Krishnan. Thanks to my friend Dr. N. Abu-Zahrah for his encouragement and instruction. Thanks to all of my dear friends in Atlanta for their continuous encouragement and support. The fun and useful times, we shared, excited me to continue on this road.

Lastly, but not least, I thank and praise my lord Allah for his mercy, sustenance, and uncountable blessings.

Table of Contents

Dedication iii

Acknowledgements iv

List of Tables iv

List of Figures v

Summary viii

1- Introduction **1**

2- Coded Modulation for Optical Communication Systems **8**

2.1 Channel Model 8

2.2 Modulation Schemes 10

2.3 Coded Modulation Schemes 13

2.4 Summary 14

3- Concatenated Codes **16**

3.1 Binary Turbo Codes 17

3.1.1 Parallel Concatenated Codes (Turbo Codes) 17

3.1.2 Serial-Concatenated Codes 21

3.1.3 Iterative Decoding 22

3.2 Turbo-Coded Modulation Techniques 24

3.2.1 Turbo Codes Combined With Gray Mapping 24

3.2.2 Turbo Trellis-Coded Modulation (TTCM) 26

3.2.2.1 Parallel Concatenated TCM 26

3.2.2.2 Serially Concatenated TCM 32
3.2.3 Multilevel Coded (MLC) Modulation 33
3.2.3.1 MLC Principles 34
3.2.3.2 Set Partitioning 36
3.2.3.3 Turbo coding with MLC 39
3.3 Summary 39

4- Two-Level Two-Pulse Position Modulation Scheme 41
4.1 Two-Level Two-Pulse Position Modulation 41
4.2 Performance of 2L2PPM 43
4.2.1 Uncoded bit-error rate 43
4.2.2 Spectral Efficiency 45
4.2.3 Cutoff rate 48
4.3 Summary 50

5- Serial-Concatenated Trellis-Coded Modulation with 2L2PPM Modulation 52
5.1 System Description 53
5.1.1 Interleaver 54
5.1.2 Inner Code 56
5.1.2.1 Inner Code Structure 57
5.1.2.2 Mapping of the Inner Code 59
5.1.3 Outer Code 60
5.1.4 Iterative Decoder 60
5.2 SCTCM Design 62
5.3 Mapping and Code Search Results 71
5.3.1 Set Partitioning For Natural Mapping 71
5.3.2 Search for Good Inner Code 77
5.3.3 Search for Good Outer Codes 81
5.4 Error Bounds and Simulation Results 82
5.5 Summary 96

6- Serial-Concatenated Trellis-Coded Modulation Based on OPPM 99
6.1 System Description 100
6.1.1 Modulation Scheme 101
6.1.2 Outer Codes 101

6.1.3 Inner Code Structure 102
6.1.4 Iterative Decoder 103
6.2 Inner Code Search 105
6.3 Simulation Results 107
6.4 Summary 113

7- Concluding Remarks 114
7.1 Summary of Results 114
7.2 Future Research Recommendations 117

References **120**

Vita **128**

List of Tables

Table 1. Coding gain at a BER equal to 10-6 for a turbo code over a Gaussian Channel [28]. 25

Table 1. 128-SCTCM natural mapping signal labels..... 75

Table 2. 256-SCTCM natural mapping signal labels..... 76

Table 3. 128-SCTCM Gray mapping signal labels..... 77

Table 4. 256-SCTCM Gray mapping signal labels..... 78

Table 5. 128-SCTCM natural mapping inner code polynomials..... 79

Table 6. 256-SCTCM natural mapping inner code polynomials..... 80

Table 7. 128-SCTCM Gray mapping inner code polynomials..... 80

Table 8. 256-SCTCM Gray mapping inner code polynomials..... 80

Table 9. Polynomials of rate 5/6 recursive systematic codes. 82

Table 10. Polynomials of rate 6/7 recursive systematic codes. 82

Table 11. Normalized power requirement, spectral efficiency, and complexity of 128-SCTCM and 256-SCTCM..... 96

Table 12. Decoding Complexity Comparison. 113

List of Figures

Figure 1. Power efficiency versus spectral efficiency for PPM, MPPM, and OPPM. 15

Figure 2. Turbo encoder structure. 19

Figure 3. The SISO device. 24

Figure 4. T-TCM encoder, shown with an example of 8-PSK modulation and N = 12 [32]. 27

Figure 5. Turbo trellis-coded modulation - decoder structure [32]. 29

Figure 6. Serial-concatenated TCM proposed by [40]. 34

Figure 7. Multilevel encoder. 35

Figure 8. Multistage decoding. 36

Figure 9. Set partitioning for 16-QAM signaling. 38

Figure 10. Power efficiency versus spectral efficiency for n-2L2PPM, OOK, L-PPM, (n,2)-MPPM, and (n,3)-MPPM modulation schemes at high optical SNR. 46

Figure 11. Continuum power spectrum of 9-2L2PPM and 12-2L2PPM. 49

Figure 12. The cutoff rate of 9-2L2PPM and 12-2L2PPM modulation schemes. 51

Figure 13. First SCTCM encoder. 54

Figure 14. Minimal systematic convolutional encoder with feedback. The code has a rate of $p/(p+1)$, parity check coefficients h_j^i, and memory m. 58

Figure 15. Iterative decoder of the proposed SCTCM-2L2PPM system. 62

Figure 16. Amplitude representation of four signals that share the same two positions. 72

Figure 17. Position representation of (9,2)-MPPM. The shaded circles represent the selected pairs of positions. 73

Figure 18. Set partitioning of 32-MPPM. 74

Figure 19. 128-SCTCM natural mapping inner code of constraint length 81

Figure 20. Gray mapping versus natural mapping for SCTCM. 84

Figure 21. Verification of the simulation (Both the outer and inner codes have 4 states, and the block length is 400). 85

Figure 22. Nonrecursive and systematic recursive outer codes. 87

Figure 23. The first 9 iterations from simulation 128-SCTCM-2L2PPM, for 8 states outer code, 4 states inner code, 2000 block length, and Gray mapping. 88

Figure 24. Upper bounds for different interleaver lengths. 89

Figure 25. The effect of the outer code memory performance of SCTCM (m is the number of memory elements in the outer code). 90

Figure 26. The effect of the inner code memory on the performance of SCTCM (mi is the constraint length of the inner code). 91

Figure 27. Simulation results for different outer code constraint lengths. 93

Figure 28. Simulation results of different inner code constraint lengths. 94

Figure 29. The two system 128-SCTCM and 256-SCTCM. Both have 8 states outer codes and 4 states inner codes, and the block length of the code is 2000 bits. 95

Figure 30. Normalized power requirement versus spectral efficiency. 97

Figure 31. Proposed SCTCM encoder with rate-1 inner code. 100

Figure 32. Memory elements governed by f(D)=D3+D+1. 103

Figure 33. Iterative decoder of SCTCM-OPPM system. 104

Figure 34. Natural mapping of one symbol of 64-OPPM. 106

Figure 35. Two symbols of 8-OPPM natural mapping. 107

Figure 36. The inner code of SCTCM-8-OPPM scheme. 108

Figure 37. The inner code of SCTCM-64-OPPM scheme. 108

Figure 38. Simulation of SCTCM-8-OPPM. The inner code has states and is the memory of the outer code. 110

Figure 39. Simulation of SCTCM-64-OPPM. The inner code has states and is the memory of the outer code. 111

Figure 40. Normalized power requirement versus spectral efficiency of proposed SCTCM-8-OPPM and SCTCM-64-OPPM compared to previous coded modulation schemes for BER = 10-6. 112

Summary

Intensity modulation and direct detection (IM/DD) is used in nearly all optical communication applications, such as wireless infrared communication links, inter-satellite links, and fiber-optic communications. IM/DD can be implemented using cheap and simple components. Pulse position-based modulation is a power efficient scheme that is used with IM/DD.

The objective of this thesis is to develop and analyze new bandwidth efficient turbo-coded modulation schemes that are well-suited to those applications that use pulse position modulation (PPM). For this purpose, the study begins with the development of a new modulation scheme that offer higher spectral efficiency than traditional PPM and multiple PPM (MPPM) schemes. The new modulation scheme is called two-level two-PPM (2L2PPM) and it is a modified version of the existing MPPM modulation. The primary modification is to allow the pulses to have more than one amplitude level. Then two different serial-concatenated trellis-coded modulation (SCTCM) schemes with iterative decoding at the receiver will be presented. The first system is a serial concatenation of two convolutional encoders and a spread-random bit-interleaver

combined with 2L2PPM. The second system has a rate-one inner code and is combined with overlapping PPM. Both SCTCM systems outperform previously reported coded modulation schemes by offering up to a 57% increase in spectral efficiency for the same power efficiency and decoding complexity.

In designing the new SCTCM codes, we started with the derivation of performance bounds of serial-concatenated convolutional codes (SCCC) developed in [1], [2], and modified them for the case of trellis-coded modulation (TCM) inner codes and spread-random bit-interleavers. Our modified design criteria will produce an increase in the effective Euclidean distance of the SCTCM codes for very large interleaver sizes compared with original SCTCM codes presented in [3]. Depending on the design criteria, we used a random search to find good inner codes that suit the two SCTCM schemes. Both Monte Carlo simulation results and upper bounds on the bit-error probability were used to evaluate the proposed turbo-coded modulation techniques. The proposed systems offer high spectral and power efficiency with low complexity decoding. The spectral efficiency, power efficiency, and decoding complexity of the proposed turbo-coded modulation schemes are addressed and compared to some previous trellis-coded modulations systems.

Chapter 1

Introduction

The widespread use of and demand for personal computers and portable communications terminals have created a strong interest in high-speed wireless links to connect portable devices and to establish local-area networks (LANs). Wireless links need to be compact and robust against background noise and interference from other users. Infrared is a strong candidate as a transmission medium for indoor wireless communications. It offers several benefits over radio. First, it has an enormous amount of unregulated bandwidth, and no interference occurs between links that operate in rooms separated by barriers. Moreover, when the link uses intensity modulation and direct detection, the nature of the wave carrier and the area of the detection devices make the link immune to multipath fading [4], [5], [6].

The most practical modulation technique in a wireless optical system is intensity modulation and direct detection (IM/DD). In this modulation technique, the information is modulated using the instantaneous power of the carrier and special detection devices such

as photocurrent diodes are used to convert the instantaneous power of the signal to an electrical current. This detection technique is simpler than coherent detection and can be implemented using inexpensive circuits. IM/DD is used in many optical communication applications, including wireless infrared communications [5], [6], [7], fiber optic communications [8], [9], deep-space communication [10], and intersatellite link (ISL) applications [11], [12]. Simpler modulation types that are commonly used with IM/DD channels are on-off keying (OOK), pulse position modulation (PPM) [13], and multiple-pulse position modulation (MPPM). OOK is the simplest modulation that can be used with IM/DD. Pulse position-based modulation (PPM and MPPM) schemes are well suited to IM/DD because they have lower duty cycles leading to higher peak to average power ratios than the other conventional modulation schemes. PPM is known for its power efficiency, but it requires more bandwidth than OOK modulation scheme. MPPM, suggested by Sugiyama and Nosu in [14], is a generalization of PPM and requires less bandwidth than PPM.

To improve the power efficiency of optical links, several trellis-coded modulation (TCM) schemes have been proposed. In [15], Lee and Kahn introduced the use of TCM [16] with PPM. They achieved good power efficiencies for different constraint lengths. However, the spectral efficiency was less than 0.25 bits/s/Hz. Trying to improve the spectral efficiency of infrared links, Park and Barry proposed a TCM-MPPM system that achieves improved power efficiency with 0.35 bits/s/Hz spectral efficiency [17], [18].

The class of parallel concatenated recursive systematic convolutional codes, or turbo codes, was first introduced by Berrou et al. [19]. The original idea of turbo coding is to combine two elements: parallel concatenation of two or more codes separated by a random interleaver at the transmitter side, and iterative decoding at the receiver side. The use of turbo codes with iterative decoding schemes achieved reliable data communications at low signal-to-noise ratios (SNRs), very close to the Shannon limit, on the additive white Gaussian noise (AWGN) channel and the interleaved Rayleigh fading channels. Motivated by the great performance results of this new class of codes, many researchers started analyzing these codes to extract and understand their power sources. Among these researchers are Benedetto and Montorsi [20]-[24], Perez et al. [25], Robertson [26], and Hagenauer et al. [27]. An equally important new class of serial concatenation codes was introduced by Benedetto et al. in [2]. This new serial concatenation scheme uses a random interleaver between the inner and outer codes and is decoded with an iterative decoder.

Parallel and serial-concatenated turbo codes were initially developed for binary modulation schemes, binary phase shift keying (BPSK) and on-off keying (OOK). Because many communication applications need spectrally-efficient modulations schemes (nonbinary modulations), the extension of turbo codes began to expand to nonbinary modulation. The first approach to utilize the substantial gain of turbo codes in the spectrally-efficient modulation schemes was presented by Le Goff et al. in [28]. With this

method, high coding gains were achieved over other conventional TCM schemes for both AWGN and fading channels.

Additionally, TCM [16], known to be a bandwidth-efficient modulation scheme, was combined with parallel concatenation scheme to form three types of parallel concatenated TCM schemes; namely, turbo TCM (TTCM), parallel concatenated TCM (PCTCM), and turbo-coded pragmatic TCM (TCPTCM). The TTCM scheme, which has been reported in [26], [29], [30], [31], [32], uses two TCM encoders and a symbol interleaver. Some improvements on the TTCM were reported in [33] and [34]. The PCTCM scheme was reported in [35], [36] and it achieves higher interleaver gains, hence more performance gains, but it is more complex to implement than TTCM. A modification of the above scheme was presented in [37], [38]. This scheme is called symbol interleaved parallel concatenated TCM (SIPCTCM). As the name implies, the modification is to have symbol interleaving instead of bit interleaving, which will increase the accuracy of the iterative decoder because it does not have to convert from symbol probabilities to bit probabilities. TCPTCM is the least complex of the three scheme types and it was introduced in [39]. The idea of TCPTCM is to apply turbo codes to pragmatic TCM. TCPTCM has a simpler design and shorter interleaver than PCTCM [35], [36]. However, all of the above turbo TCM schemes, which are based on parallel concatenation, have two disadvantages. These schemes do not utilize all the available interleaver length, which will result in sacrificing some interleaver gain. Secondly, the constituent codes need large constraint length to

avoid parallel transitions in the trellis, and this disadvantage increases the decoding complexity.

In addition to the previous studies, Benedetto et al. suggested a serial-concatenated trellis-coded modulation (SCTCM) with iterative decoding [3]. The rate of the proposed code is $2b/(2b+2)$. The proposed system is a serial concatenation of a convolutional outer code, followed by an interleaver, which is followed by a TCM inner code. Another serially concatenated punctured TCM, with a rate of $b/(b+1)$, has been suggested by Ogiwara and Bajo in [40]. To achieve this rate with two TCM codes, the parity bits are alternatively punctured. In this method, symbol interleavers were used instead of bit interleavers. Two problems are associated with using symbol interleavers. The first is the restriction of avoiding parallel transitions, which increase the decoding complexity to at least $2^{2(b-1)}$. The second problem is the limitation of the interleaver gain because the size of the symbol interleavers is $1/(b-1)$ the size of bit interleavers.

This thesis considers the application of SCTCM with iterative decoding to improve the power and bandwidth efficiencies of optical communications and all other communication systems that use IM/DD. Chapter 2 covers necessary background material on optical communications. Chapter 3 discusses issues related to turbo codes, iterative decoding, and turbo-coded modulation schemes. Chapter 4 studies a new modulation scheme that is suitable for optical communications. The uncoded BER performance of this modulation

technique is compared with OOK, PPM and MPPM modulation schemes that are already used in this field. The cutoff rate is employed to evaluate the power efficiency of this modulation when combined with coded modulation techniques. In Chapter 5, a SCTCM is constructed. Both the coding and iterative decoding of this system are described. The performance error bounds for serial-concatenated convolutional codes was modified for TCM inner codes to derive the design criteria for the SCTCM encoder. Monte Carlo simulations and performance error bounds were used to evaluate the performance of this system. The complexity of the iterative decoding of SCTCM is compared to that of previous TCM techniques. In Chapter 6, a less complex SCTCM encoder, with rate one inner code, is presented. The performance of this technique is studied using Monte Carlo simulations and performance error bounds. Finally, Chapter 7 summarizes the key results of this thesis and suggests directions for future research on this topic.

The contributions of this work include:

- Introduction of two-level two-pulse position modulation (2L2PPM), a new modulation scheme which has better bandwidth efficiencies than PPM and MPPM modulations. Also, the new modulation scheme is found to outperform OOK in terms of power efficiency.
- Introduction of a SCTCM combined with 2L2PPM and iterative decoding that is well-suited to optical communication systems. This scheme outperforms

previously reported coded modulation by up to a 57% increase in the spectral efficiency, and offers the same power efficiency.

- Introduction of a low-complexity SCTCM, with rate-one inner code combined with overlapping pulse position modulation. This SCTCM scheme offers the same spectral efficiency as the previous one, but has better power efficiency performance in the low range signal to noise ratio.
- Development of new design criteria for SCTCM systems with S-random interleavers are presented. These design criteria offer up to a 100% increase in the effective minimum Euclidean distance of SCTCM schemes.

Chapter 2

Coded Modulation for Optical Communication Systems

Intensity modulation with direct modulation (IM/DD) favors low-duty cycle modulation schemes such as pulse position modulation (PPM) and multiple PPM (MPPM). In the following, the channel model over IM/DD is introduced. Then, a brief summary is given about some of the modulation techniques used in this area. Finally, some of the coded modulation techniques are reviewed.

2.1 Channel Model

The most practical modulation technique in wireless and nonwireless optical communication systems is intensity modulation and direct detection (IM/DD). The IM/DD modulation systems are simpler and cheaper than coherent modulation techniques. The idea of IM/DD stems from transmitting the information on the instantaneous power of the carrier signals. The receiver has a photo-diode that responses

to the received signal by generating an electrical current that is proportional to the instantaneous power of the received signal.

The appropriate channel model for optical communication systems depends on the intensity of the background noise. For the case of low background noise the received signal is modeled as a Poisson Process with rate $\lambda_r(t) = \lambda_s(t) + \lambda_n$, where $\lambda_s(t)$ is proportional to the instantaneous optical power of the received signal, and λ_n is proportional to the background light. The channel is called quantum limited if λ_n is zero. If λ_n is very large and the receiver exploits a wideband photodetector, or if the background light is very intense even after using narrowband optical filters, then the optical communication channel, with intensity modulation (IM/DD), can be accurately modeled by a baseband additive white Gaussian noise (AWGN) model [5]

$$y(t) = x(t) + n(t), \tag{1}$$

where $y(t)$ represents the instantaneous current of the receiving photodetector, $x(t)$ represents the instantaneous optical power of the transmitter, and $n(t)$ depicts the additive white Gaussian noise with $N_o/2$ power spectral density. In this model, the instantaneous transmitted power $x(t)$ is constrained by

$$P_t = \lim_{T \to \infty} \frac{1}{2T} \int_{-T}^{T} x(t)dt, \tag{2}$$

where P_t is the average optical power at the transmitter. From the above equation, we can see that the amplitude of $x(t)$ is constrained, while the energy of $x(t)$ determines the performance of the system. By allowing $x(t)$ in the modulation scheme to have a very small duty cycle we can produce high energy modulation schemes that will definitively outperform conventional modulation schemes such as QAM that are appropriate for radio or wireless channels. Hence, special kinds of modulation schemes are introduced under the constraints of IM/DD.

2.2 Modulation Schemes

The common and simple modulation scheme that can be used with IM/DD channels is on-off keying (OOK) modulation. OOK works as follows: for the average optical power P and bit rate of R_b, the OOK transmitter emits a rectangular pulse of duration $1/R_b$ and of intensity $2P$ to convey a one bit and no pulse to convey a zero bit. The rough estimate of the OOK spectral efficiency is 1.0 bits/s/Hz.

For high SNR, the minimum Euclidean distance ($d_{\min}$) between any pair of valid signals is

$$d_{\min}^2 = \min_{i \neq j} \int (x_i(t) - x_j(t))^2 dt . \quad (3)$$

The minimum Euclidean distance ($d_{\min}$) could be used to estimate the bit-error probability of OOK as follows:

$$Pr[\text{bit error}] \approx Q\left(\frac{d_{\min}}{\sqrt{2N_0}}\right) = Q\left(\frac{P}{\sqrt{R_b N_0 / 2}}\right). \tag{4}$$

PPM [13] is another modulation scheme that is common with IM/DD modulation systems. PPM is known for its good power efficiency, however, it has less spectral efficiency than OOK. In the PPM format, there are L symbols, each of duration T. Each symbol is divided into L chips (with duration $T_c = T/L$). The PPM duty cycle is $\alpha_{\text{PPM}} = 1/L$. The transmitter sends an optical pulse in only one of these chips at a time. The intensity of each pulse is LP. The spectral efficiency of PPM modulation is

$$\eta_{\text{PPM}} = \log_2(L)/L \text{ bit/s/Hz.} \tag{5}$$

Multiple-pulse position modulation (MPPM), suggested by Sugiyama and Nosu [14], is a generalization of PPM and has a higher spectral efficiency than the PPM. In MPPM, each symbol is divided into n chips and the transmitter sends w pulses every symbol duration. The number of possible signals is

$$L = \binom{n}{w} \text{ signals.} \tag{6}$$

The duty cycle of MPPM is $\alpha_{\text{MPPM}} = w/n$. The spectral efficiency of MPPM modulation is

$$\eta_{\text{MPPM}} = \log_2(L)/n \text{ bit/s/Hz.} \quad (7)$$

Furthermore, overlapping PPM (OPPM), suggested in [14] and used in [41], is another form of pulse modulation scheme. For this modulation, each b bits are mapped into one of $L = 2^b$ symbols and transmitted to the channel. The symbol interval of duration T is partitioned into n chips. Each chip has a duration T/n. The transmitter sends a rectangular optical pulse that spans w chips beginning from any of the first $L = n - w + 1$ chips to convey one of the L symbols. The reason for using w consecutive chips for every symbol is to increase the spectral efficiency. As we can see, information is conveyed by the positions of the chips, and the symbols are allowed to overlap; this is why this modulation format is called overlapping PPM. The most important parameters of modulation scheme are L, n, and w, and only two of them completely define the modulation scheme. The three parameters are related by

$$L = n - w + 1. \quad (8)$$

The duty cycle of this modulation scheme is $\alpha = w/n$. For an information rate of R_b bits/second, the bandwidth requirement of the uncoded modulation is $n/(wT)$, where $T = \log_2(L)/R_b$. So, the bandwidth requirement of the noncoded OPPM compared with

the bandwidth of the on-off keying (OOK) modulation scheme could approximated by [42]

$$BW_{OPPM}/R_b = \frac{n/w}{\log_2(n-w+1)}. \quad (9)$$

which results in a spectral efficiency of

$$\eta_{OPPM} = \frac{\log_2(n-w+1)}{n/w} \text{ bit/s/Hz.} \quad (10)$$

2.3 Coded Modulation Schemes

To improve the power and spectral efficiencies of infrared links, trellis-coded modulation schemes [16] were used. In [15], Lee and Kahn introduced the use of trellis-coded modulation (TCM) [16] with PPM. By using 8-TCM-PPM, a range of 7.0-8.2 dB power efficiency was achieved with a spectral efficiency of 0.25 bit/s/Hz. In this thesis the power efficiency is always computed with respect to the power required by OOK modulation schemes to achieve the same bit-error rate (BER) of 10^{-6}. In addition, 8.2-9.4 dB power efficiency was achieved by 16-TCM-PPM; but, the normalized spectral efficiency of 16-TCM-PPM is 0.19 bit/s/Hz. Searching for better spectral efficiency TCM codes, Park proposed the use of MPPM instead of PPM modulations [17]. By using 128-TCM-MPPM, high power efficiencies of 7.0-8.5 dB were achieved with spectral efficiency of 0.35 bit/s/Hz.

2.4 Summary

In this chapter, we have seen several types of pulse position-based modulation techniques: PPM, MPPM and OPPM. We have also shown some of the coded modulation schemes in this area. In the following, Fig. 1 shows the power efficiency versus the spectral efficiency of PPM and MPPM, for different values of n. For comparison purposes, we also showed the performance of OOK. The y-axis represents the power efficiency compared to the OOK power requirement for BER = 10^{-6}. The x-axis represents the spectral efficiency in terms of bits/s/Hz. The figure shows that PPM modulation scheme is the most power efficient modulation scheme, and that MPPM modulation outperforms PPM in the spectral efficiency. In addition to the uncoded modulation schemes, the figure shows the performance of 8-TCM-PPM, 16-TCM-PPM [16], and 128-TCM-MPPM [17].

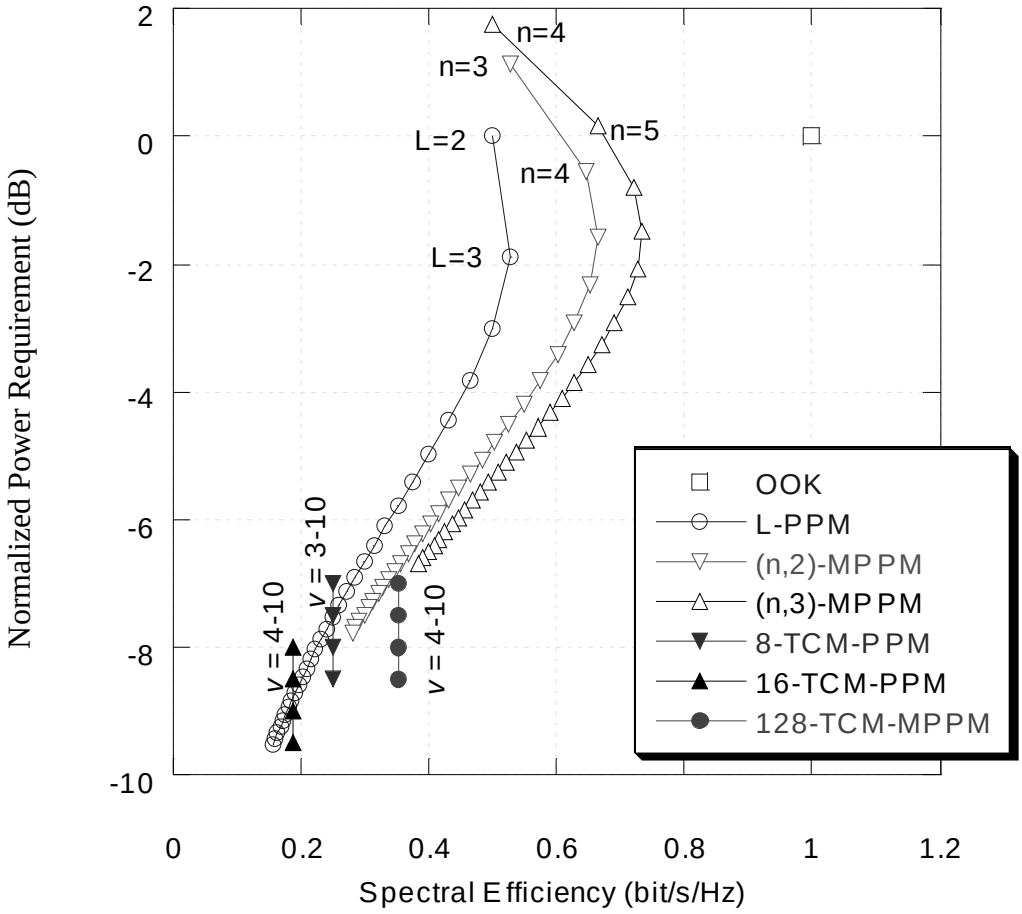

Figure 1. Power efficiency versus spectral efficiency for PPM, MPPM, and OPPM.

Chapter 3

Concatenated Codes

Before considering the new coded modulation schemes proposed in chapters 5 and 6, this chapter reviews background material on concatenated codes, including binary turbo codes and turbo coded modulation techniques. Concatenated codes were first introduced by Forney [43]. The structure of concatenated codes consists of two encoders and an interleaver connected in series, a nonbinary outer code, and a binary inner code. Usually, the interleaver is implemented as a rectangle that writes row-wise and reads column-wise. The role of the interleaver is to break up the error bursts produced by the inner decoder. Moreover, the interleaver is seen as a device that transforms the outer channel into a memoryless channel. The classical method of concatenation is decoded by a series of hard-decision decoders for the inner code, followed by a hard-decision decoder for the outer code. The performance of such a system can be improved by using a soft-output decoding algorithm such as MAP or SOVA to decode the inner code.

In 1993, a new parallel concatenated code was introduced by Berrou et al. [19]. This new parallel concatenated code with iterative decoding scheme is called a turbo code. A brief explanation of binary turbo codes follows.

Section 3.1 reviews binary turbo codes and iterative decoding technique. Then, different types of turbo coded modulation techniques are reviewed in Section 3.2.

3.1 Binary Turbo Codes

Berrou's turbo code [19] is a parallel concatenation code that includes at least two constituent codes, a random interleaver (instead of the rectangular interleaver used in classical concatenated codes) and iterative decoding. The random interleaver and iterative decoding elements were discovered to increase the performance of code concatenation systems. In 1996, Benedetto et al. [2] introduced new serial concatenation codes, which also had at least two constituent codes, a random interleaver, and iterative decoding. Similar to the parallel concatenated codes, the strength of the serial concatenation comes from the random interleaver and iterative decoding. The following discussion focuses on the basics of parallel concatenated codes, serial-concatenated codes, and iterative decoding.

3.1.1 Parallel Concatenated Codes (Turbo Codes)

Figure 2 shows the structure of a turbo encoder, which consists of two encoders and a random interleaver. Both encoders are systematic convolutional codes. The same

information is encoded twice in the case of two encoders, but the information bits are interleaved by the bit-wise random interleaver before the second encoder. Although the information bits are encoded twice, they are transmitted once to increase the code rate. The role of the multiplexer/puncturer block (see Figure 2) is to control the code rate by puncturing some parity bits from the encoders' outputs. The code components do not have to be identical.

With recursive encoders, the length of the interleaver plays an important role in the performance of turbo codes [21][23][24][25]. More importantly, increasing the interleaver's length does not add complexity to the iterative decoders of the turbo codes. A great advantage of turbo codes is that one can increase the performance without increasing the decoding complexity, as far as latency and cost are affordable.

Turbo codes are linear because their components are linear and they are analyzed using the same methods used for linear codes. For recursive systematic convolutional codes, the generator matrix is

$$G_{RSC}(D) = \left[1 \ \frac{g_1(D)}{g_2(D)}\right], \tag{11}$$

where 1 stands for the systematic part, which appears directly in the output, and the ratio $g_1(D)/g_2(D)$ is responsible for the recursive nature of the turbo codes.

For an input data sequence $\boldsymbol{d}$ of weight $w(\boldsymbol{d})$, the weight of the turbo code output $\boldsymbol{c}$ is $w(\boldsymbol{c}) = w(\boldsymbol{d}) + w(\boldsymbol{p_1}) + w(\boldsymbol{p}_2)$, where $\boldsymbol{p_1}$ and $\boldsymbol{p}_2$ are the parity bit sequences of the two encoders, respectively. The role of the interleaver is to reorder the data sequence $\boldsymbol{d}$, such that $w(\boldsymbol{p_1})$ and $w(\boldsymbol{p}_2)$ are not small simultaneously. If $\boldsymbol{d}$ produced $\boldsymbol{p_1}$ with small weight and small probability, the probability that the interleaved version of $\boldsymbol{d}$ will produce $\boldsymbol{p}_2$ with small weight is very small. Also, it is known that finite weight code outputs require that the polynomial $\boldsymbol{d}(D)$ be divisible by $g_2(D)$, which means that $w(\boldsymbol{d})$ is greater than or equal to 2 for nontrivial $g_2(D) \neq 1$. Therefore, the interleaver must be selected in a manner that avoids generating simultaneous low weight parity outputs.

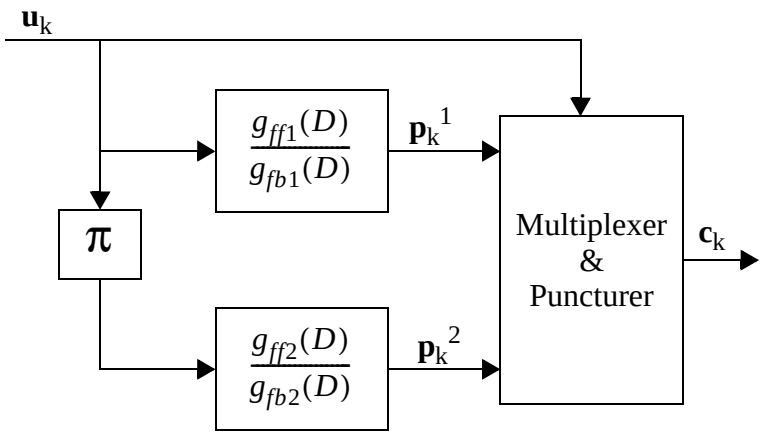

Figure 2. Turbo encoder structure.

In addition to previous studies, Perez et al. studied the turbo code spectrum. Their analysis shows that for any code word of Hamming distance d, there is an effective multiplicity number M_d, which is the number of possible code words of Hamming distance d. The smaller the effective multiplicity, the better the performance of the code becomes because the number of errors that correspond to the code word of weight d will be less. Perez et al. states that turbo codes have thin code spectrum in contrast to convolutional codes, which have a dense code spectrum [25].

The bit-error rate (BER) of turbo codes might be upper bounded, if we assume the use of maximum likelihood (ML) decoders. The BER for a BPSK modulation and a block code of length N, in the presence of additive white Gaussian noise (AWGN) [20][22] is shown as

$$P_b \leq \sum_{d = d_{free}}^{N} \left[\frac{A_d \tilde{w}_d}{N}\right] Q\left(\sqrt{d^2 \frac{R_c E_b}{N_o}}\right), \tag{12}$$

where A_d is the number of code words of weight d, and $\tilde{w}_d$ is the average weight of information sequences corresponding to code words of weight d. The union bound approximation of BER is valid in moderate and high SNR, because the above sum is dominated by code words with weight equal to the minimum free distance of the code.

The union bound was also used to approximate the BER of turbo codes in moderate and high SNR [24]:

$$P_b \cong A_{d_{free}} \tilde{w}_{d_{free}} Q\left(\sqrt{d_{free,\,eff} \frac{2R_c E_b}{N_o}}\right), \tag{13}$$

where $d_{free,\,eff}$ is the effective free distance, defined as $d_{free,\,eff} = 2 + z_{min}$, where z_{min} is the weight of the lowest weight parity sequence of one of the recursive systematic convolutional (RSC) encoders, caused by an input sequence of weight 2.

3.1.2 Serial-Concatenated Codes

Serial-concatenated codes, with iterative decoding, were introduced by Benedetto et al. [2]. These new serial concatenation schemes use a random interleaver between the inner and the outer codes, and it is decoded with an iterative decoder. The information bits are encoded by the outer encoder. The output of the outer encoder is interleaved by the bit-wise random interleaver and then encoded by the inner encoder. With the assumption of maximum likelihood receiver and uniform interleavers, the analysis of the BER reveals the following upper bound [2]

$$\lim_{N \to \infty} P_b \leq B_{\text{non-recursive}} N^{\alpha_m} \exp\left(\frac{-h_m R_c E_b}{N_o}\right), \tag{14}$$

when the inner code is nonrecursive. However, for recursive inner codes, the BER upper bound becomes

$$P_b \le \begin{cases} B_{\text{even}} N^{\frac{-d_f^o}{2}} \exp\left(\frac{-d_f^o d_{f,eff}^2}{2} R_c E_b / N_b\right) & \text{, for } d_f^o \text{ even} \\ B_{\text{odd}} N^{-\frac{d_f^o + 1}{2}} \exp\left(-\left[\frac{(d_f^o - 3) d_{f,eff}^2}{2} + h_m^{(3)}\right] R_c E_b / N_b\right) & \text{, for } d_f^o \text{ odd} \end{cases}, \qquad (15)$$

where N is the size of the interleaver, d_f^o is the free distance of the outer code, $h_m^{(3)}$ is the minimum weight of sequence of the input code corresponding to weight 3, α_m is a positive constant, and $B_{\text{non-recursive}}$, B_{even}, and B_{odd} are positive constants that depend on codes. Serial-concatenated codes are reported to not have error floor compared to parallel concatenated codes [2]. When the inner code is nonrecursive, equation (14), the exponent of N is always positive, which means there is no interleaving gain. However, when recursive inner codes are used, equation (15), the exponent of N is always negative. Hence, the inner component code should be recursive. Also, we can see that the interleaving gain is affected by the free Hamming distance of the outer code.

3.1.3 Iterative Decoding

Both parallel and serial-concatenated codes use iterative decoders. The performance of these suboptimal decoders approaches the bound of maximum likelihood (ML) decoders for the moderate and high SNRs. Berrou et al. used the symbol-by-symbol maximum a

posteriori (MAP) algorithm reported by Bahl et al. in [44]. The algorithm is known as the BCJR algorithm. Most of the current turbo decoders use a modified version of the BCJR algorithm. Many researchers have studied the iterative decoding algorithms for turbo codes [45], [46].

A modification of the BCJR algorithm is utilized in building soft-input soft-output (SISO) maximum a posteriori (MAP) modules to decode parallel and serial-concatenated codes [46], [47], [48], [49]. The SISO algorithm can be implemented in both multiplicative and additive forms. Figure 3 shows the structure of the SISO module, a four-port device that is built on a certain code. The module accepts two sequences of probabilities about the input and output of the code, and it produces two sequences of probability distributions about the input and output of the code. The inputs are $P_k(u;I)$ and $P_k(c;I)$. The outputs are $P_k(u;O)$, and $P_k(c;O)$. The two inputs, $P_k(u;I)$ and $P_k(c;I)$, represent a priori information about the input and output, respectively. The device uses its input information, which is called extrinsic information, and knowledge about the code to produce its outputs, which represent the a posteriori information about the input and output. The SISO module, which is used in decoding parallel and serial-concatenated codes, is general for binary and nonbinary codes.

Figure 3. The SISO device.

3.2 Turbo-Coded Modulation Techniques

Parallel and serial-concatenated turbo codes were designed for binary modulation schemes. The need in many communication applications for bandwidth efficient modulations schemes (non-binary modulation), led to extensions of turbo codes to non-binary modulation. This section of research provides a detailed overview of the structure and operation of the extensions of turbo coding schemes for non-binary modulation. We will start with a simple combination of turbo codes and mapping of bandwidth efficient modulation schemes. Then, we will discuss turbo TCM (TTCM), parallel concatenated TCM (PCTCM), and serial-concatenated TCM (SCTCM). Finally, we will address the multilevel coding (MLC) strategy and various research done to use turbo codes as component codes in MLC.

3.2.1 Turbo Codes Combined With Gray Mapping

Le Goff et al. presented the first approach to utilize the substantial gain of turbo codes in bandwidth-efficient modulation schemes [28]. They proposed the utilization of binary

turbo codes as component codes of a multilevel code, with higher order modulation (8-PSK, 16-QAM, 64-QAM) and Gray mapping. The systematic outputs form the higher-order bits and the parity code outputs form the lower-order bits of a symbol vector. The system has an interleaver between the code and the Gray mapper to obtain symbols that are affected by uncorrelated noises. The spectral efficiency of this system is $\Gamma = R \log_2 M$ bits/s/Hz, where R is the rate of the turbo code and M is the size of the modulation signal constellation. With this method, higher coding gains over conventional TCM schemes for both AWGN and fading channels are achieved. The following data show the simulation results of this scheme, see Table 1.

Table 1. Coding gain at a BER equal to 10^{-6} for a turbo code over a Gaussian Channel [28].

Turbo Rate	1/2	2/3	3/4	2/3
Modulation	16-QAM	8-PSK	16-QAM	64-QAM
Spectral Efficiency (bits/s/Hz)	2.0	2.0	3.0	4.0
Coding gain at 10^{-6} over uncoded modulation	6.0 dB	5.5 dB	7.8 dB	5.8 dB
Coding gain at 10^{-6} over 64 state TCM	2.4 dB	1.9 dB	2.6 dB	2.2 dB

3.2.2 Turbo Trellis-Coded Modulation (TTCM)

Turbo codes provide significant coding gains over AWGN and fully interleaved Rayleigh fading channels. However, this coding gain is achieved only through use of more bandwidth (extra parity bits have to be transmitted). In this section, we discuss the use of turbo codes in conjunction with trellis-coded modulation (TCM), which is known as a bandwidth-efficient modulation scheme [16], [50]. The addition of such a combination is that coding gains can be achieved without bandwidth expansion.

3.2.2.1 Parallel Concatenated TCM

The first coded modulation scheme, called turbo TCM (TTCM), is reported in [29], [32]. In [30] Ungerboeck codes are employed as constituent codes in a turbo code. The idea of this structure stems from two incentives. First, Ungerboeck codes combine modulation and coding by optimizing the Euclidean distance and achieve high spectral efficiency through signal set expansion [16]. Second, soft-output decoding algorithms exist for decoding these codes [50]. When Ungerboeck codes are used as constituent codes in a turbo coding scheme, the coding gain of the turbo coding scheme can be combined with the spectral efficiency of the TCM scheme. The encoder structure is shown in Figure 4.

The decoder structure is similar to the one used for the binary case, with a few changes to make it fit the nonbinary encoder. The first difference is that the interleaver has to work on the input symbols and not on the input bits themselves. Because the systematic

component and the parity are not transmitted separately, the systematic part of the second encoder is deinterleaved to retain the order of the systematic outputs as they are in the output of the first encoder, which is another constraint on the interleaver. So, for the two-bit symbols (8-PSK and 2 bits/s/Hz), the interleaver has to map symbols in odd positions to odd positions and symbols in even positions to even positions. Also, a deinterleaver has to be introduced after the second encoder to ensure the correct order in which the symbols are transmitted. For the $b/(b+1)$ TTCM, there are 2^{b-1} transitions from each state of the encoders. As a result, the soft-outputs generated and passed between the component decoders are vectors of length 2^b, of the form $[\lambda_0, \lambda_1, \lambda_2, ..., \lambda_K]$, where $K = 2^b$ and $\lambda_i = \log Pr(d_k = i)$.

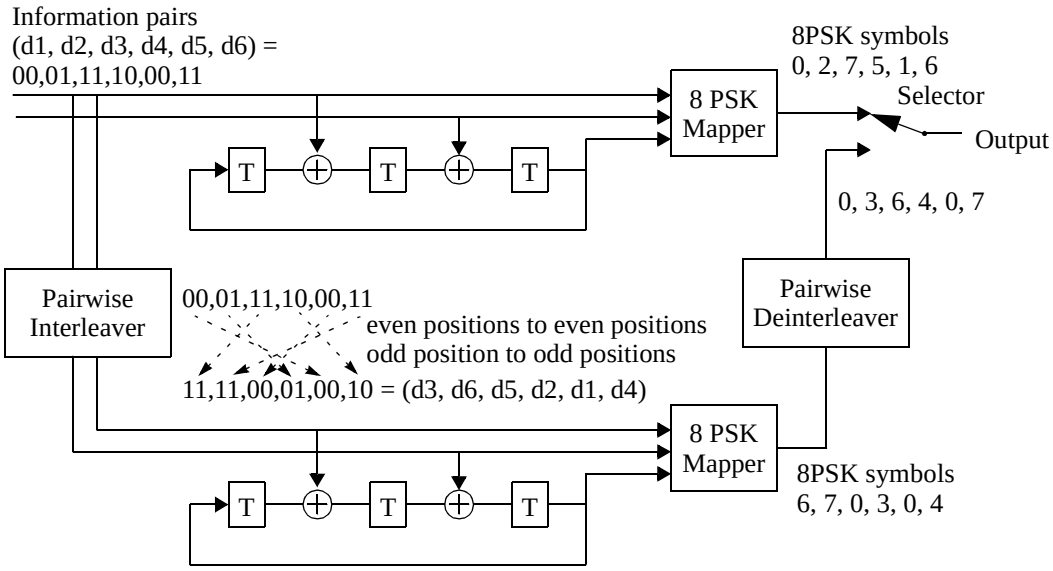

Figure 4. T-TCM encoder, shown with an example of 8-PSK modulation and $N = 12$ [32].

Furthermore, we note that the symbols are punctured before transmission, which means that the systematic information for these punctured symbols is not available to the two decoders. The solution for this is to obtain the systematic information of the punctured symbols in the first decoder from the second decoder, and vise versa. By passing the systematic information from one decoder to another, two pieces of information are passed from one decoder to another: extrinsic information and systematic information (channel information). For the first stage, the first decoder estimates the systematic information of its punctured symbols, because they are not available yet. This estimation takes place with the assumption that the parity bits are equally likely. The calculation takes place in the block called “metric” in Figure 5. As reported in [29], a coding gain of about 1.7 dB can be achieved over Ungerboeck’s TCM codes at a BER of 10^{-4}. Also, it achieved about a 0.5 dB over the results of [28], in which a Gray mapping is used.

In the scheme of [29], parallel transitions occur, because one of the data lines $\boldsymbol{D_1}$ or $\boldsymbol{D_2}$ is not encoded. The occurrence of parallel transitions causes one error event to start appearing in both encoders simultaneously, which limits the minimum free distance of the turbo encoder. One solution is to prevent parallel transitions, but doing so will result in avoiding the best-known TCM codes, which are know to have parallel transitions with small constraint lengths. An alternative solution is to use a mapper after the interleaver, as suggested in [33], to change the order of the bits in every symbol. Hence, parallel transition in one encoder results in a multistep error in the other encoder. This idea

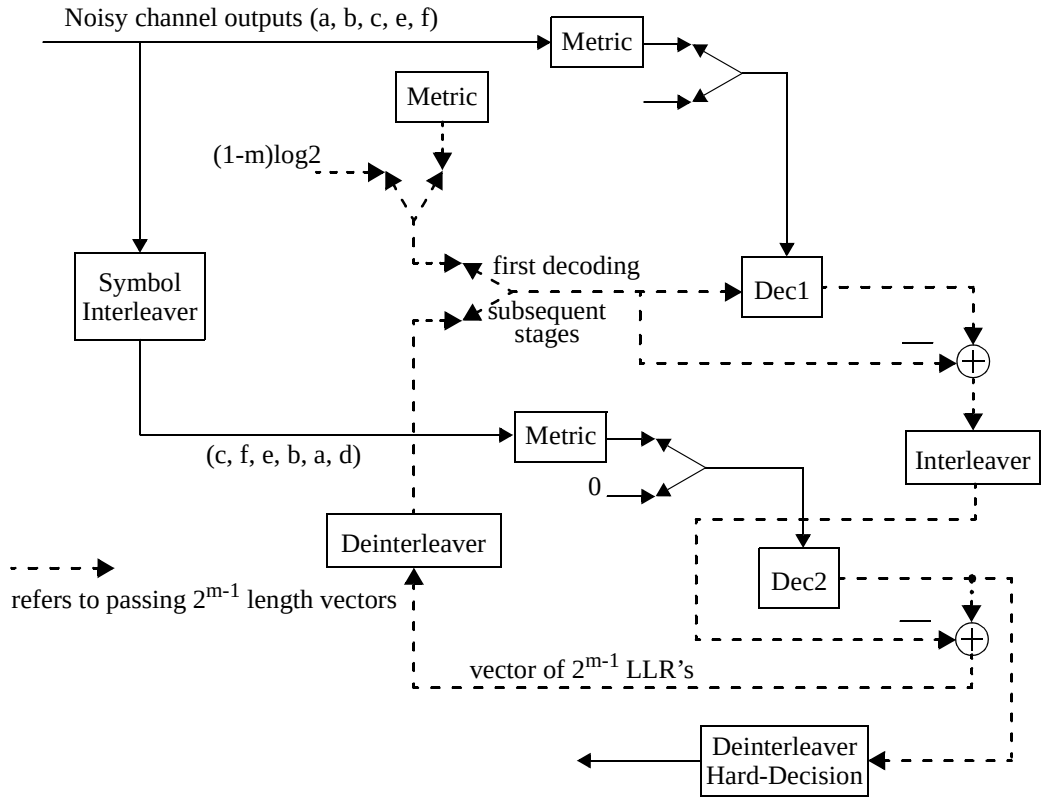

Figure 5. Turbo trellis-coded modulation - decoder structure [32].

involves using the best-known small constraint length codes with parallel transitions. This modification improves the performance of the turbo-TCM scheme for the first few iterations of the decoding. However, the performance of both schemes becomes identical as the number of iterations increases.

In [34], an improvement of Robertson's system has been introduced through removal of two obstacles. The first obstacle is the odd and even constraint on the interleaver. Second, in Robertson's system, the extrinsic and channel parts are transferred from one branch of the decoder to the other, although the extrinsic information is the only part that needs to be transferred between the two branches of the decoder of the modified system. Removing the first constraint on the interleaver cuts the delay to half, and removing the second constraint simplifies the decoding process. The simulation of this new system shows that a BER of 10^{-6} is obtained at 0.4 dB from the Shannon limit for the case of a two-bits/symbol transmission with 8PSK modulation.

Another scheme, called parallel concatenated TCM, is reported in [35], [36]. The encoder consists of two TCM encoders, two interleavers, and the modulation mapper. In this new scheme, the data sequence $\boldsymbol{D}$ is split to two sequences, $\boldsymbol{D}_1$ and $\boldsymbol{D}_2$. The complete data sequence is fed to both encoders. The first TCM encoder takes the two data sequences and produces a parity bit per symbol. Then, the two data sequences are interleaved separately by the two interleavers. The output of the interleavers is fed to the second TCM encoder to produce the second parity bit per symbol. The first data sequence,

together with the output of the first encoder, is fed to the I-channel. The second data sequence, together with the output of the second encoder, is fed to the Q-channel.

To improve the scheme's performance, the effective free Euclidean distance, which is a fundamental parameter of turbo codes, of the complete encoder is maximized. In the same reference, two additional mappings were used with the Ungerboeck mapping. The iterative decoder deals with bit log-likelihoods instead of symbol log-likelihoods. To achieve that, an algorithm was implemented to convert from symbol log-likelihoods to bit log-likelihoods. This method takes advantage of the attributes of turbo codes more than the other schemes. The new scheme is studied over 8-PSK and 16-QAM signal constellations with a rate of two-bits/s/Hz. The result shows a 1.0 dB from the Shannon limit for a BER of 10^{-6}.

A modification of the above scheme, which is presented in [37], is called symbol interleaved parallel concatenated TCM (SIPCTCM). As the name implies, the modification is to have symbol interleaving instead of bit interleaving, which will increase the accuracy of the iterative decoder because it does not have to convert from symbol probabilities to bit probabilities. The simulation shows that this scheme converges at a lower SNR. However, it has a higher error floor than the above schemes. This indicates that schemes with bit interleaving have a higher effective distance than those with symbol interleaving.

A less complex scheme than those presented above was introduced in [39]. The idea is to apply turbo codes to pragmatic TCM. This scheme, called turbo-coded pragmatic TCM (TCPTCM), has a simpler design and shorter interleaver than PCTCM [35], [36]. It is worth mentioning that the performance achieved by this scheme is only 1.0 db from the performance reported by [35], [36] at a BER of 10^{-6}.

3.2.2.2 Serially Concatenated TCM

Benedetto et al. suggested a serial concatenated TCM scheme with iterative decoding [3]. The rate of the proposed code is $2b/(2b+2)$. The proposed system is a serial concatenation of a convolutional outer code, followed by an interleaver, which is followed by a TCM inner code. The outer code is a nonrecursive convolutional code and the inner code is a recursive TCM code. The TCM code is optimized such that the minimum Euclidean distance is maximized for the input sequences of weight two. The resultant minimum Euclidean distance is called the effective free Euclidean distance of the TCM code and is denoted by $d_{f,\,eff}$. If the free distance of the outer code is denoted by d_f^o and the minimum Euclidean distance of the inner (TCM) code resulting from the weight three

input sequence by $h_m^{(3)}$, the authors expect the bit-error rate of the serial-concatenated TCM system to be

$$P_b \leq \begin{cases} B_{\text{even}} N^{\frac{-d_f^o}{2}} \exp\left(-\left(\frac{d_f^o d_{f,eff}^2}{2}\right)\left(\frac{E_s}{4N_o}\right)\right) & \text{, for } d \text{ even} \\ B_{\text{odd}} N^{\frac{-(d_f^o+1)}{2}} \exp\left(-\left[\frac{(d_f^o-3)d_{f,eff}^2}{2} + h_m^{2\,(3)}\right]\left(\frac{E_s}{4N_o}\right)\right) & \text{, for } d \text{ odd} \end{cases}, \qquad (16)$$

where E_s/N_o is the M-ary symbol signal-to-noise ratio. The above system has a performance of 1.1 dB from the Shannon limit, for 8-PSK modulation, 2 bits/s/Hz spectral efficiency, and interleaver size of 16384.

A serially concatenated punctured trellis-coded modulation, with a rate of $b/(b+1)$ is presented in [40]. To achieve this rate with two TCM codes, the parity bits are alternatively punctured. The structure of the system is shown in Figure 6. A simulation of this scheme indicates an improvement on the parallel concatenated system because there is no flattening effect associated with it, up to BER of 10^{-6}. In the simulation, a BER of 10^{-6} can be realized at E_b/N_0 = 4.43 dB.

3.2.3 Multilevel Coded (MLC) Modulation

Multilevel coding (MLC), introduced by Hirakawa et al. in [51], is considered to be an efficient way to separate error correction and multilevel coding problems. The idea behind

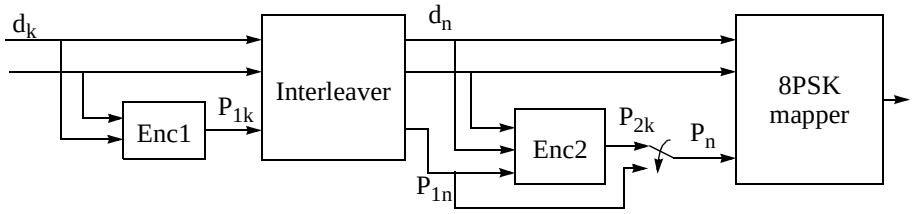

Figure 6. Serial-concatenated TCM proposed by [40].

TCM and MLC is to optimize the code in Euclidean space instead of dealing with the Hamming distance, which is used in the classical coding techniques.

3.2.3.1 MLC Principles

MLC, as the name implies, is a combination of several error correction codes applied to subsets of a signal constellation. MLC depends on set partitioning as the TCM. It starts with partitioning a signal constellation S into L steps, thereby producing a partitioning chain $S_0/S_1/S_2/.../S_{L-1}$. The structure of the MLC encoder is shown in Figure 7.

In [51], the multilevel code is decoded suboptimally using a multistage decoder. Multistage decoders are discussed in [52], [53], [54], [55], [56]. The decoding process starts with Decoder 1 of C_1 based on the received signal. Then, based on the received signal and the estimated code word of C_1, Decoder 2 starts decoding C_2. Thus, Decoder i decodes the code C_i for $i = 2, 3,..., L$ based on the received signal and the estimated

code words of C_1, C_2,..., C_{i-1}, and does not use the higher level codes C_{i+1}, C_{i+2},..., C_L. Multistage decoders are suboptimal because the decoding at stage i does not depend on the information from higher level decoders. However, they lower the complexity of decoding, see Figure 8.

Capacity of MLC systems: Huber et al., in [57], [58], [59], [60], and Kofmann et al., in [61], [62], showed that multilevel codes combined with multistage decoding can achieve the capacity of the modulation schemes.

Design Rules: To design the different code rates of various code branches of the MLC system, many design rules have been suggested, [63], [64]. Setting the code rates to the

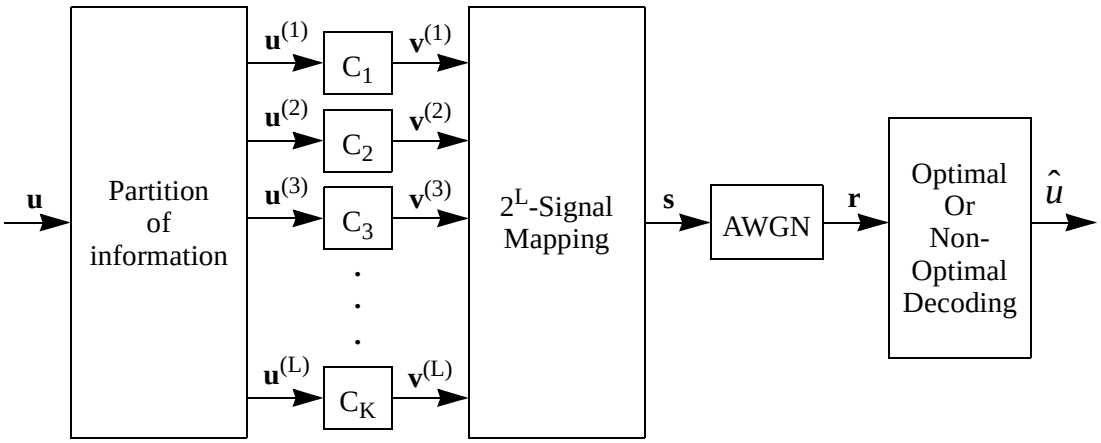

Figure 7. Multilevel encoder.

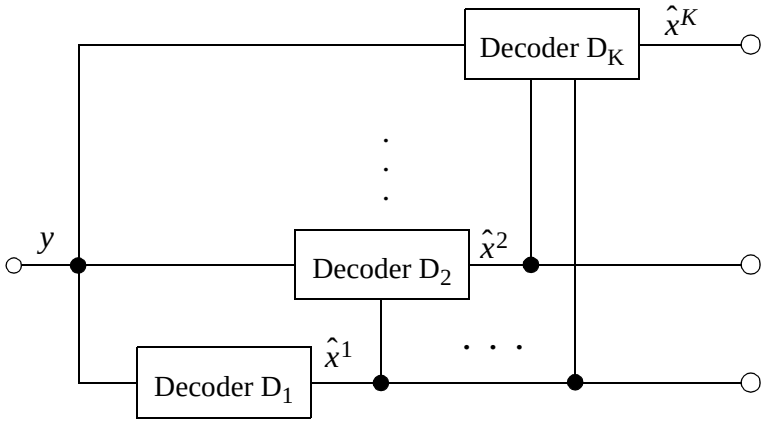

Figure 8. Multistage decoding.

capacity of the levels is called the capacity design rule. Other design rules were reported, namely, balanced distance rule, coding exponent rule, cut-off rate rule, and equal error probability or bounds. For the lower levels of the MLC scheme, the number of nearest points is more than for high levels. As a result, the balanced distance design method is not appropriate because it does not account for this fact [59], [60]. Also, it is reported that the best way to design MLC codes is through the use of random coding exponents or the capacity of the equivalent channels.

3.2.3.2 Set Partitioning

Set partitioning for a signal set S of M elements, where $M = 2^L$, is done in L steps. In the first step, the set S is divided into two subsets. In the division process, a certain

criterion related to the Euclidean distance between the elements of the subset is used. For example, the intrasubset Euclidean distance is maximized in the case of Ungerboeck's partitioning, although it is minimized in the case of block partitioning. Then, in the second step, every resultant subset is divided. For Ungerboeck's partitioning, see Figure 9.

In studying the power efficiency of MLC, with different set partitioning strategies, multiple information theory measures are conducted in [60]. First, the sum of the cut-off rate of the equivalent channels is compared in the case of two different set partitionings: Ungerboeck's partitioning and block partitioning. The sum of cut-off rates of the equivalent channels of MLC system with Ungerboeck's partitioning excels over MLC system with block partitioning. Also, the two systems are tested for the case of different code word lengths. The results of [60] explain that both systems' capacities do not differ for infinite block lengths. However, in the case of finite code word lengths, the system with Ungerboeck's partitioning reveals more capacity than the system with block partitioning.

With the use of multistage decoding, block partitioning offers no error propagation from the lower levels of MLC to the higher levels. So, this partitioning technique is used in some applications, which need to have different amounts of error protection. For example, consider the case of 8-ASK modulation where the three levels are coded with the same rate of 0.5, and block partitioning and multistage decoding technique are used. Then, over a 10.0 dB range, the degree of reliability of all levels varies as the SNR increases. At

high SNR, a 1.5 bit/symbol could be received reliably. For medium SNR, a 1.0 bit/symbol could be received. At the same time, the transmission on the highest bit becomes impossible. At low SNR, only 0.5 bit/symbol could be received reliably at the lowest level, whereas the transmission becomes impossible at high levels. This example supports the theory that MLC systems are the best candidates for applications for which the transmitted data could be classified to sensitive and nonsensitive. Broadcasting systems and mobile communications, which require transmission of video and audio information are considered examples of such applications.

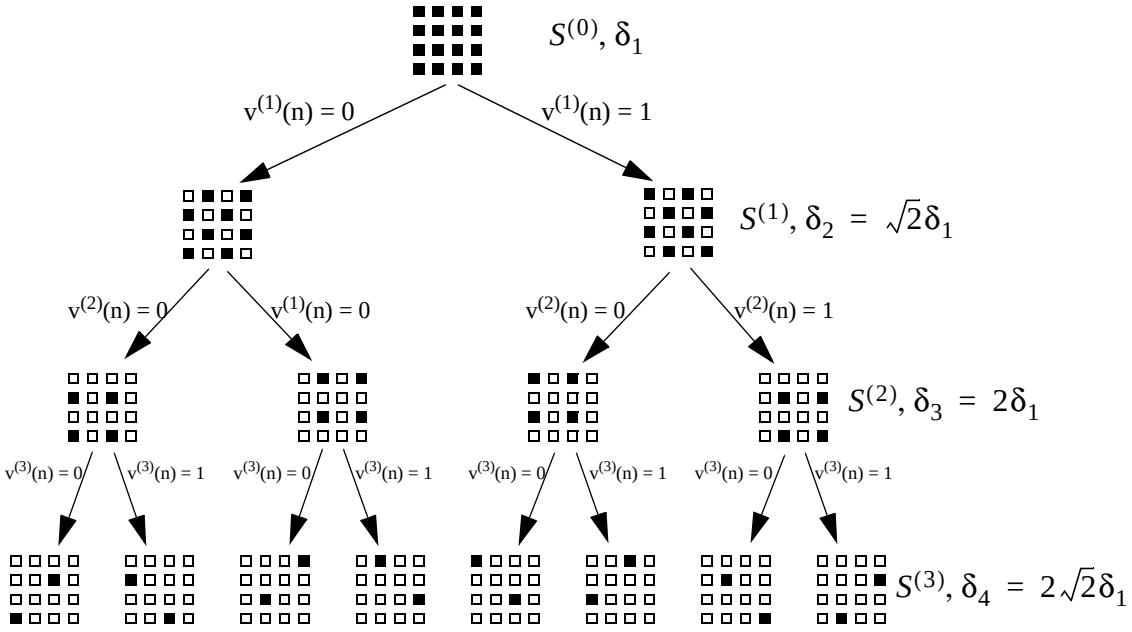

Figure 9. Set partitioning for 16-QAM signaling.

3.2.3.3 Turbo coding with MLC

In [65], it is shown that achieving capacity of a modulation scheme via MLC could be done without going through specific set partitioning; capacity could be received with any set partitioning. In that paper, two set partitionings have been used, namely, Ungerboeck's partitioning and block partitioning. As presented earlier, the intrasubset minimum Euclidean distance is maximum in the case of the first, and it is minimum in the second.

Because turbo codes depend on the whole spectrum of the code, [64] reports that balancing the error rates for the multilevel coding component codes is more practical than the other design rules. The turbo codes were applied to multilevel coding in [63], [66], [67]. In [66], the code rates of the turbo codes were designed using the random coding bound, which is considered more practical than using the capacity. The results provide up to 1.6 dB from the Shannon limit for the case 8-PSK modulation and up to 1.9 dB for the case of 32-QAM, with an interleaver length of 20,000. A modified block interleaver was used, in [67], to improve the performance of turbo codes with short interleavers. These new interleavers outperforms the random interleavers at bit-error rates greater than 10^{-7}.

3.3 Summary

In this chapter, we reviewed binary turbo codes, iterative decoding and turbo coded modulation techniques. We have seen that TTCM and PCTCM schemes do not utilize all the available interleaving gain. In addition to that, both schemes are constrained by

parallel transitions leading to higher decoding complexity. MLC schemes with turbo codes components are not good candidates to utilize the available interleaving gain because of the error propagation problem in low SNR range. On the other hand, SCTCM schemes with bit-interleaving utilize all the available interleaving gain and do not have constraints from parallel transitions.

Chapter 4

Two-Level Two-Pulse Position Modulation Scheme

To achieve good power and spectral efficiencies with a coded modulation system, the underlying modulation must be selected carefully. For IM/DD, PPM and MPPM have good power efficiencies but low spectral efficiencies. On the other hand, PAM achieves excellent spectral efficiencies but with poor power efficiency. In the following discussion, we will introduce a new modulation scheme that combines multiple-level and multiple-pulse position. We will begin with the description of the modulation scheme, then we present its performance in terms of uncoded BER and cutoff rate.

4.1 Two-Level Two-Pulse Position Modulation

Multi-level modulation techniques are powerful in terms of spectral efficiency, whereas pulse position modulation is strong in terms of power efficiency. To benefit from the strength of two modulation categories, we introduced a modulation scheme that has

two pulses for every symbol time period and each pulse can take two amplitude levels instead of one amplitude level, as in PPM and MPPM. We call this modulation two-level two-pulse position modulation (2L2PPM).

In this modulation format, each word of b bits is mapped into one of $L = 2^b$ waveforms and transmitted to the channel. The symbol interval of duration T is partitioned into n chips. Each chip has a duration T/n. Of the n, only two contain pulses, each of which can take one of two levels (A_1, A_2) to convey one of the L symbols. The two levels are introduced to increase the spectral efficiency. In the conventional pulse position modulation (PPM), only one amplitude level and one position is used. In conventional multiple pulse position modulation (MPPM), two or more pulses are used, but each pulse takes only one amplitude level. The new modulation scheme achieves more spectral efficiency than conventional PPM and MPPM modulation schemes because we allow pulses to have two amplitude levels. The two amplitude levels, A_1 and A_2, are chosen so that the average optical power is P, and the relationship between the two levels is a design parameter. In addition to that, the number of the signal waveforms in the 2L2PPM signal set is

$$L = 4\binom{n}{2} = \frac{2n!}{(n-2)!} = 2n(n-1), \tag{17}$$

where n is the number of pulse positions. L is usually not a power of two, so we generally must discard some of the resulting signals to achieve $L = 2^b$.

In this research, two different cases are explored. In the first case, n is chosen to be 9, producing 144 possible signals, and n is chosen to be 12 for the second case producing 264 possible signals. The two cases are denoted by 9-2L2PPM and 12-2L2PPM, respectively.

4.2 Performance of 2L2PPM

To evaluate the effectiveness of this modulation scheme we use two different performance measures: uncoded bit-error rate and cutoff rate.

4.2.1 Uncoded bit-error rate

In determining error probability, we assume maximum-likelihood (ML) detection. The transmitter sends information at a rate of R_b bits/s by transmitting one of its L available signals $\{x_1(t), x_2(t), \ldots, x_L(t)\}$ every $T = \log_2 L / R_b$ seconds. The channel adds white Gaussian noise with power spectrum $N_o/2$. The signal set satisfies the constraint of power limitation $\frac{1}{T}\int_0^T x(t)dt = P$, where P is the average optical power. We also assume high SNR, which allows us to approximate the BER from the Euclidean distance between the nearest two signals $d_{\min}$, where

$$d_{\min}^2 = \min_{i \neq j} \int (x_i(t) - x_j(t))^2 dt . \tag{18}$$

and the BER is roughly bounded by

$$\text{BER} \approx Q\left(\frac{d_{\min}}{\sqrt{2N_o}}\right). \tag{19}$$

For the uncoded 2L2PPM the ratio between the 2nd amplitude level to the first is

$$A_2 = (1 + \sqrt{2})A_1 . \tag{20}$$

Using the power constraint we can find that

$$A_1 = (nP)/(2 + \sqrt{2}), \tag{21}$$

$$A_2 = nP(1 + \sqrt{2})/(2 + \sqrt{2}). \tag{22}$$

Looking to the signal constellation of 2L2PPM modulation scheme, it is not difficult to show that the minimum Euclidean distance square of this modulation scheme is going to be:

$$(d_{\text{2L2PPM}})^2 = \frac{2nP^2 \log_2(2n(n-1))}{(2 + \sqrt{2})^2 R_b} \tag{23}$$

Similar to the discussion in [41], we can write the ratio between the power needed for 2L2PPM to the power needed for OOK for the same BER as the inverse ratio between the minimum Euclidean distance of the two modulations,

$$P_{\text{2L2PPM}} / P_{\text{OOK}} \approx d_{\text{OOK}} / d_{\text{2L2PPM}} = \frac{2(2+\sqrt{2})}{\sqrt{2n\log_2(2n(n-1))}}. \quad (24)$$

Figure 10 shows the power efficiency versus the spectral efficiency of 2L2PPM for different values of n. For comparison purposes, we also showed the performance of OOK, L-PPM, (n,2)-MPPM and (n,3)-MPPM modulation schemes. The y-axis represents the normalized power requirement for BER = 10^{-6}. The x-axis represents the spectral efficiency in terms of bits/s/Hz. The figure shows that 2L2PPM modulation scheme is more spectrally efficient than PPM and MPPM modulation schemes. It also shows that the power efficiency of 2L2PPM is still better than OOK for $n \geq 5$. The curve shows that the power efficiencies of 9-2L2PPM and 12-2L2PPM are -2.2 and -3.0 dB, respectively.

4.2.2 Spectral Efficiency

There are several ways to define the bandwidth of signals in communications [68]. One of the simplest estimates of the bandwidth requirement of 2L2PPM is the inverse of the shortest pulse width, and the estimate is equivalent to the width of the main spectral lobe of the modulation scheme [41]. More accurate measures of the bandwidth requirement come after specifying the power spectral density (PSD) of the modulation

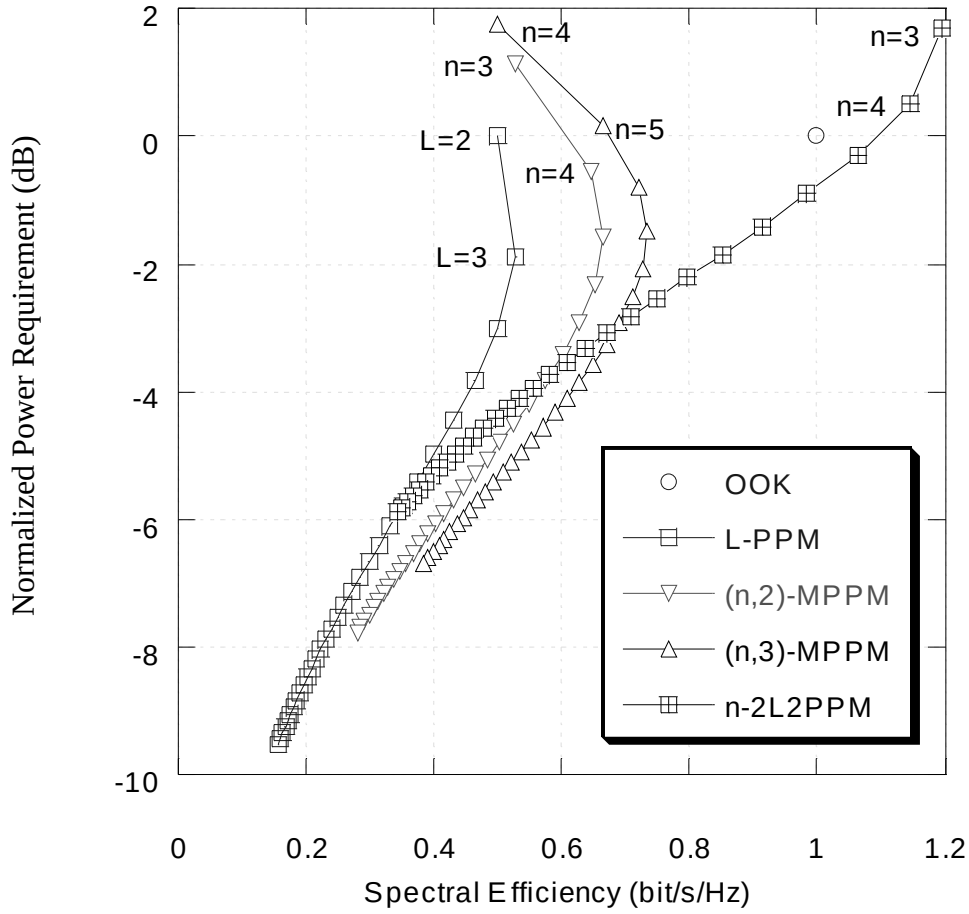

Figure 10. Power efficiency versus spectral efficiency for n-2L2PPM, OOK, L-PPM, (n,2)-MPPM, and (n,3)-MPPM modulation schemes at high optical SNR.

scheme, and the bandwidth that includes an x-percentage of the signal power is called B_x [69]. If the input symbols to the modulator are assumed to be chosen independently and with equal probability, then a general expression for the PSD of any L-ary modulation scheme is given in [42] as

$$P(f) = \frac{1}{L^2 T_s^2} \sum_{n=-\infty}^{\infty} \left| \sum_l P_l\left(\frac{n}{T_s}\right) \right|^2 \delta\left(f - \frac{n}{T_s}\right) + \frac{1}{T_s}\left[\sum_l \frac{1}{L} |P_l(f)|^2 - \left| \sum_l \frac{1}{L} P_l(f) \right|^2 \right], \qquad (25)$$

where $P_l(f)$ is the Fourier transform of the signal corresponding to the l-th symbol, and T_s is the symbol period. The first term is discrete and represents the spectral lines. The second term represents the continuous part of the spectrum.

For rectangular pulses, Figure 11 shows the continuous part of the PSD of 9-2L2PPM and 12-2L2PPM. In each curve, the first null of the spectrum corresponds to the inverse of the shortest pulse-width, which is used as an approximation for the bandwidth requirement of the modulation scheme. According to this approximation, the normalized bandwidth requirements of the two cases are 1.26 and 1.49, and they contain 91.4% and 91.1% of the signal power, respectively. Since more than 90% of the signal power is contained in main spectral lobe, the above approximation of the bandwidth requirement is justified.

In addition to that, the spectral density is defined as the inverse of the bandwidth requirement. When the above approximation is used, we can show that the spectral efficiency of 2L2PPM modulation scheme is

$$\eta_{2L2PPM} = \frac{\log_2 L}{n} = \frac{\log_2(2n(n-1))}{n}. \tag{26}$$

Out of the 144 possible signals in 9-2L2PPM modulation scheme, 128 signals are used with a serial concatenated encoder as we see in chapter 5 to get 128-SCTCM-2L2PPM system. Similarly, only 256 of 264 signals in 12-2L2PPM modulation scheme are used with serial concatenated encoder to form 256-SCTCM-2L2PPM system.

4.2.3 Cutoff rate

According to [70], the cutoff rate is believed to be a figure of merit for all modulation schemes. For an arbitrary L-ary modulation scheme, the cutoff rate R_o is defined when the input code words are i.i.d. with a uniform distribution $p(x_k) = 1/L$ as

$$R_o = -\log_2\left(\frac{1}{L^2}\sum_{l=0}^{L-1}\sum_{m=0}^{L-1}\exp(-\|v_l - v_m\|^2/8)\right) \text{ bits/codeword}, \tag{27}$$

where $v = x/(\sqrt{N_o})$.

The cutoff rate is used to evaluate efficiency of the above modulation scheme. From Figure 12, we can see that when $n = 9$ we have $R_o = 5$ at -6.8 dB normalized power efficiency. For $n = 12$, $R_o = 6$ at a normalized power efficiency of -7.1 dB. Later on in the simulation results of SCTCM-2L2PPM, we can see that these power efficiencies are

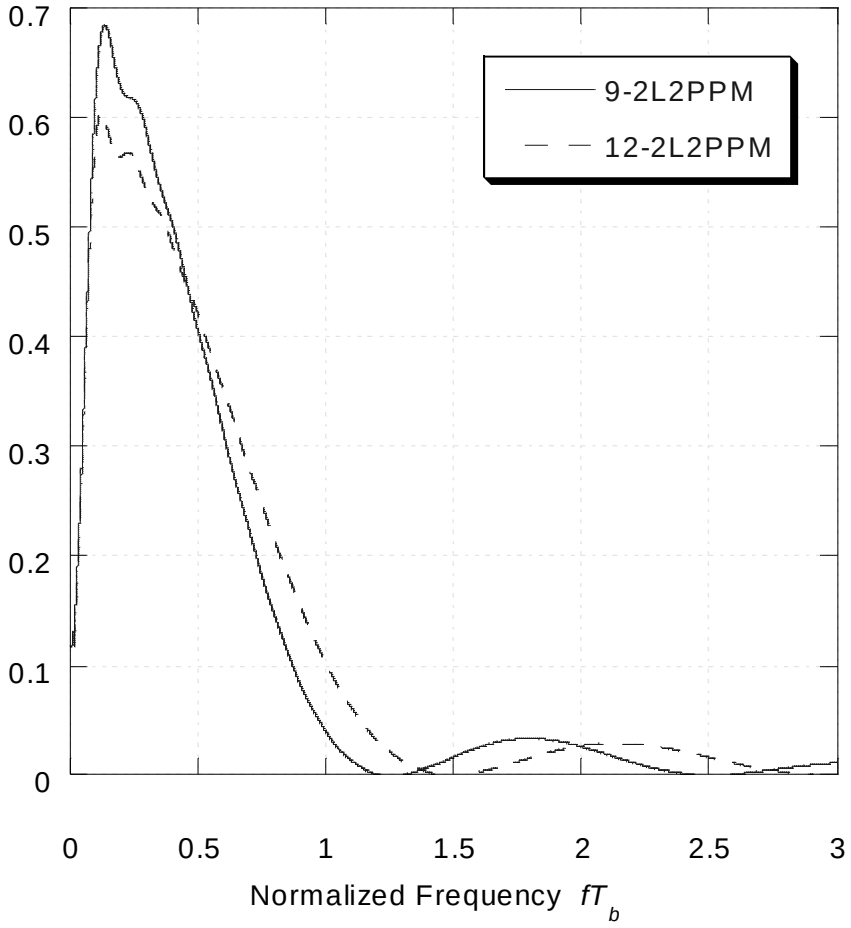

Figure 11. Continuum power spectrum of 9-2L2PPM and 12-2L2PPM.

approachable with the use of 128-SCTCM and 256-SCTCM for medium size interleavers ($N = 10000$).

4.3 Summary

In this chapter, we introduced a new modulation scheme that is suitable for optical communications. The new modulation is a combination of MPPM and multilevel modulation techniques. The uncoded BER performance of this modulation technique shows it is more spectrally efficient than PPM and MPPM. The cutoff rate curves of the new modulation scheme indicate that up to 6.7-7.1 dB of power efficiencies and 0.55-0.5 bits/sec./Hz spectral efficiencies could be obtained by using 128 and 256 symbols 2L2PPM modulation. This modulation scheme is utilized in chapter 5 with serial-concatenated trellis-coded modulation systems.

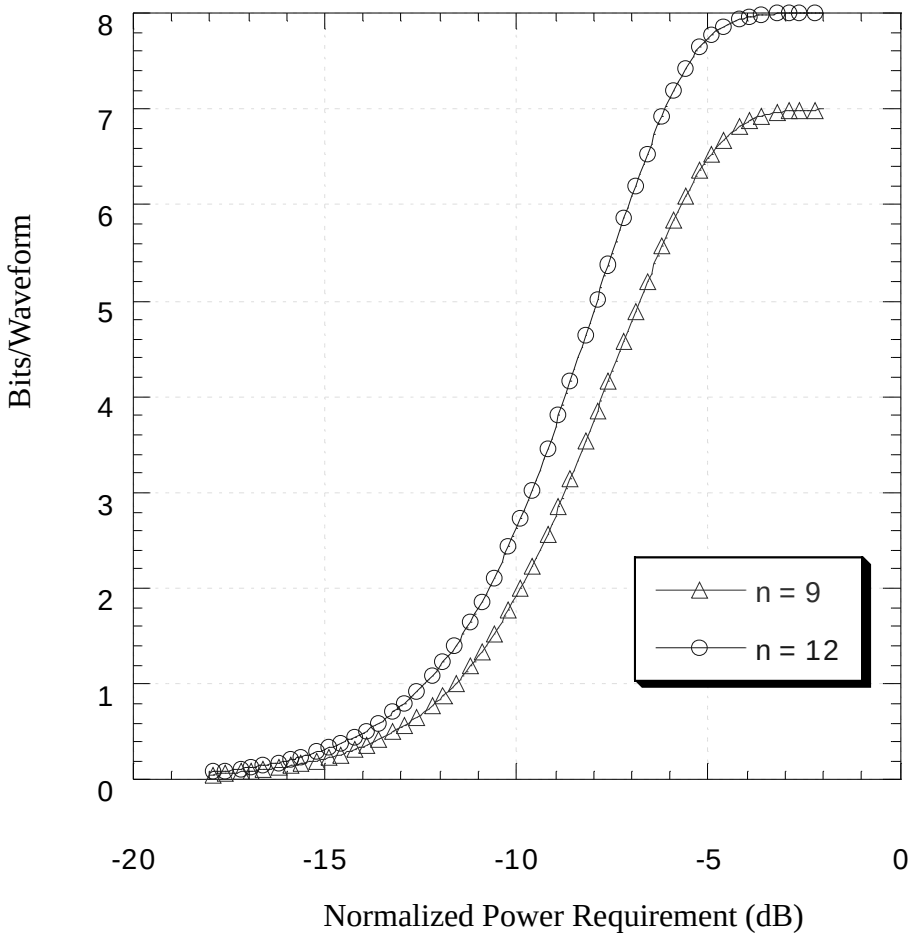

Figure 12. The cutoff rate of 9-2L2PPM and 12-2L2PPM modulation schemes.

Chapter 5

Serial-Concatenated Trellis-Coded Modulation with 2L2PPM Modulation

As we have seen in chapter 3, serial-concatenated trellis-coded modulation (SCTCM) schemes with bit-wise interleavers achieve excellent performance and they outperform both turbo trellis-coded modulation (TTCM) and parallel-concatenated trellis-coded modulation (PCTCM) techniques in utilizing the interleaver gain. For the same reason, they outperform SCTCM schemes with symbol-wise interleavers. Additionally, constituent codes of symbol interleaved SCTCM have to meet the conditions of not allowing parallel transitions to occur, which increase the constraint length of both the outer and inner codes and, hence, increase the complexity of the decoding. Moreover, SCTCM are found to have lower error floor bounds compared with TTCM and PCTCM.

In this chapter, we present a SCTCM with spread-random (S-random) bit interleavers and two-level two-pulse position modulation (2L2PPM). A description of the system and

the performance error bounds of serial-concatenated convolutional codes (SCTCM) [2] are rederived, with the difference of having a trellis-coded modulation (TCM) inner code, to find the design criteria for the system. The mapping and code search results are given. Finally, Monte Carlo simulations and performance error bounds are presented for the proposed SCTCM.

5.1 System Description

The structure of this proposed system is shown in Figure 13. The proposed transmitter of the system consists of a serial concatenation of an outer code, interleaver, an inner code, and a 2L2PPM modulator. As we saw in chapter 4, the 2L2PPM modulation scheme has excellent uncoded power and spectral efficiencies. The outer code is chosen to be a convolutional code of rate $(b-2)/(b-1)$. We used both systematic and non-systematic convolutional codes for the implementation of the outer code. The interleaver is a bit spread-random interleaver [71]. The inner code is a recursive systematic convolutional code of rate $(b-1)/b$ and is combined with the modulation mapper. The modulation scheme is two-level two-pulse position modulation (2L2PPM). The signal constellation has a size of $M = 2^b$ signals. Because the rate of the outer code is $(b-2)/(b-1)$ and the rate of the inner code is $(b-1)/b$, the total coding rate becomes $(b-2)/b$. From the spectral efficiency point of view, the rate of the 2L2PPM modulation scheme is b/n and

when combined with the total coding rate it produces a total spectral efficiency of $(b-2)/n$ bits/s/Hz for the SCTCM-2L2PPM system.

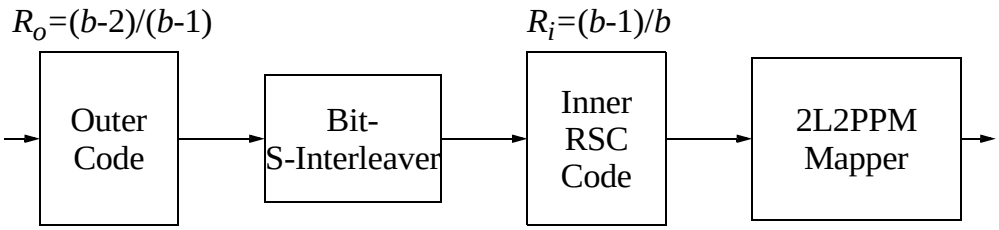

Figure 13. First SCTCM encoder.

The following presentation is a brief explanation of the type of interleaver used. Then, the structure of the outer and the inner codes, and the types of mapping to the modulation signal space are described.

5.1.1 Interleaver

S-random interleavers are used to improve the performance of parallel or serial concatenated systems. Through the use of S-random interleavers, the effective Euclidean distance of the serial concatenated encoder will increase to at least the product of the Hamming distance of the outer code and the minimum Euclidean distance of the inner TCM code as in the following theorem:

Theorem: With the use of very long spread-bit-interleavers in the serial concatenated trellis-coded modulation encoder, which consists of non-systematic convolutional outer code and a recursive inner code, the effective minimum Euclidean distance of the system will be bounded by:

$$d^{s}_{E,\,eff} \geq d^{o}_{H} d^{i}_{E}\,, \tag{28}$$

where d^{o}_{H} is the outer code free Hamming distance and d^{i}_{E} is the minimum Euclidean distance of the inner code.

Proof: In the serial concatenated TCM encoders, we have an outer code of rate R^{o}, an inner code of rate R^{i}, and an interleaver. If the information block length is N then the interleaver length N_i is

$$N_i = N/R^{o}\,. \tag{29}$$

According to [71] S-random interleavers could be found easily for the parameter S

$$S \leq \sqrt{N_i/2} = \sqrt{N/(2R^{o})}\,. \tag{30}$$

If two information bits are located at positions i and j such that $|i-j| \leq S$ before interleaving, they will be mapped to two positions $f(i)$ and $f(j)$, such that $|f(i)-f(j)| > S$. One of the properties of convolutional codes is that the first d^{o}_{H} ones of the output of a codeword is within a limited depth relative to the constraint length of the code [72]. This

property is used frequently by the algorithms that find the minimum Hamming distance of convolutional codes. So, for the considered outer code and large S-interleavers, at least d_H^o ones will fall in a span less than S. This will result in an interleaver output that has at least d_H^o ones, each of them is at least S away from the other (d_H^o-1) ones. If S is very large, then the minimum Euclidean distance of such sequences is $d_H^o d_E^l$. This result is also applicable to the case of recursive outer codes.

5.1.2 Inner Code

The inner code structure and its mapping to the modulation space are critical to the performance of SCTCM schemes. As will be seen in the design of SCTCM, the inner code has to be recursive. Thus, for the proposed SCTCM-2L2PPM scheme, we selected the inner code to be a systematic recursive convolutional code. We used two methods to map the outputs of the inner code to the signal space: natural mapping and Gray mapping techniques. More details about the structure and the output mappings of the inner code, are given below.

5.1.2.1 Inner Code Structure

Figure 14 shows the minimal systematic encoder structure with feedback. This convolutional encoder is uniquely specified by the parity-check matrix $H = \{ h_j^i \}$. According to [16], we have to set $h_0^0 = h_m^0 = 1$ and

$$h_0^i = h_m^i = 0, \ \mathrm{i} = 1, 2, \ldots, p. \tag{31}$$

In this case, we have an excessive number of parallel transitions, and the minimum Euclidean intra-distance does not always increase between the successive partitionings. Hence, we decided to change the conditions of Ungerboeck on the code polynomials. For natural mapping (see the next section), we will set $h_0^0 = h_m^0 = 1$ and leave h_0^i and h_m^i, for $i = 1, 2, \ldots, p$, free. This will decrease the maximum number of parallel transitions by one half. For Gray mapping (next section), we set $h_0^0 = h_m^0 = 1$ and $h_0^i = 0$ for $i = 1, 2, \ldots, p$, to facilitate the mapping process. Moreover, to ensure the minimization of the parallel transitions, we require H to be of maximum rank. Since the trellis codes are linear, the minimum Euclidean distance of the all-zero path is not necessarily the minimum distance to any other trellis path. For this reason, in looking for the minimum Euclidean distance, we used an algorithm presented in [73], but modified to keep record of the Hamming weight of the path that has the minimum Euclidean distance.

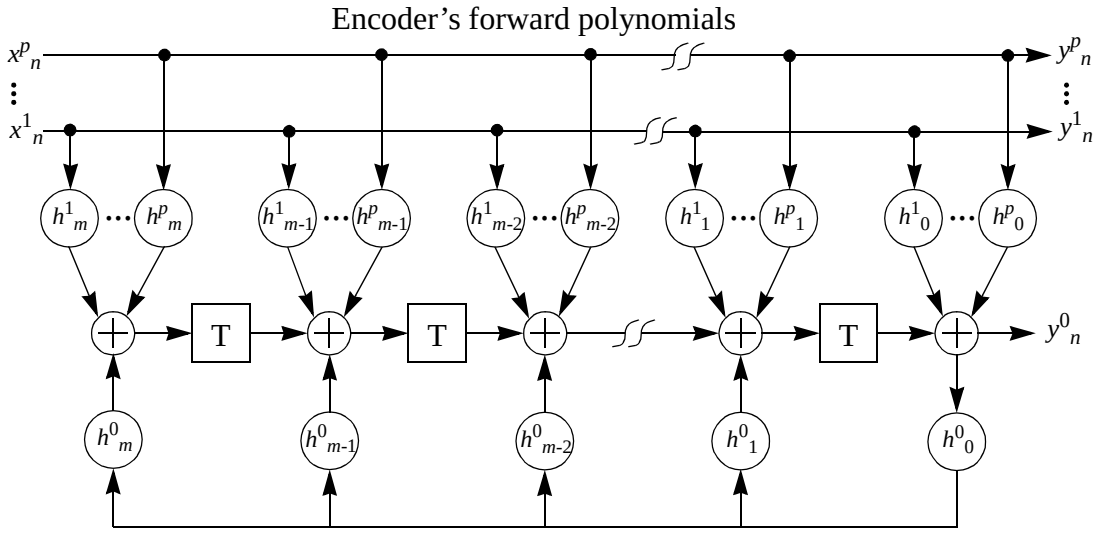

Figure 14. Minimal systematic convolutional encoder with feedback. The code has a rate of $p/(p+1)$, parity check coefficients h^i_j, and memory m.

5.1.2.2 Mapping of the Inner Code

In this study, the outputs of the inner code to the signal space are mapped using two methods: natural mapping and Gray mapping. In TCM, natural mapping is always guaranteed to maximize the minimum Euclidean distance. However, Gray mapping produces lower bit-error rate (BER) if it has the same minimum Euclidean distance [74], [75].

Natural Mapping. Natural mapping is based on successively partitioning the signal set into subsets with increasing Euclidean distance [16]. In natural mapping, output labels are decided by the set partitioning of the signal set and the classical way of selecting the output labels of the code, but they affect the realization of the inner code. In this system, recursive systematic convolutional encoders are used, so for every selection of arbitrary forward and feedback polynomials we need to do a linear transformation of the output labels to match the set partitioning result. For input mapping, it is essential that any two input sequences that have a difference of one between their Hamming weights result in two output sequences of symbols that are separated with infinite Euclidean distance. This objective can be assured by using non-zero forward polynomials.

Gray Mapping. Natural mapping guarantees minimization of event error rate (EER). In most applications BER is more important than the EER. For this reason, the authors of [74], [75] found that using Gray mapping with trellis-coded modulation produces lower BER than the TCM codes that use natural mapping on the same signal sets. They

concluded that both mappings will result in the same probability of error event, but the average number of information bit-errors is less with Gray mapping than with natural mapping when the Euclidean distance is small. Also, when the Euclidean distance is large, the average number of information bit-errors is less with natural mapping than with Gray mapping. They concluded that it is necessary to encode all of the information-bits in Gray mapping, yet some of the information-bits could be left uncoded in natural mapping. In our system, Gray mapping will further decrease the BER because of the nature of the iterative decoding technique.

5.1.3 Outer Code

In this research, we proposed both recursive and nonrecursive convolutional codes as an outer code. The nonrecursive are punctured codes [76]. The recursive codes are chosen to be a minimal systematic encoder with feedback, shown in Figure 14.

5.1.4 Iterative Decoder

Optimum maximum likelihood (ML) decoding algorithms for serial concatenation TCM codes are complex, due to the presence of the interleaver, but iterative decoding of such codes is feasible and often leads to or approaches ML decoding. Iterative decoding involves iterations between constituent decoders, with an exchange of soft information between iterations. The constituent decoders are a posteriori probability (APP) decoders which compute the posterior probability.

The receiver uses a unit-energy filter $f(t)$, which is matched to the pulse shape, and samples the output at the chip rate n/T producing n samples for each symbol. Each n samples are grouped in one block. The soft de-mapper will receive the samples to produce N_s vectors of soft information, where N_s represents the number of symbols in every codeword. Then, these N_s vectors of soft information will be used by the soft decoder. The soft decoder is composed of four blocks: the inner decoder, the bit de-interleaver, the outer decoder, and the bit interleaver. A block diagram of the iterative decoder is shown in Figure 15. Each decoder is a symbol-APP detector, which operates on the probability of the symbols rather than the bit probabilities. The interleaver works on the bits. Hence, the iterative decoder needs to perform symbol-to-bit probability conversion before the interleaver and deinterleaver and, it needs bit-to-symbol probability conversion after them. These conversions are not shown on the block diagram of the iterative decoder, but they are included in the block diagram of the constituent decoders.

The most complex receiver blocks are the inner and the outer decoders; their complexity reflects the complexity of the whole receiver. Hence, for the calculation of decoder complexity we will depend on the total number of branches per bit in the trellises of the outer and the inner codes.

Iterative decoders are suboptimal but their performance approach the bound of ML decoders for the moderate and high SNR. Symbol by symbol a posteriori decoder reported

by Bahl et al. [44] and known as the BCJR algorithm, is used in both the outer and inner decoders.

5.2 SCTCM Design

In the design of SCTCM we rely on error performance bounds. We begin the derivation of performance bounds for the SCTCM exactly as the performance bounds of the serial-concatenated convolutional codes (SCCC) [1][2]. The only difference appears in the enumeration of the inner code because the inner code is connected to a nonbinary channel. Hence, Euclidean distances are enumerated instead of enumerating the Hamming distances, as is the case with binary modulation schemes. Because we are using binary

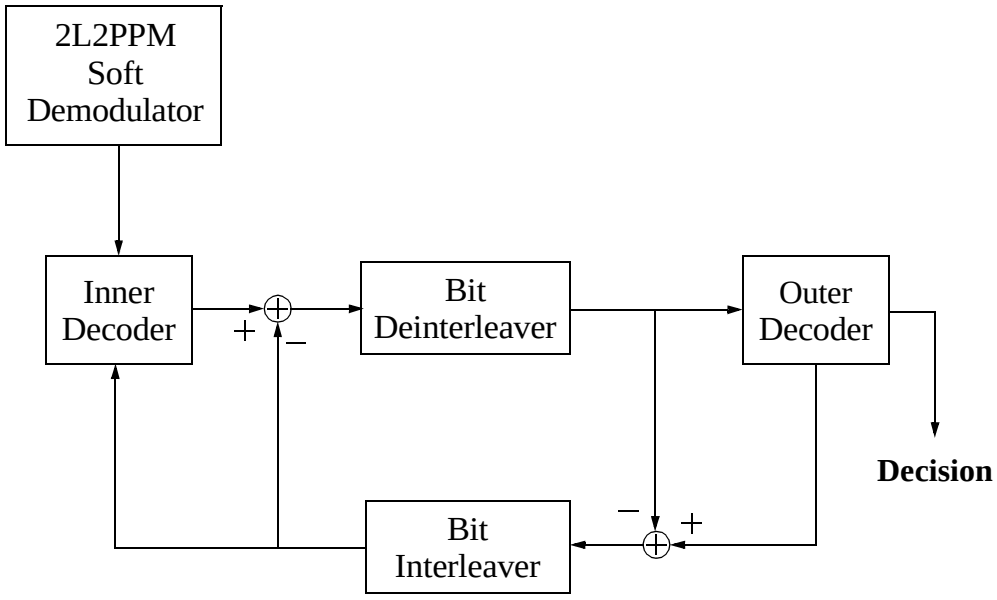

Figure 15. Iterative decoder of the proposed SCTCM-2L2PPM system.

interleavers and binary outer encoders we can still enumerate the outer code using Hamming distances.

The inner codes utilized in this research are non-regular because of the signal space [77]. In non-regular codes, every correct path in the trellis has a different enumerating function. This fact makes it impossible to use the all-zeros codeword as a reference. Therefore, in enumerating the inner code between any two points in the trellis, we will randomly pick a finite number of correct trellis paths between these two points and consider the average enumeration function between the two points as the average of the enumerating functions with respect to each selected path,

$$A_{\text{average}} = \frac{1}{M} \sum_{i=1}^{M} A_i . \tag{32}$$

For the inner codes in this research, we use the average distance spectrum, which shows the average number of codewords that have specific input Hamming distance and Euclidean distance for any possible combination of Hamming distance and Euclidean distance. The distance spectrum for the SCTCM codes can be determined using the code spectrums of both the outer code and the inner code, with a uniform interleaver.

Consider the concatenation of two linear convolutional constituent codes, C_o and C_i, connected by a bit-wise random interleaver π. The outer code C_o has a rate

$R_o = (b-2)/(b-1)$ and the inner code C_i has rate $R_i = (b-1)/b$, which gives rise in an overall SCTCM rate $R_s = (b-2)/b$. The interleaver length is N and it is an integer multiple of $(b-1)$. Every b bits that come out of the inner code constitute one of the 2^b waveforms that are mapped to the signal space. If the code termination is neglected, the block size is NR_o and the spectral efficiency is $(b-2)$ information bits per symbol. In deriving the bounds, the assumption of uniform interleaver is used. The uniform interleaver is a probabilistic device that permutes an input word of Hamming distance l, randomly to every possible permutation with the same probability. The Hamming distance of the output is l, which makes the number of possibilities equal to $\binom{N}{l}$ for an interleaver of length N. Every possibility is equi-probable with a uniform probability

$$Prob = 1/\binom{N}{l}. \tag{33}$$

By averaging over the ensemble of all interleavers, we can obtain a good bound on the performance of the serial-concatenated TCM. The performance bounds obtained using the uniform interleaver technique are useful because at least one real interleaver is guaranteed to exist that meets these bounds [24]. It is also assumed that both the outer and inner codes start from state zero for every block and terminate to the same state at the end of the block.

This assumption helps calculate the weight enumerating functions of the codes from the constituent codes.

For the outer code, the weight enumerating function is

$$A^{C_o}(W, H) = \sum_{w, h} A^{C_o}_{w, h} W^w H^h, \tag{34}$$

which is a polynomial in the dummy variables W and H, where $A^{C_o}_{w, h}$ is the number of codewords of the code with input Hamming weight w, and output Hamming weight h. The inner code has a distance spectrum

$$B^{C_i}(W, D) = \sum_{w, \{d\}} B^{C_i}_{w, d} W^w D^d, \tag{35}$$

It is also a polynomial in the dummy variables W and D, where $B^{C_i}_{w, d}$ is the average number of codewords of C_i with input Hamming weight w and squared Euclidean distance d. The summation with respect to d covers all the possible values of d. From the above polynomial, we can derive the spectral lines for all codewords with input Hamming weight w

$$B^{C_i}(w, D) = \frac{1}{l!} \frac{\partial^w}{\partial W^w} B^{C_i}(W, D)\big|_{W = 0}. \tag{36}$$

With the assistance of the uniform interleaver, any code word of C_o with output Hamming weight l will result in a code word of C_i, of input Hamming weight l with probability $1/\binom{N}{l}$.

Considering a total of $A_{w,l}^{C_o}$ such codewords, with input Hamming weight w and output Hamming weight l in C_o, will result in an average of $B_{l,d}^{C_i}$ codewords with squared Euclidean distance d in C_i. Hence, the multiplicity of codewords of the SCTCM C_s with input Hamming weight w and squared Euclidean distance d becomes

$$B_{w,d}^{C_s} = \sum_{l=0}^{N} \frac{A_{w,l}^{C_o} \times A_{l,d}^{C_i}}{\binom{N}{l}}. \tag{37}$$

The upper bound to the BER of the SCTCM is

$$P_b \leq \sum_{w=1}^{NR_o} \sum_{d \in \{d_i\}} B_{w,d}^{C_s} \frac{w}{NR_o} Q(\sqrt{d/N_o}). \tag{38}$$

By concatenating the error events of the convolutional codes C_o, we can write

$$A_{w,l}^{C_o} = \sum_{j} E_j^{C_o}, \tag{39}$$

where $E_j^{C_o}$ represents all the errors that rejoin the zero-code path j times

$$A_{w,l}^{C_o} = \sum_{z,j} M[N/k, z, j] A_{w,l,z,j}^{C_o}, \tag{40}$$

where $M[N/k, z, j]$ represents the total number of error possibilities that have z depth and result from concatenating j single event errors for a block length N/k. Whereas, $A_{w,l,z,j}^{C_o}$ represents the total number of error events that have an input Hamming weight w, an output Hamming weight one, a depth of z and consists of j single error events. For large N/k, $M[N/k, z, j]$ can be approximated by

$$M[N/k, z, j] = \binom{N/k + j - z}{j}. \tag{41}$$

When the block length N/k is large, only the small values of j determine the performance of the convolutional codes, which makes the following approximation valid

$$M[N/k, z, j] \approx \binom{N/k}{j}. \tag{42}$$

By the same discussion for the inner codes, (37) could be rewritten as

$$B_{w,d}^{C_s} = \sum_{l=d_H^o}^{N} \sum_{j^o} \sum_{j^i} \frac{\binom{N/p}{j^o}\binom{N/p}{j^i}}{\binom{N}{l}} A_{w,l,j^o}^{C_o} B_{l,d,j^i}^{C_i}, \tag{43}$$

where d_H^o is the free Hamming distance of the outer code. If the asymptotic approximation of the binomial function is used, the equation (43) becomes

$$B_{w,d}^{C_s} \approx \sum_{l=d_H^o}^{N} \sum_{j^o} \sum_{j^i} N^{j^o + j^i - l - 1} \frac{l!}{p^{j^o + j^i} j^o! j^i!} A_{w,l,j^o}^{C_o} B_{l,d,j^i}^{C_i}, \tag{44}$$

from which $\Pr[\text{bit error}]$ can be written as

$$\Pr[\text{bit error}] = \sum_{w=1}^{NR^v} \sum_{d} \sum_{l=d_H^o}^{N} \left(\sum_{j^o} \sum_{j^i} N^{j^o + j^i - l - 1} \frac{l!}{p^{j^o + j^i} j^o! j^i!} A_{w,l,j^o}^{C_o} B_{l,d,j^i}^{C_i} \right) Q\left(\sqrt{\frac{d}{N_o}} \right). \tag{45}$$

In the above equation, the maximum exponent of N decides the interleaver gain of the SCTCM.

$$\alpha(d) = \max_{j^o + j^i} \{ j^o + j^i - l - 1 \}. \tag{46}$$

So the objective should minimize this parameter $\alpha(d)$.

By allowing the inner code to have codewords with input Hamming weight one, the maximum of j^i becomes l which makes $\alpha(d)$

$$\alpha(d) = \max_{j^o} \{ j^o - 1 \}, \tag{47}$$

which is always positive (no interleaver gain). In this case, the performance of SCTCM does not benefit from the interleaver gain. This result is also applicable for nonrecursive inner codes. By designing the inner codes to have infinite Euclidean distance for input sequences with input Hamming weight one, the maximum of j^i becomes $\left\lfloor \frac{l}{2} \right\rfloor$, which results in

$$\alpha(d) = \max_{j^o} \left\{ j^o - \left\lfloor \frac{l+1}{2} \right\rfloor - 1 \right\}. \tag{48}$$

Moreover, since the free Hamming distance of the outer code is d_H^o, then

$$j^o \leq \left\lfloor \frac{l}{d_H^o} \right\rfloor. \tag{49}$$

If S-interleavers are used, then the single error events, that have small output Hamming weights, of the outer code will have depths less the parameter S of the interleaver. This idea will increase the minimum j^i to d_H^o. Now, for $j^o = 2$ the minimum of l becomes $(2d_H^o)$, so

$$\alpha(d) = \max_{d_H^o} \left\{ 1 - \left\lfloor \frac{2d_H^o + 1}{2} \right\rfloor \right\} = 1 - d_H^o. \tag{50}$$

The minimum squared Euclidean distance of the SCTCM will increase to

$$d_H^o \cdot d_{min}^i, \tag{51}$$

where d_{min}^{i} is the minimum squared Euclidean distance of the inner code.

The previous analysis of the bit-error bound of SCTCM encoders gives rise to the following design criteria for SCTCM systems:

- The outer code can be a recursive or nonrecursive convolutional code. However, it should have a maximum free Hamming distance.
- The interleaver should be a bit-wise S-interleaver to utilize full interleaving gain and maximize the effective Euclidean distance of the SCTCM.
- The inner TCM code should use recursive convolutional codes rather than nonrecursive ones, which do not offer any interleaving gain.
- The inner TCM code should have an infinite squared Euclidean distance for any input sequence of Hamming weight one. This criterion is specially important when the TCM code has parallel transitions. If there are no parallel transitions in the inner TCM, it is enough to restrict the inner code to be recursive.
- In searching for the inner TCM code, the minimum squared Euclidean distance should be maximized for any input sequence that has Hamming weight greater than one.

5.3 Mapping and Code Search Results

In this section, we will give a brief explanation for the set partitioning process used in natural mapping. Furthermore, mapping and code search results are listed in tables.

5.3.1 Set Partitioning For Natural Mapping

In our system we used the 2L2PPM modulation scheme. The signal constellation of this case can be visualized in many ways. First, we can visualize the modulation in four-dimensional space, where the first two axes are reserved for the two pulse positions and the other two axes are assigned for two amplitudes of the two pulses. However, set partitioning on four-dimensional space is a very difficult operation. Hence, we used an enhanced visualization technique, in which each four signals that share the same positions are grouped together. On the group level, the four signals are represented by a two-dimensional plane, see Figure 16. The first axis represents the amplitude of the first pulse and the second axis is reserved for the amplitude of the second pulse. Next, every group of four signals sharing the same two positions are presented as one point on a two-dimensional plane called the plane of positions, see Figure 17. In the plane of positions, the horizontal depicts the position of the first pulse and the vertical axis represents the position of the second pulse.

The set partitioning of the whole signal constellation is done in three steps. In the first step, each group of four signals that share the same positions is partitioned using the usual set partitioning technique (similar to QAM signals). In the second step, which is totally

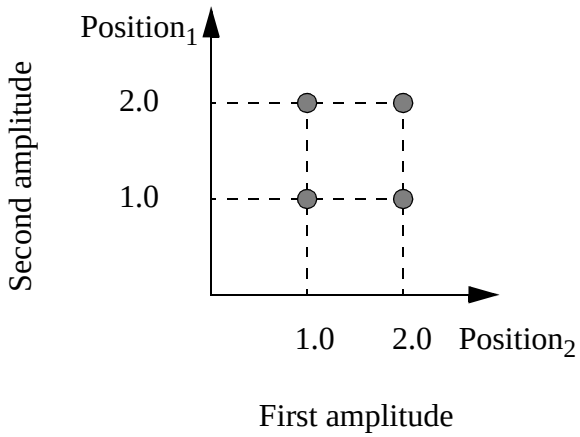

Figure 16. Amplitude representation of four signals that share the same two positions.

independent from the first, a special set partitioning is done on the plane of positions of the groups. This special set partitioning of the arbitrary groups is similar to the set partitioning mentioned in [78]. In the third step, we use the result of the first partitioning step to form four different subsets A00, A01, A10 and A11, such that if we use the second partitioning on each subset, we form a resultant partitioning that maximizes the Euclidean distance for the last two levels. After doing the set partitioning, we decide the output labels of the inner code accordingly. According to natural mapping technique, Tables 1 and 2 show the signal labels of the two modulation schemes of 128-2L2PPM and 256-2L2PPM. In each row of the table we can see two positions and the output labels of the four signals that share two positions.

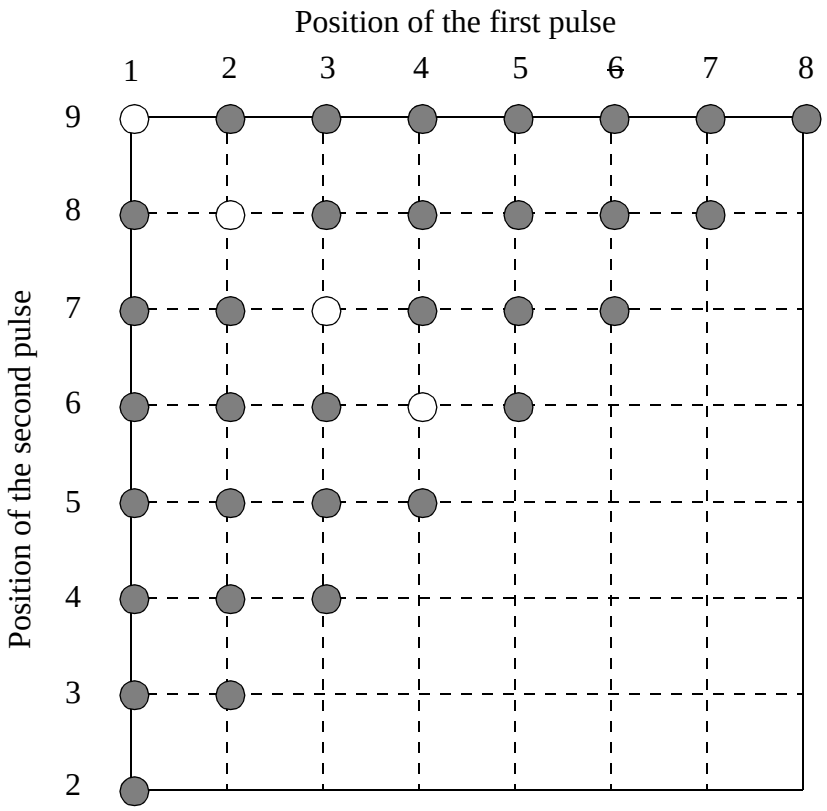

Figure 17. Position representation of (9,2)-MPPM. The shaded circles represent the selected pairs of positions.

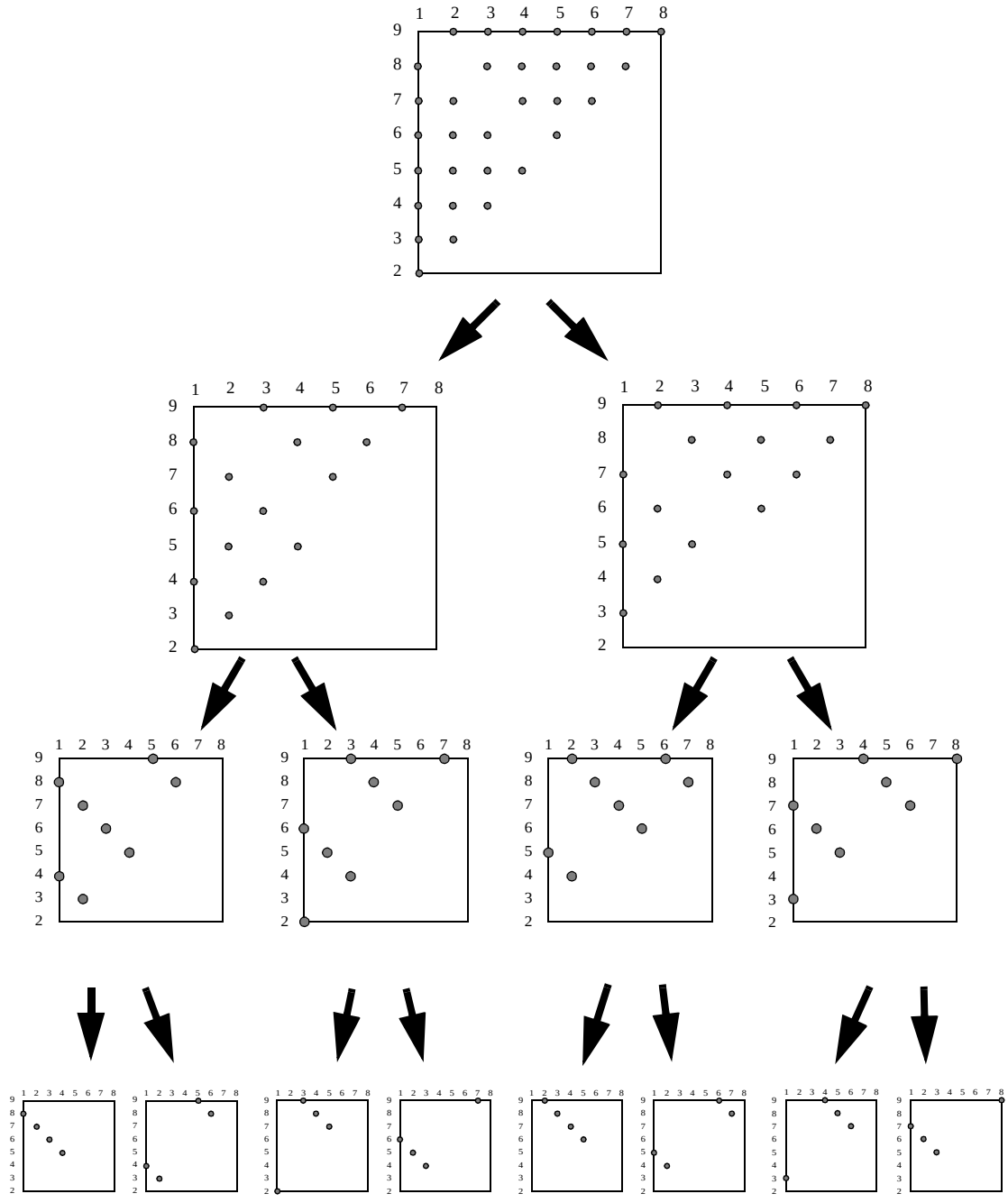

Figure 18. Set partitioning of 32-MPPM.

Table 1. 128-SCTCM natural mapping signal labels.

Positions		Amplitudes					Positions		Amplitudes			
1st Pos.	2nd Pos.	1,1	1,2	2, 2	2, 1		1st Pos.	2nd Pos.	1, 1	1, 2	2, 1	2, 2
1	5	0	1	2	3		2	4	64	65	66	67
1	4	4	5	6	7		2	3	68	69	70	71
1	7	8	9	10	11		2	6	72	73	74	75
1	6	12	13	14	15		2	5	76	77	78	79
2	9	16	17	18	19		3	8	80	81	82	83
1	8	20	21	22	23		2	7	84	85	86	87
1	3	24	25	26	27		4	9	88	89	90	91
1	2	28	29	30	31		3	9	92	93	94	95
6	9	32	33	34	35		7	8	96	97	98	99
5	9	36	37	38	39		6	8	100	101	102	103
3	5	40	41	42	43		8	9	104	105	106	107
3	4	44	45	46	47		7	9	108	109	110	111
4	7	48	49	50	51		5	6	112	113	114	115
3	6	52	53	54	55		4	5	116	117	118	119
5	8	56	57	58	59		6	7	120	121	122	123
4	8	60	61	62	63		5	7	124	125	126	127

At high optical SNR most erroneous symbols are within the minimum Euclidean distance from the correct ones. The objective of Gray mapping is to minimize the information bit error rate for the case of small Euclidean distance between the correct and erroneous symbols. In TCM applications Gray mapped TCM is better than Naturally mapped TCM in terms of BER. For 2L2PPM modulation, every four signals share the same two positions and they have different amplitude level combinations. Hence, we assigned two bits to the amplitude variations and we mapped them as we map QAM

Table 2. 256-SCTCM natural mapping signal labels

Positions		Amplitudes					Positions		Amplitudes			
Pos 1	Pos 2	1,1	1,2	2, 1	2, 2		Pos 1	Pos 2	1, 1	1, 2	2, 1	2, 2
11	12	0	1	2	3		1	6	128	129	130	131
10	12	4	5	6	7		6	8	132	133	134	135
9	12	8	9	10	11		10	11	136	137	138	139
1	7	12	13	14	15		2	6	140	141	142	143
7	12	16	17	18	19		8	11	144	145	146	147
2	12	20	21	22	23		3	11	148	149	150	151
5	12	24	25	26	27		6	11	152	153	154	155
1	3	28	29	30	31		2	10	156	157	158	159
4	11	32	33	34	35		5	10	160	161	162	163
6	12	36	37	38	39		7	11	164	165	166	167
1	12	40	41	42	43		2	11	168	169	170	171
3	10	44	45	46	47		5	11	172	173	174	175
2	9	48	49	50	51		3	8	176	177	178	179
1	9	52	53	54	55		2	8	180	181	182	183
1	8	56	57	58	59		2	7	184	185	186	187
1	11	60	61	62	63		3	9	188	189	190	191
2	5	64	65	66	67		3	4	192	193	194	195
1	5	68	69	70	71		2	4	196	197	198	199
1	4	72	73	74	75		2	3	200	201	202	203
3	5	76	77	78	79		4	8	204	205	206	207
9	10	80	81	82	83		1	2	208	209	210	211
4	10	84	85	86	87		5	9	212	213	214	215
7	10	88	89	90	91		8	9	216	217	218	219
4	12	92	93	94	95		9	11	220	221	222	223
6	9	96	97	98	99		7	8	224	225	226	227
8	10	100	101	102	103		4	9	228	229	230	231
5	8	104	105	106	107		6	7	232	233	234	235
7	9	108	109	110	111		8	12	236	237	238	239
4	7	112	113	114	115		5	6	240	241	242	243
3	7	116	117	118	119		4	6	244	245	246	247
3	6	120	121	122	123		4	5	248	249	250	251
5	7	124	125	126	127		6	8	252	253	254	255

constellations. The remaining bits are used to map the position domain. In Gray mapping the position domain, we exploited the Manhattan distance instead of the Euclidean distance. Gray mapping signal labels for 128-SCTCM are shown in Table 3 and Gray mapping signal labels for 256-SCTCM are shown in Table 4.

Table 3. 128-SCTCM Gray mapping signal labels.

Positions		Amplitudes				Positions		Amplitudes			
Pos. 1	Pos. 2	1,1	1,2	2, 1	2, 2	Pos. 1	Pos. 2	1, 1	1, 2	2, 1	2, 2
2	9	104	105	106	107	4	5	20	21	22	23
3	4	40	41	42	43	3	5	52	53	54	55
1	4	8	9	10	11	1	5	80	81	82	83
2	4	24	25	26	27	2	5	84	85	86	87
3	9	56	57	58	59	8	9	92	93	94	95
3	8	120	121	122	123	3	6	16	17	18	19
1	3	88	89	90	91	1	6	64	65	66	67
2	3	48	49	50	51	2	6	68	69	70	71
5	9	44	45	46	47	6	9	76	77	78	79
5	8	12	13	14	15	6	8	72	73	74	75
5	6	28	29	30	31	1	8	96	97	98	99
5	7	60	61	62	63	6	7	100	101	102	103
4	9	124	125	126	127	7	9	108	109	110	111
4	8	112	113	114	115	7	8	32	33	34	35
1	2	116	117	118	119	1	7	36	37	38	39
4	7	4	5	6	7	2	7	0	1	2	3

5.3.2 Search for Good Inner Code

The number of polynomials in the inner code are between seven and eight, which makes the exhaustive search time consuming. Hence, a random search is done to find

Table 4. 256-SCTCM Gray mapping signal labels

Positions		Amplitudes					Positions		Amplitudes			
Pos 1	Pos 2	1,1	1,2	2, 1	2, 2		Pos 1	Pos 2	1, 1	1, 2	2, 1	2, 2
1	12	0	1	2	3		1	5	128	129	130	131
2	12	4	5	6	7		2	5	132	133	134	135
4	12	8	9	10	11		4	5	136	137	138	139
3	12	12	13	14	15		3	5	140	141	142	143
8	12	16	17	18	19		10	12	144	145	146	147
7	12	20	21	22	23		2	4	148	149	150	151
5	12	24	25	26	27		11	12	152	153	154	155
6	12	28	29	30	31		3	4	156	157	158	159
1	11	32	33	34	35		1	6	160	161	162	163
2	11	36	37	38	39		2	6	164	165	166	167
4	11	40	41	42	43		4	6	168	169	170	171
3	11	44	45	46	47		3	6	172	173	174	175
8	11	48	49	50	51		9	11	176	177	178	179
7	11	52	53	54	55		1	3	180	181	182	183
5	11	56	57	58	59		5	6	184	185	186	187
6	11	60	61	62	63		1	2	188	189	190	191
1	9	64	65	66	67		1	8	192	193	194	195
2	9	68	69	70	71		2	8	196	197	198	199
4	9	72	73	74	75		4	8	200	201	202	203
3	9	76	77	78	79		3	8	204	205	206	207
8	9	80	81	82	83		10	11	208	209	210	211
7	9	84	85	86	87		7	8	212	213	214	215
5	9	88	89	90	91		5	8	216	217	218	219
6	9	92	93	94	95		6	8	220	221	222	223
1	10	96	97	98	99		1	7	224	225	226	227
2	10	100	101	102	103		2	7	228	229	230	231
4	10	104	105	106	107		4	7	232	233	234	235
3	10	108	109	110	111		3	7	236	237	238	239
8	10	112	113	114	115		9	10	240	241	242	243
7	10	116	117	118	119		2	3	244	245	246	247
5	10	120	121	122	123		5	7	248	249	250	251
6	10	124	125	126	127		6	7	252	253	254	255

good inner codes with maximum minimum Euclidean distance. Moreover, in the random search, we kept all forward polynomials non-zeros, to assure infinite Euclidean distances for input sequences of weight one.

The inner codes are not regular; thus it is not enough to check the all-zero path for the minimum squared Euclidean distance. For this reason, we used two phases in the search for good codes. First, the minimum squared Euclidean distance of the all-zero path is found. For all codes that pass the first test, we use a more complex algorithm, which was reported in [73], to check the minimum squared Euclidean distance of every possible path. For natural mapping, the code search results are listed in Tables 5 and 6. The code search

Table 5. 128-SCTCM natural mapping inner code polynomials.

Constraint Length (v)	h_0	h_1	h_2	h_3	h_4	h_5	h_6	Min. Euclidean Distance
3	7	2	3	3	3	4	1	2.0
4	13	04	01	15	13	13	04	2.0
5	37	10	36	35	23	24	35	4.0
6	45	36	27	32	74	55	61	4.0

results for Gray mapping are listed in Tables 7 and 8. For example, the actual encoder of 128-SCTCM natural-mapping inner code of constraint length $v = 3$ is shown in Figure 19.

Table 6. 256-SCTCM natural mapping inner code polynomials.

Constraint Length (v)	h_0	h_1	h_2	h_3	h_4	h_5	h_6	h_7	Min. Euclidean Distance
3	7	2	3	3	3	3	4	1	2.0
4	17	04	03	11	12	11	02	16	2.0
5	37	04	21	13	26	22	21	01	2.0
6	55	20	12	11	02	52	10	37	4.0

Table 7. 128-SCTCM Gray mapping inner code polynomials.

Constraint Length (v)	h_0	h_1	h_2	h_3	h_4	h_5	h_6	Min. Euclidean Distance
3	7	2	3	3	3	4	1	2.0
4	13	04	01	15	13	13	04	2.0
5	37	10	36	35	23	24	35	3.0
6	45	36	27	32	74	55	61	4.0

Table 8. 256-SCTCM Gray mapping inner code polynomials.

Constraint Length (v)	h_0	h_1	h_2	h_3	h_4	h_5	h_6	h_7	Min. Euclidean Distance
3	7	2	3	3	3	3	4	1	2.0
4	17	04	03	11	12	11	02	16	2.0
5	37	04	21	13	26	22	21	01	2.0
6	55	20	12	11	02	52	10	73	3.0

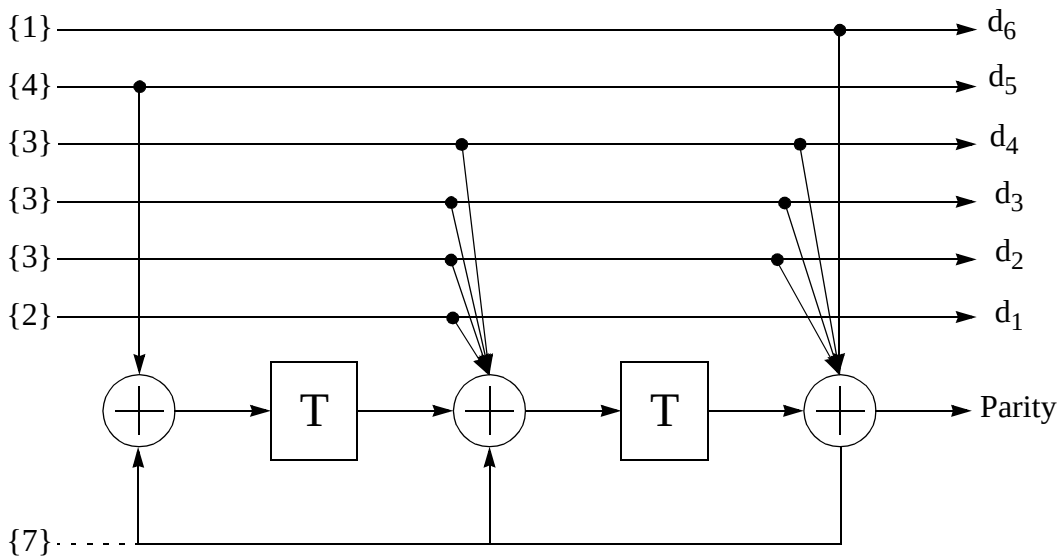

Figure 19. 128-SCTCM natural mapping inner code of constraint length $\nu = 3$.

5.3.3 Search for Good Outer Codes

One of the design criteria of SCTCM is to choose outer codes with maximum free Hamming distance. The non-systematic outer codes are produced by puncturing rate 1/2 binary convolutional codes, and hence, their free Hamming distances are not guaranteed to be the maximum possible for the specified rate [76]. For the recursive outer codes, we performed a random search to find good codes with maximum free Hamming distance. The results of the random search are shown on the following two tables: Table 9 and Table 10.

Table 9. Polynomials of rate 5/6 recursive systematic codes.

Constraint Length (ν)	h_0	h_1	h_2	h_3	h_4	h_5	Free Hamming Distance
3	5	5	5	6	7	7	2
4	15	05	07	17	11	13	3
5	25	33	36	23	35	31	4
6	51	43	75	66	57	71	4
7	107	101	125	177	163	151	4

Table 10. Polynomials of rate 6/7 recursive systematic codes.

Constraint Length (ν)	h_0	h_1	h_2	h_3	h_4	h_5	h_6	Free Hamming Distance
3	7	3	5	5	7	3	3	2
4	15	13	16	14	17	12	11	3
5	35	33	17	27	25	23	31	4
6	51	45	55	47	37	61	63	4
7	131	061	105	167	137	127	173	4

5.4 Error Bounds and Simulation Results

In this research, two systems are proposed: 128-SCTCM-2L2PPM and 256-SCTCM-2L2PPM. Both modulation schemes are two-pulse and two-level. The first modulation scheme has 9 positions and the second has 12 positions. The spectral efficiencies are 0.56 and 0.5 bits/s/Hz, respectively. Unless it is stated otherwise, the x-axis, in the following

figures represents the normalized power requirement with respect to the power requirement of the un-coded on-off keying (OOK) to achieve a BER of 10^{-6}, the y-axis represents the BER, and Gray mapping is used. The nonrecursive outer codes are taken from [76] and the recursive ones are found in Tables 9 and 10.

Figure 20 shows the difference between Gray mapping and natural mapping for 128-SCTCM-2L2PPM with 8 states outer code, 4 states inner code and an interleaver of length 2400. In this figure, it is clear that Gray mapping is better than natural mapping by 0.1 dB. The constraint length of the inner or outer codes increases this difference. Gray mapping is designed to minimize the BER in the inner decoder, which explains the improved BER we have seen.

In Figure 21, the BER is shown versus the normalized power requirement for both an upper bound on the performance of Gray-mapped 128-SCTCM-2L2PPM and the 20th iteration of simulation of the same system. In evaluating the error bounds we used the equations derived before, see Section “SCTCM Design” on page 62. We only consider the terms that had Euclidean distance in this range

$$d_{\text{SCTCM, eff}} \leq d \leq 3d_{\text{SCTCM, eff}}. \tag{52}$$

It is found that the terms with greater Euclidean distances do not effect the bound at high optical SNR.

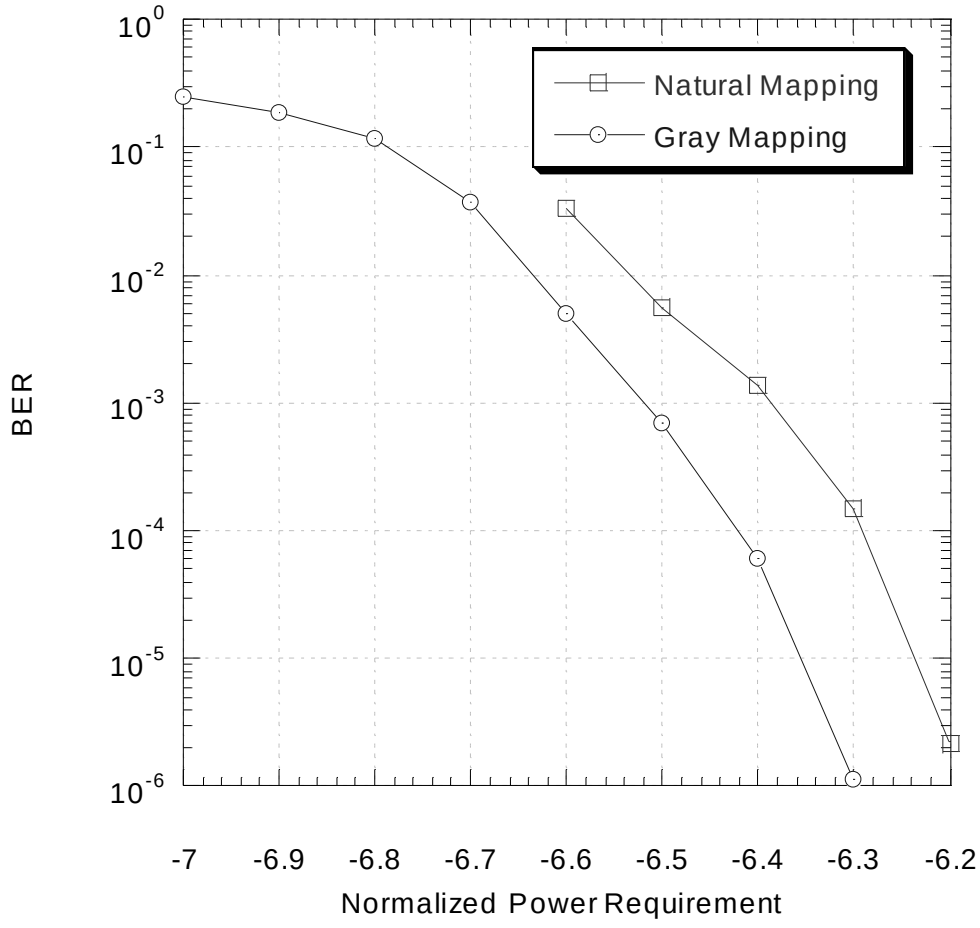

Figure 20. Gray mapping versus natural mapping for SCTCM.

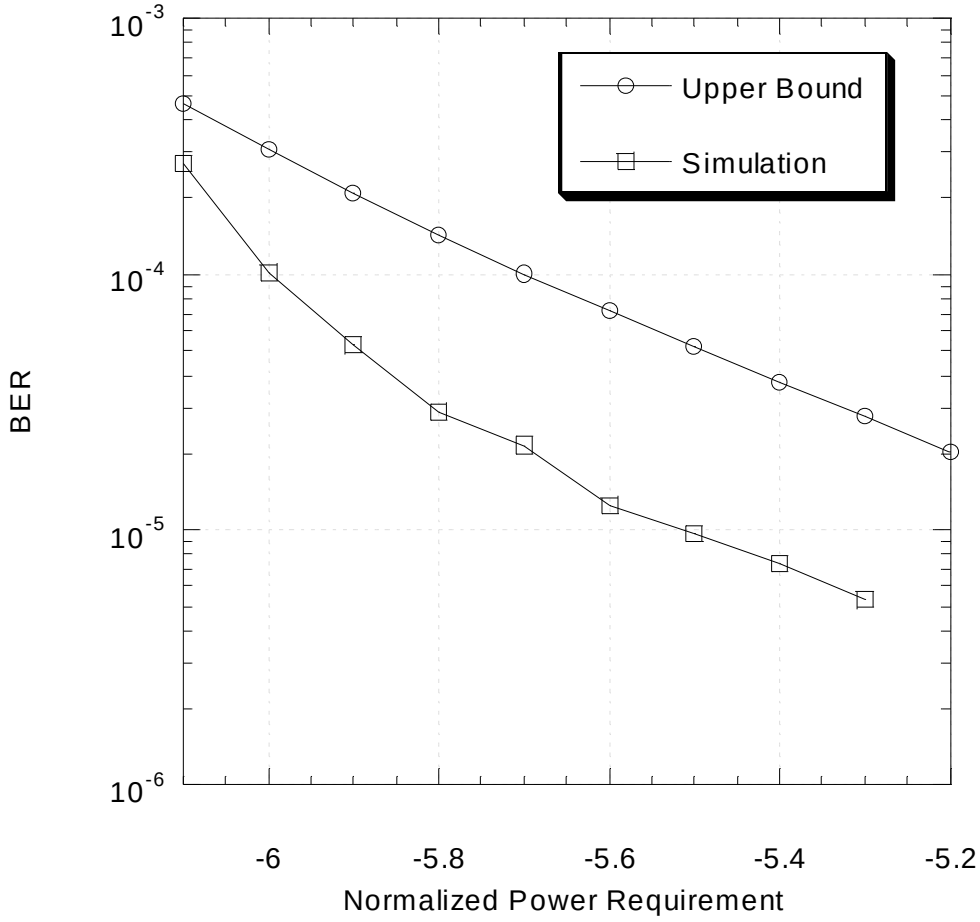

Figure 21. Verification of the simulation (Both the outer and inner codes have 4 states, and the block length is 400).

Figure 22 shows the simulation of 128-SCTCM-2L2PPM for two types of outer codes: nonrecursive and systematic recursive. In both cases we have 4 states inner code s-interleaver of length 2400, and Gray mapping. Both the outer codes are of maximum free Hamming distance. The figure shows that the nonrecursive outer codes are slightly better than the recursive systematic ones in the high range SNR, while the recursive systematic outer codes are better in the low range SNR.

Figure 23 shows the first nine iterations from the simulation of 128-SCTCM-2L2PPM for the case of 8 states outer code, 4 states inner code, 2000 block length (2400 interleaver length), and Gray mapping. As we can see from the figure, most of the gain comes in the first six iterations, then the gain decreases as the number of iterations goes up.

In Figure 24, the error bonds of the 128-SCTCM-2L2PPM are used to show the effect of increasing the information block length on power efficiency. In this figure, both the outer code and the inner code have four states and Gray mapping is used. This increase in the interleaver length will increase the latency of the system.

Figure 25 and Figure 26 show the effect of increasing the outer code constraint length and the inner code constraint length, respectively. This figure illustrates that the power efficiency of SCTCM could be increased by increasing the memory of the outer code, increasing the memory of the inner code, or increasing both.

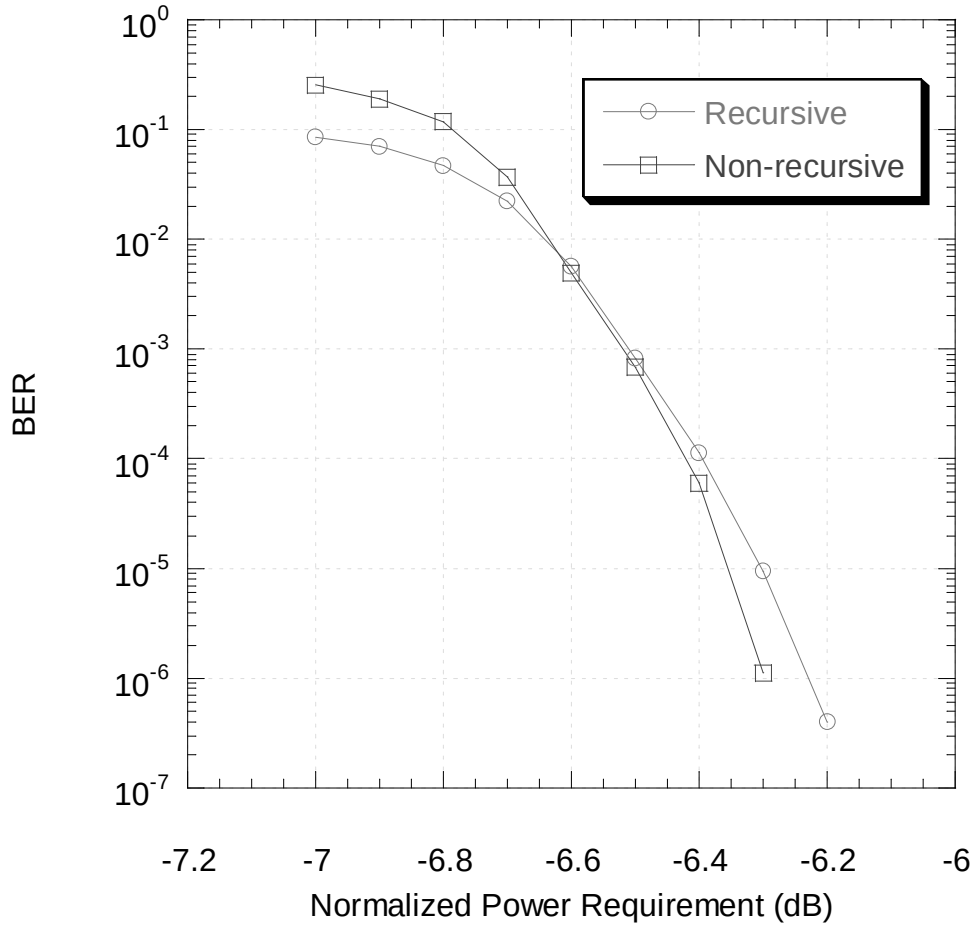

Figure 22. Nonrecursive and systematic recursive outer codes.

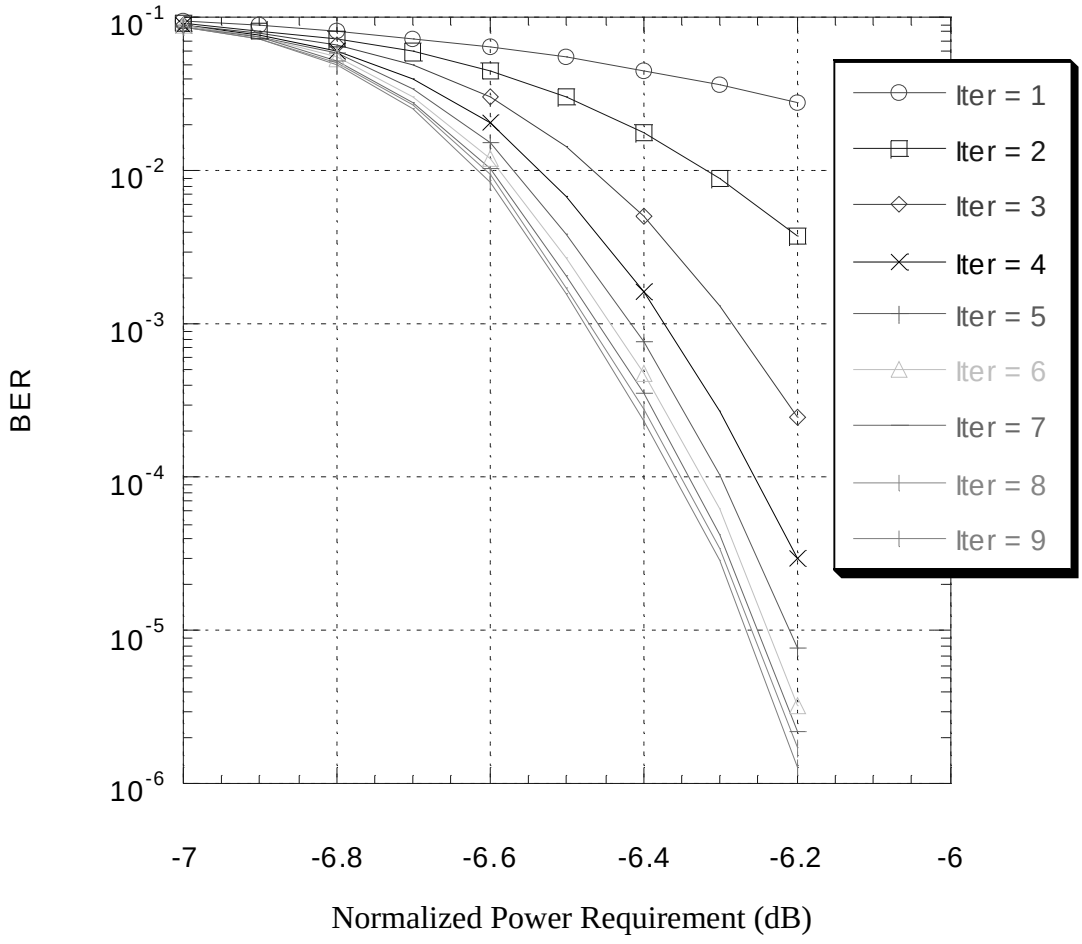

Figure 23. The first 9 iterations from simulation 128-SCTCM-2L2PPM, for 8 states outer code, 4 states inner code, 2000 block length, and Gray mapping.

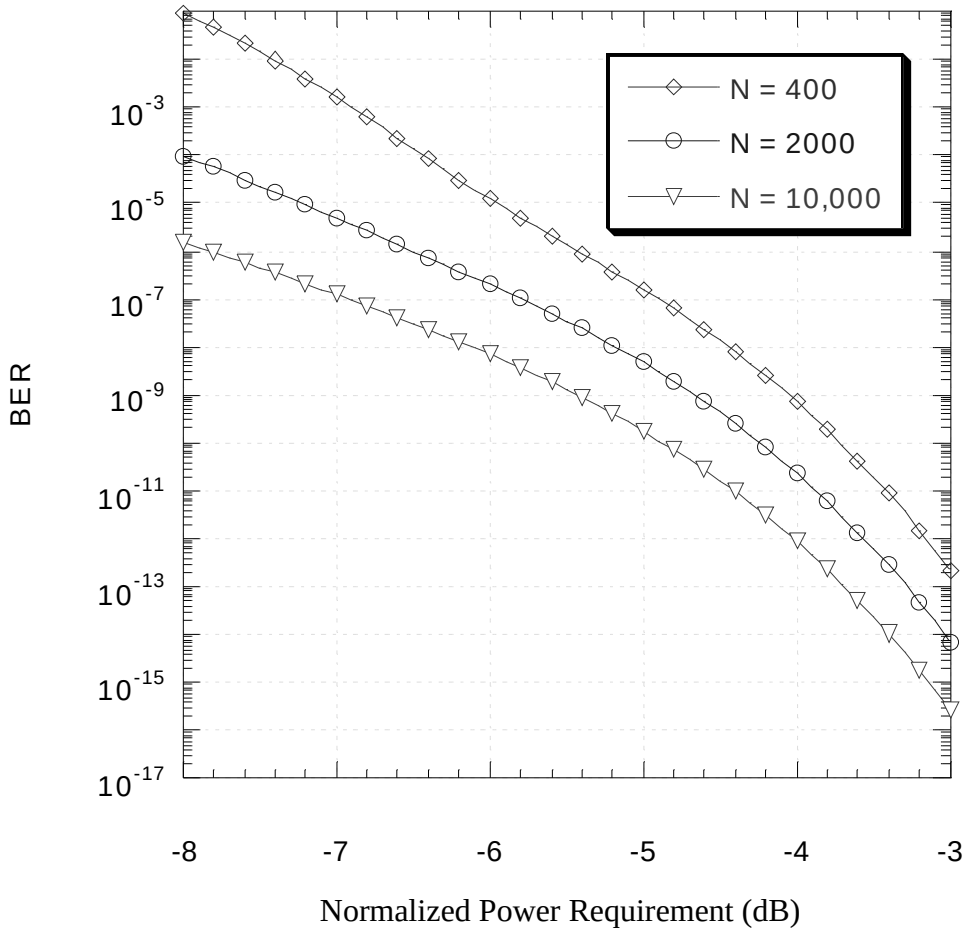

Figure 24. Upper bounds for different interleaver lengths.

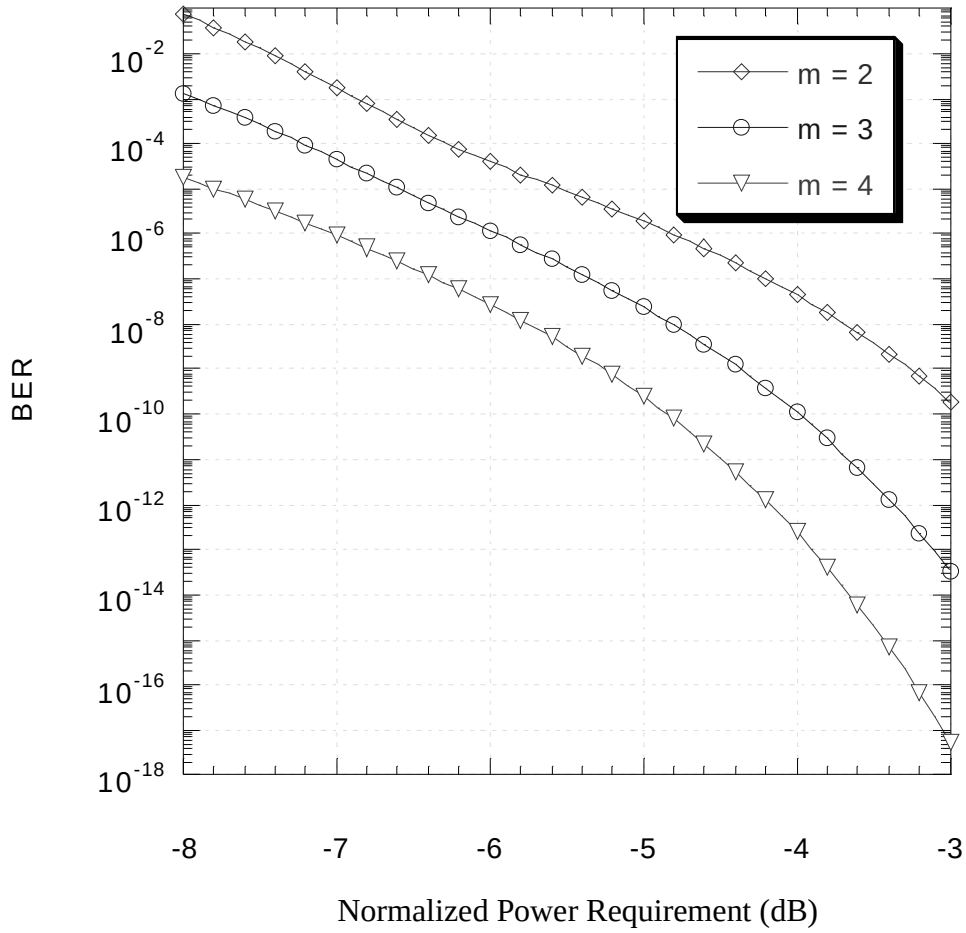

Figure 25. The effect of the outer code memory performance of SCTCM (m is the number of memory elements in the outer code).

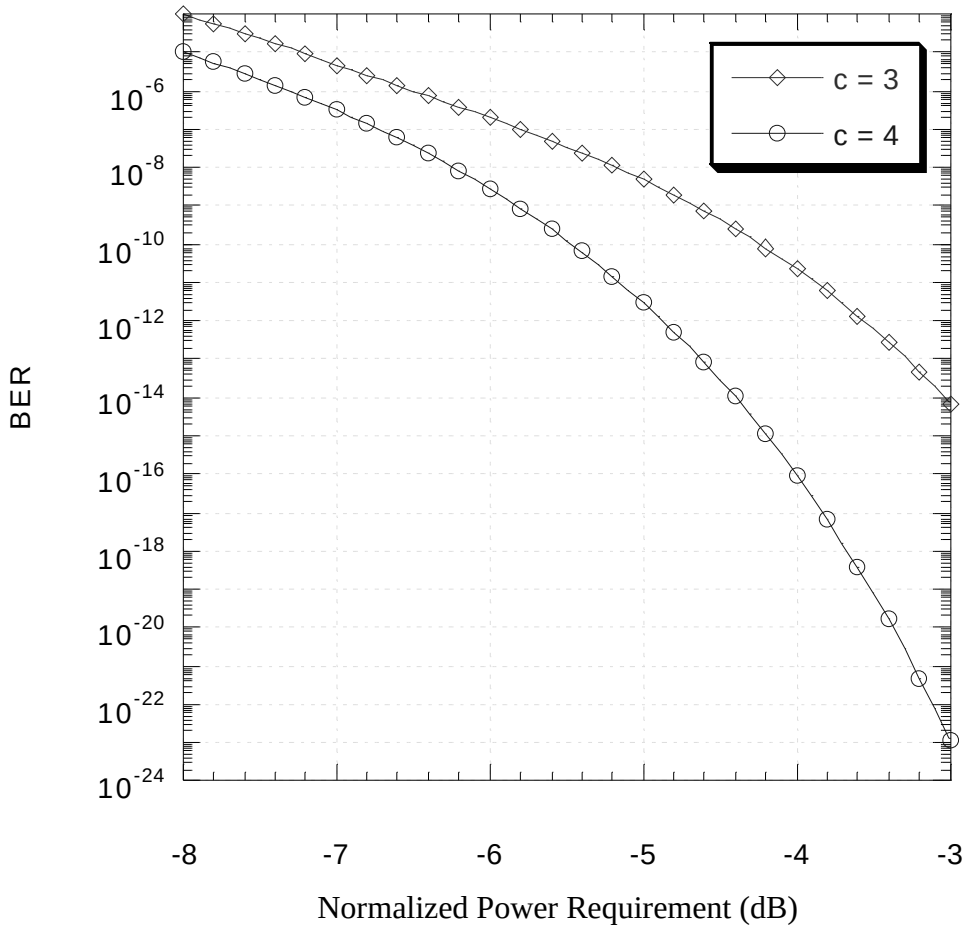

Figure 26. The effect of the inner code memory on the performance of SCTCM (m_i is the constraint length of the inner code).

Figure 27 shows simulation results for different outer code constraint lengths. For low BERs, the performance is better with low memory outer codes. For high BERs, the performance of the large memory outer codes becomes superior. This figure suggests two modes of operation depending on the received power. Figure 28 shows the simulation results of different inner code constraint lengths. Similarly, this figure suggests two modes of operation. The performance error bounds of 128-SCTCM and 256-SCTCM for 8 states outer code and 4 states inner code are shown on Figure 29.

Table 11 presents the normalized power requirement, the spectral efficiency, and the complexity of our proposed systems with input block length of 10,000 information bits, compared to 8-TCM-PPM, 16-TCM-PPM, and 128-TCM-MPPM systems [15][17]. We can see from the table that 128-SCTCM-2L2PPM and 256-SCTCM-2L2PPM have achieved both power and spectral efficiencies with low decoding complexity. In the table, we considered the complexity of both the outer and inner codes. For higher block lengths (higher than 10000), the power efficiency will even exceed what is shown in the table. In the following, Figure 30 shows the normalized power requirement versus the spectral density of the proposed 128-SCTCM-2L2PPM and 256-SCTCM-2L2PPM with other previously coded modulation schemes, uncoded PPM and uncoded MPPM modulation schemes.

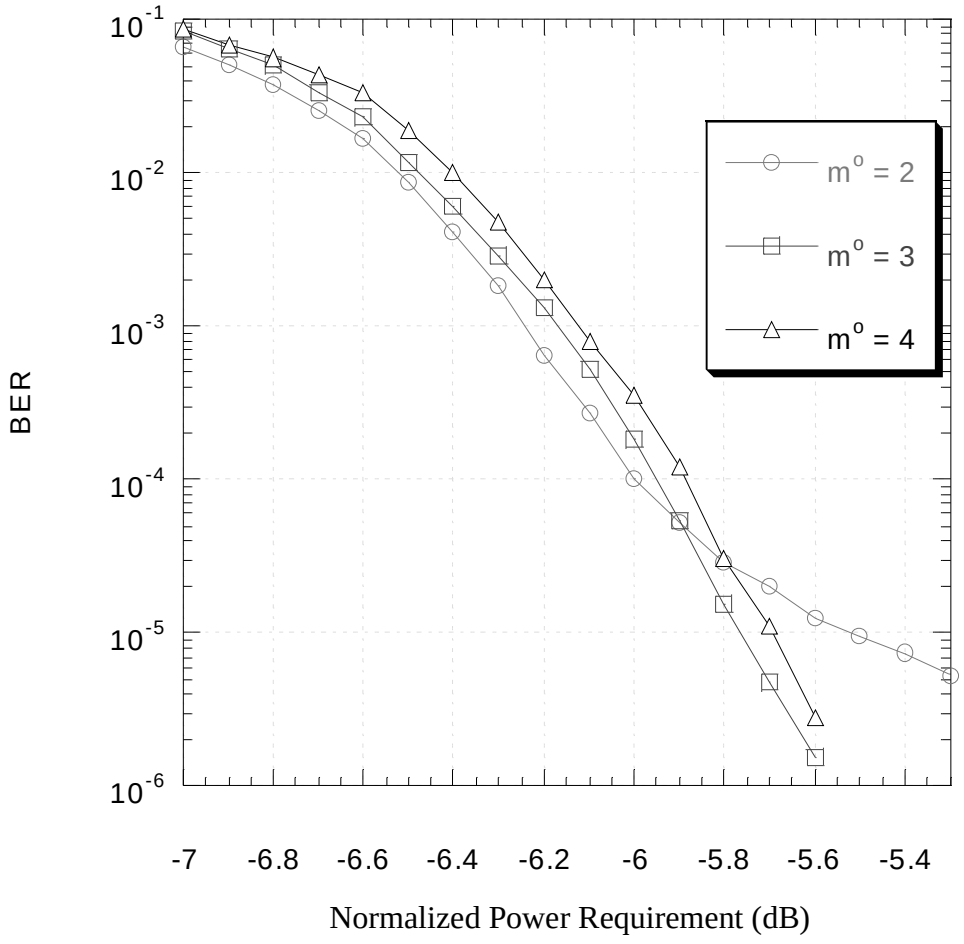

Figure 27. Simulation results for different outer code constraint lengths.

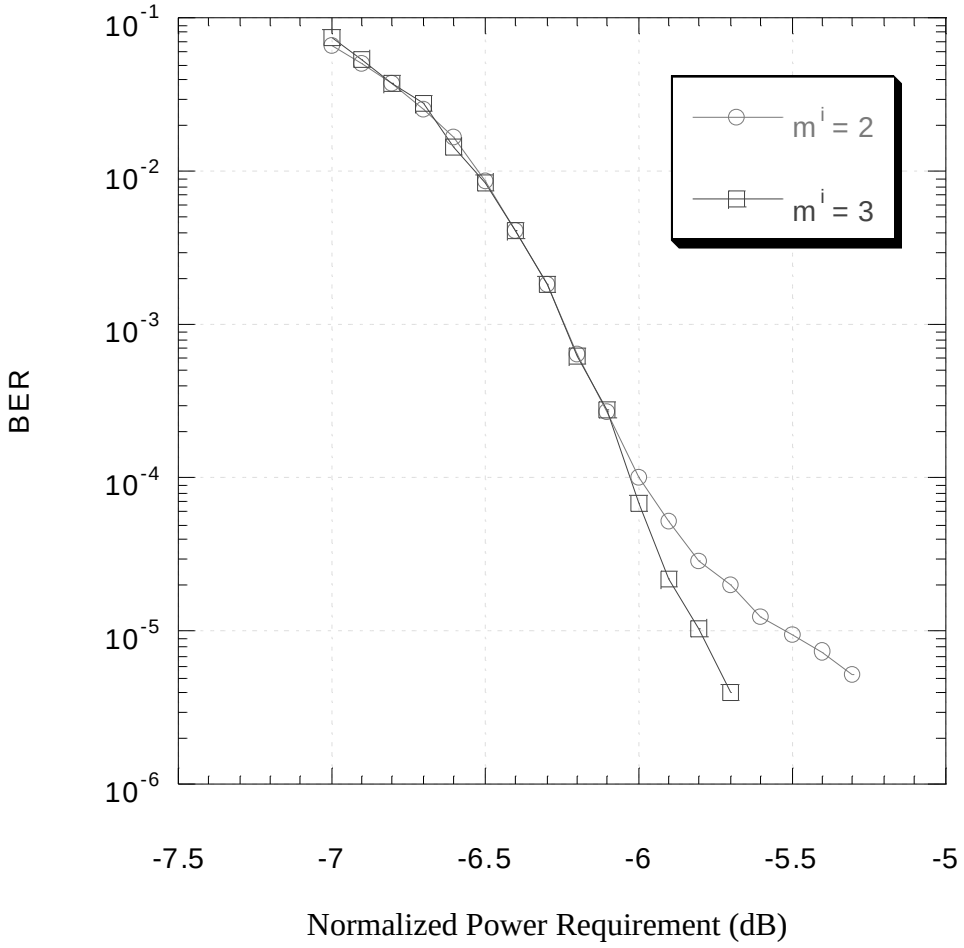

Figure 28. Simulation results of different inner code constraint lengths.

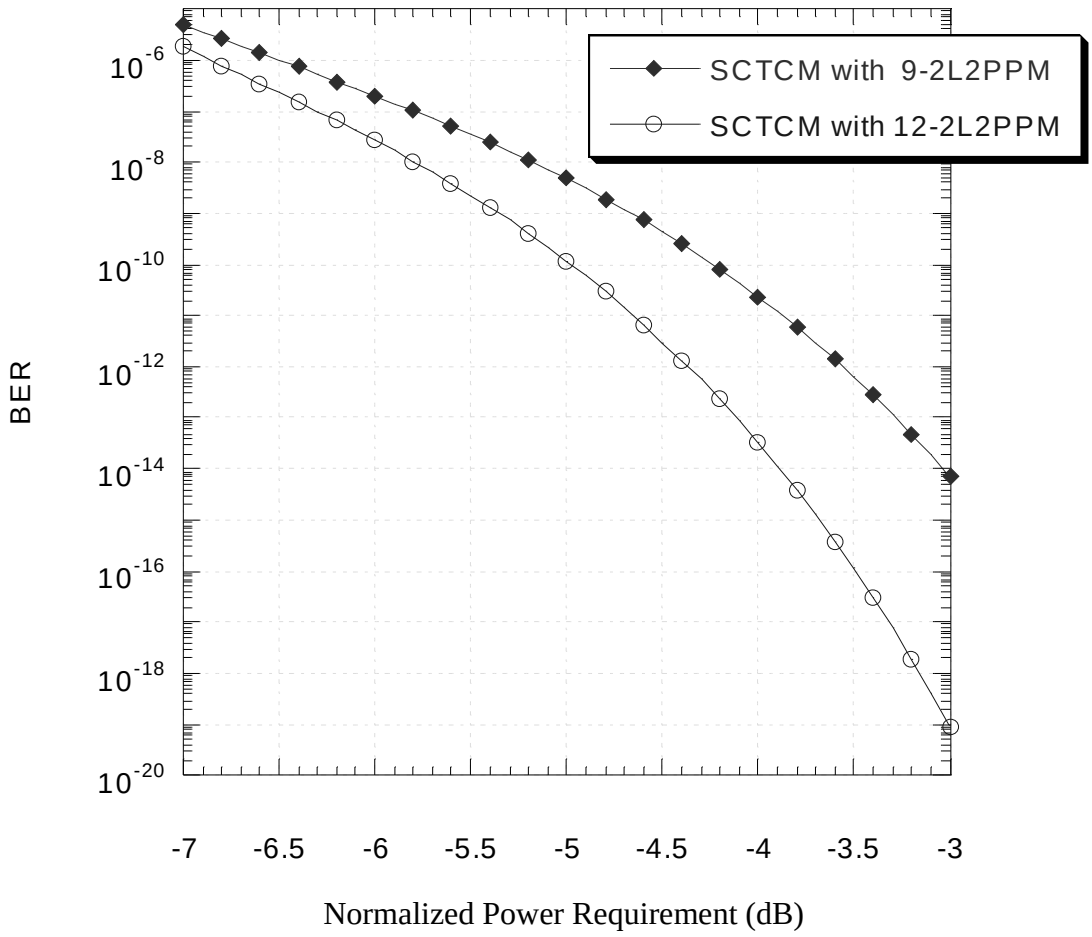

Figure 29. The two system 128-SCTCM and 256-SCTCM. Both have 8 states outer codes and 4 states inner codes, and the block length of the code is 2000 bits.

Table 11. Normalized power requirement, spectral efficiency, and complexity of 128-SCTCM and 256-SCTCM.

	Normalized power requirement	Spectral efficiency	Complexity (edges per bit)	Cut-off rate	Gain from cut-off rate
8-TCM-PPM [15]	7.0-8.2 dB	0.25 bits/s/Hz	16-1024	8.35 dB	1.35-0.15 dB
16-TCM-PPM [15]	8.2-9.4 dB	0.19 bits/s/Hz	21-682	11.25 dB	3.05-1.85 dB
128-TCM-MPPM [17]	7.0-8.5 dB	0.35 bits/s/Hz	85-21,845	9.15 dB	2.15-0.65 dB
128-SCTCM-2L2PPM	6.3 dB	0.56 bits/s/Hz	512	6.75 dB	2.0-0 dB
256-SCTCM-2L2PPM	6.8 dB	0.5 bits/s/Hz	853	7.05 dB	2.0-0 dB

5.5 Summary

In this chapter, we developed a SCTCM combined with 2L2PPM modulation. The system was decoded with an iterative decoder. The performance error bounds for SCTCM were rederived for the case of TCM inner codes. Assuming large S-random interleavers, the effective minimum Euclidean distance of the SCTCM is found to be the product of the free Hamming distance of the outer code and the minimum Euclidean distance of the inner code. This result is at least double the effective minimum Euclidean distance of SCTCM encoder with just random interleavers. Random searches were conducted to find good inner codes that satisfy the derived design criteria. Using Monte Carlo simulation, Gray mapping is found to be better than natural mapping by 0.1 dB for the case of 8 states outer

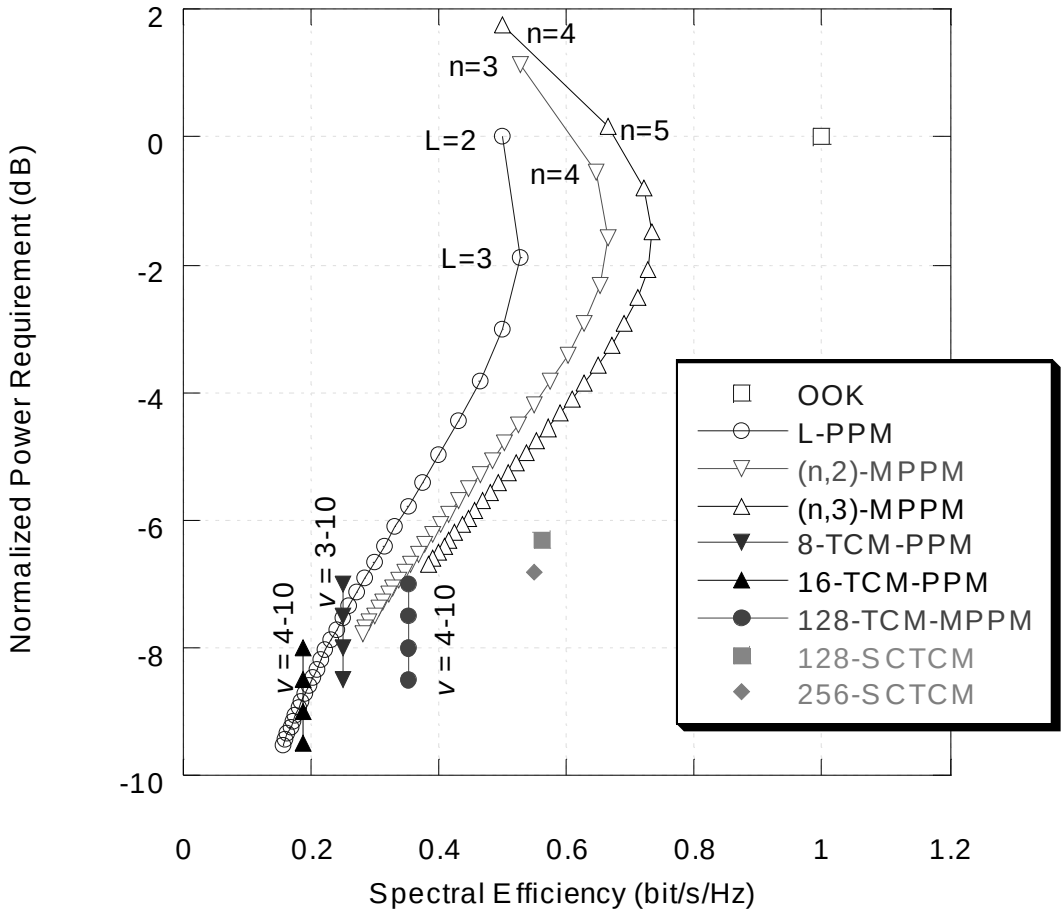

Figure 30. Normalized power requirement versus spectral efficiency.

code and 4 states inner code. Moreover, short constraint length outer and inner codes outperform the ones with larger constraint lengths in small and medium optical SNRs. We also employed the performance error bounds to gauge SCTCM's performance at very low BER that is not feasible by Monte Carlo simulations. Finally, a comparison was made between the performance of the proposed SCTCM and some previous trellis-coded modulations in the area of infrared communications. The comparison was done in terms of normalized power requirement, spectral efficiency, decoding complexity, and distance to the cut-off rates.

Chapter 6

Serial-Concatenated Trellis-Coded Modulation Based on OPPM

The previous chapter proposed coded modulation on 2L2PPM. In this chapter we propose serial concatenated trellis-coded modulation based on a different modulation scheme, namely overlapping pulse position modulation (OPPM). One of the desirable properties of OPPM is the low bandwidth requirement compared to MPPM. The change in modulation scheme calls for different inner and outer codes. We propose two variations of OPPM with this simplified SCTCM, because of their good normalized power requirement in the required range of spectral efficiency. In the second section, SCTCM with inner code of rate-1, combined with OPPM modulation scheme, is presented with some simulation results of that system.

The following section presents a basic description of this coded modulation, followed by inner code search and simulation results.

6.1 System Description

The proposed system includes a serial concatenation of an outer code, an interleaver, and an inner code of rate-1 and one memory element, combined with an OPPM modulation. The outer code is chosen to be a non-systematic convolutional code. The inner code is recursive convolutional code of rate-one and is combined with the modulation mapper. A bit spread-random interleaver [71] is used. The modulation scheme is overlapping pulse position modulation (OPPM). The signal constellation has a size of $M = 2^b$ signals. The rate of the outer code is $(b-1)/b$ and the rate of the inner code is 1.0, which will result in a system of total rate $(b-1)/b$. Even though the outer code is selected to be non-systematic convolutional code, the results of this research still apply for other kinds of convolutional outer codes as far as its free Hamming distance is maximized for the given rate and constraint length.

The encoder shown in Figure 31 is composed of an outer code, S-interleaver, and inner code connected to the OPPM signal mapper. The outer code is non-recursive

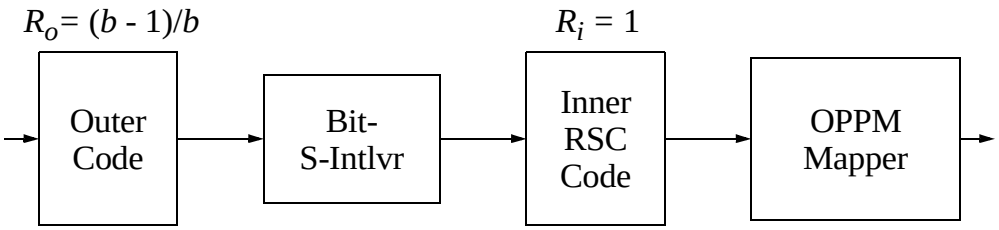

Figure 31. Proposed SCTCM encoder with rate-1 inner code.

convolutional code; the inner code is a recursive convolutional code. The interleaver works on the stream of bits coming out of the outer code.

The following presentation sheds light on the description of the modulation scheme and the structure of the inner code presented in this case.

6.1.1 Modulation Scheme

With this serial concatenation scheme, OPPM modulation scheme is selected. The first objective is to look for modulation schemes that result in a total spectral efficiency of greater than 0.5 bits/s/Hz. With this specification, we used two OPPM cases which have high minimum Euclidean and spectral efficiency of 0.56 and 0.5 bits/s/Hz, respectively. The first case resulted from choosing the parameters of OPPM to be $L = 8$, $n = 9$ and $w = 2$. For this case, the output of the inner code is mapped to two-symbol durations to give 64 symbols and an effective spectral efficiency of 0.56 bits/s/Hz. In the second case, the parameters of OPPM are chosen to be $L = 64$, $n = 70$ and $w = 7$. The inner code is connected to one symbol duration to produce 64 symbols and with 0.5 bits/s/Hz spectral efficiency.

6.1.2 Outer Codes

One of the design criteria of SCTCM is to choose outer codes with maximum free Hamming distance. The outer codes are chosen to be non-systematic convolutional codes, which are generated from puncturing rate 1/2 binary convolutional codes [76]. The

Hamming distances of these codes are not guaranteed to be the maximum possible for the specified rate.

6.1.3 Inner Code Structure

For good performance of serial concatenation encoders, the inner code has to be recursive; therefore, a general structure of recursive convolutional codes is used. A general convolutional encoder with p inputs, n outputs, and m memory elements can be described by state space equations over GF(2):

$$\begin{aligned} s_{j+1} &= s_j A + u_j B \\ y_j &= s_j C + u_j D \end{aligned}, \tag{53}$$

where s_j is the state vector of dimension $1 \times m$, y_j is the output vector of dimension $1 \times m$, u_j is the input vector of dimension $1 \times k$, matrix B has dimension $k \times m$, matrix C has dimension $m \times n$, and matrix D has dimension $k \times n$. Matrix A determines the way the m memory elements are connected. If the encoder is with a feedback, A is the companion matrix of the encoder's feedback polynomial. For instance, the memory elements in Figure 32 can be described by the following feedback polynomial

$$f(D) = D^3 + D + 1, \tag{54}$$

and can also be described by the following companion matrix [80]

$$A = \begin{bmatrix} 0 & 1 & 0 \\ 0 & 0 & 1 \\ 1 & 1 & 0 \end{bmatrix}. \tag{55}$$

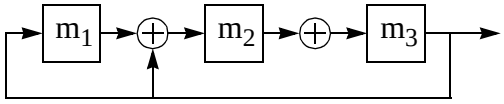

Figure 32. Memory elements governed by $f(D)=D^3+D+1$.

6.1.4 Iterative Decoder

Optimum maximum likelihood (ML) decoding algorithms for serial concatenation TCM codes are complex, due to the presence of the interleaver, but iterative decoding of such codes is feasible and often leads to or approaches ML decoding. Iterative decoding involves iterations between constituent decoders, with an exchange of soft information between iterations. The constituent decoders are a posteriori probability (APP) decoders which compute the posterior probability.

The receiver uses a unit-energy filter $f(t)$, which is matched to the pulse shape, and samples the output at the chip rate n/T producing n samples for each symbol. Each n samples are grouped in one block. The OPPM soft demodulator will receive the samples to produce N_s vectors of soft information, where N_s represents the number of symbols in every codeword. Then, these N_s vectors of soft information will be used by the soft

decoder. The soft decoder is composed of four blocks: the inner decoder, the bit deinterleaver, the outer decoder, and the bit interleaver. A block diagram of the iterative decoder is shown in Figure 33. Each decoder is a symbol-APP detector, which operates on the probability of the symbols rather than the bit probabilities. The interleaver works on the bits. Hence, the iterative decoder needs to perform symbol-to-bit probability conversion before the interleaver and deinterleaver and, it needs bit-to-symbol probability conversion after them. These conversions are not shown on the block diagram of the iterative decoder, but they are included in the block diagram of the constituent decoders.

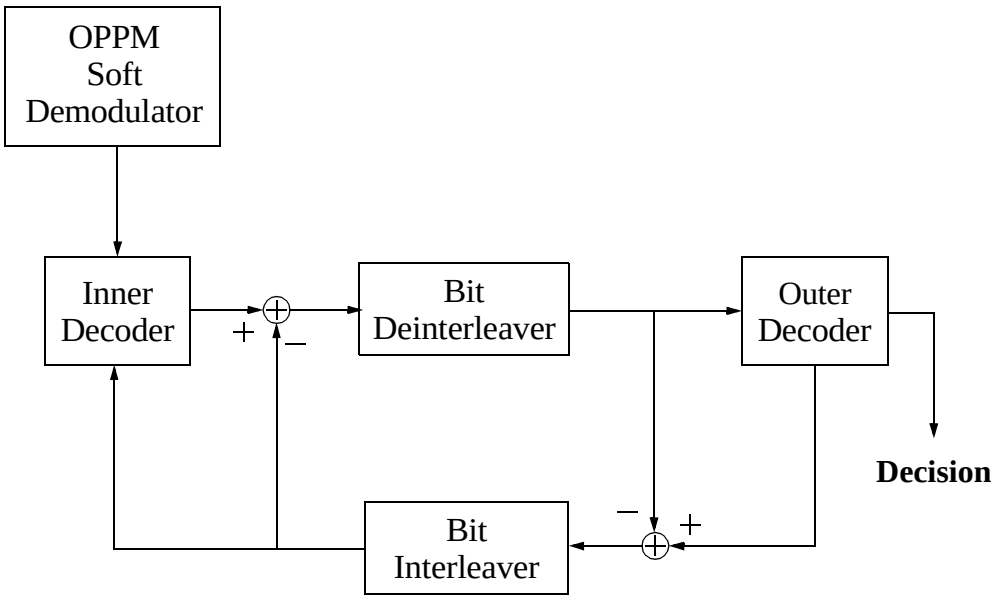

Figure 33. Iterative decoder of SCTCM-OPPM system.

Iterative decoders are suboptimal but their performance approach the bound of ML decoders for the moderate and high SNR. Symbol by symbol a posteriori decoder reported by Bahl et al. [44] and known as the BCJR algorithm, is used in both the outer and inner decoders.

6.2 Inner Code Search

The error probability of the SCTCM scheme depends on the Euclidean distance spectrum (EDS) of the inner code. In the search for optimum or good inner codes, we have to evaluate the inner code's EDS with respect to every possible codeword. Zehavi and Wolf [81] observed that it is enough to evaluate the code's EDS with respect to the all-zero codeword if the signal constellation is symmetric. The symmetry condition requires that every level of partitioning results in two subsets with identical Euclidean distance profiles. More detailed works on the performance evaluation of TCM schemes, with different degrees of symmetry, are provided by Benedetto in [82].

The output of the inner code is naturally mapped to the OPPM signal constellation. Figure 34 shows the mapping of one symbol of 64-OPPM scheme, where the axis shows the time index of the first pulse in the symbol. Figure 35 shows the mapping of two-symbols of 8-OPPM. In the figure, the starting time of the first symbol is assigned to the x-axis and the starting time of the second symbol is assigned to the y-axis. A close look to

the two mappings shows that we have symmetric signal constellation. Hence, it is enough to check the all-zero path to find the Euclidean distance spectrum of the inner code.

In this research, we are using inner codes of single-memory (2-states) and rate $= 6/6$. First of all, since the code memory is one, we have the matrix $A = [1]$. Moreover, one of the design criteria of SCTCM in the previous chapter is to avoid codewords that have input Hamming weight equals to one. This design criterion is satisfied here, by forcing the matrix B to have non-zero rows. Since the size B is 6×1, it is not difficult to show that the only B that satisfies this criterion is $B = [1, 1, 1, 1, 1, 1]^T$. The two matrices C and D have 6 and 36 entries, respectively, and to do an exhaustive search to find them will be time consuming. Hence, a random search is done to find C and D that have good Euclidean distance spectrum. After conducting a limited random search, the found inner codes for SCTCM-8-OPPM and SCTCM-64-OPPM are shown in Figure 36 and Figure 37, respectively.

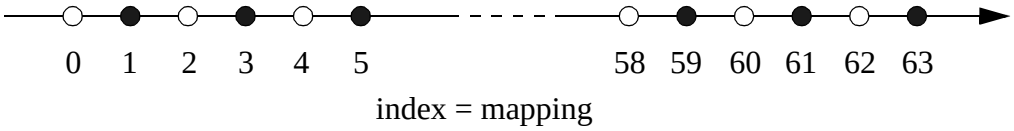

Figure 34. Natural mapping of one symbol of 64-OPPM.

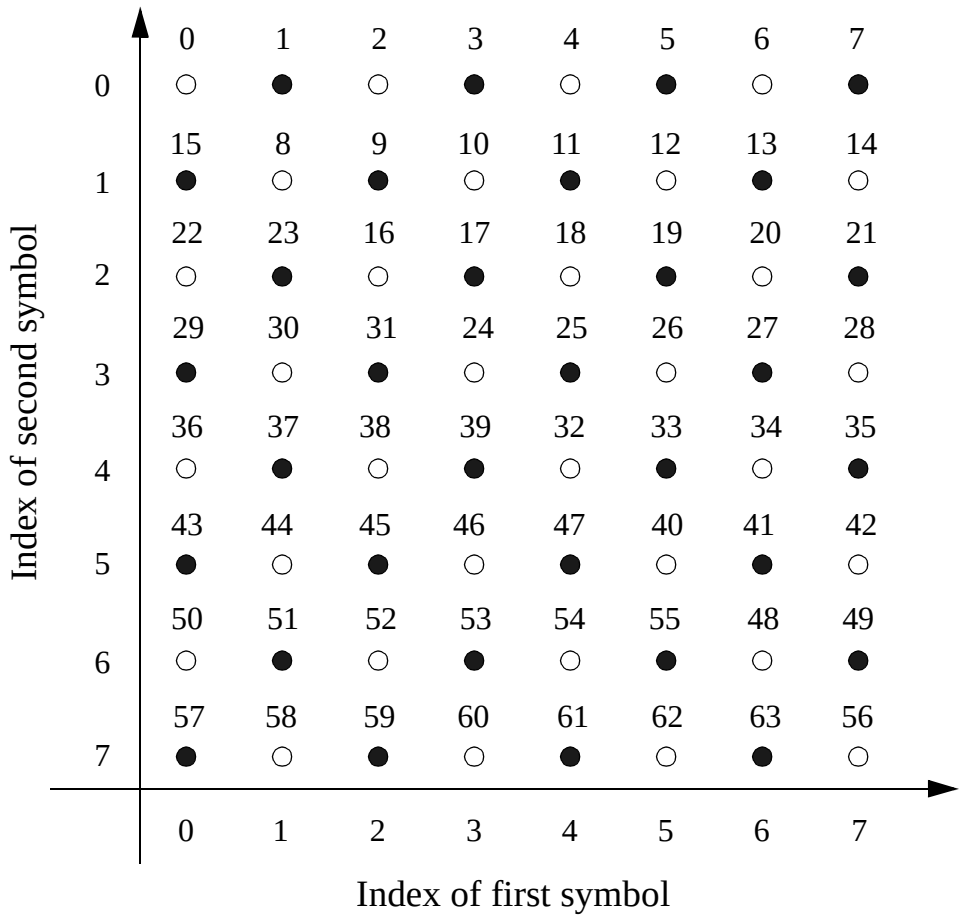

Figure 35. Two symbols of 8-OPPM natural mapping.

6.3 Simulation Results

Figure 38 illustrates the simulation of SCTCM-8-OPPM with two cases of outer codes: 4 states and 8 states. As you can see from the figure, the normalized power requirement is about 6.22 dB. For this simulation, the information block length is 2000,

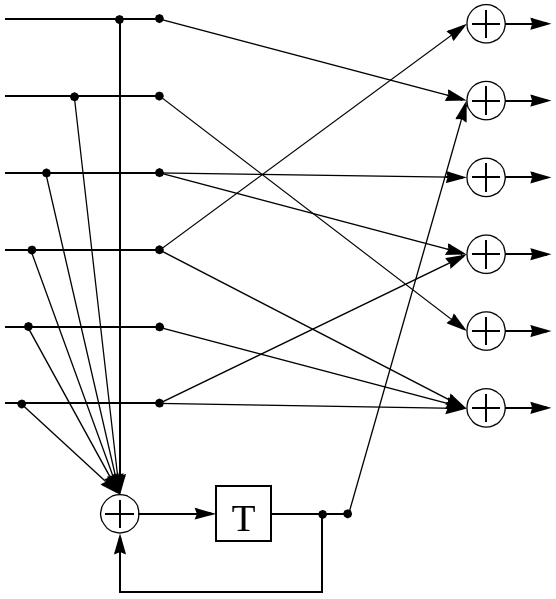

Figure 36. The inner code of SCTCM-8-OPPM scheme.

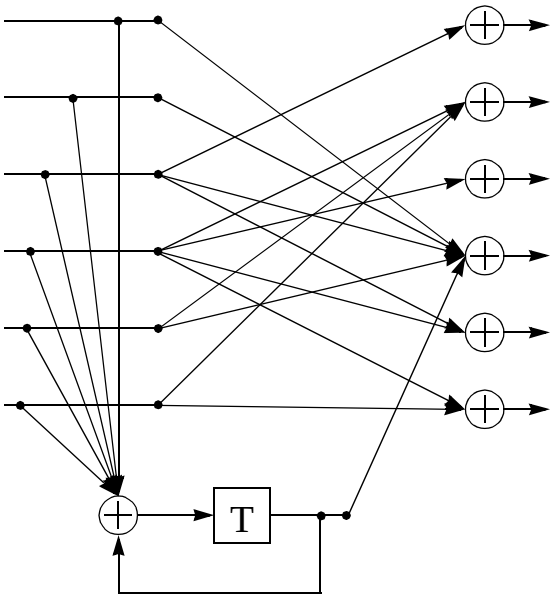

Figure 37. The inner code of SCTCM-64-OPPM scheme.

which makes the interleaver length equal 2400, because the outer code rate is $(5/6)$. Using an outer code of 8 states ($m^o = 3$) is better for high SNR (more than 6.25 normalized power requirement).

Figure 39 shows the simulation of SCTCM-64-OPPM for 2-states inner code and two cases of outer code. For this simulation, the information block length is 2000 and the interleaver length equals 2400. The figure points out that using an outer code of 8 states ($m^o = 3$), is better for high SNR (more than 8.1 normalized power requirement). A normalized power requirement of 7.2 dB could be extrapolated from the figure. Higher power efficiencies are expected if we increase the information block length.

Figure 40 shows the normalized power requirement versus the spectral efficiency of the proposed SCTCM-8-OPPM and SCTCM-64-OPPM with other previously coded modulation schemes [18], and uncoded PPM modulation schemes. The figure shows that the proposed schemes outperform the previous coded system by a 42% to 57% increase in the spectral efficiency for a comparable normalized power requirement. The figure also shows the performance of 128-SCTCM-2L2PPM and 256-SCTCM-2L2PPM schemes, which are discussed in chapter 5. It is clear from the figure that the proposed 64-OPPM-based SCTM scheme outperforms the 256-SCTCM-2L2PPM scheme by about 0.9 dB in the power requirement and 64% decrease in the decoding complexity.

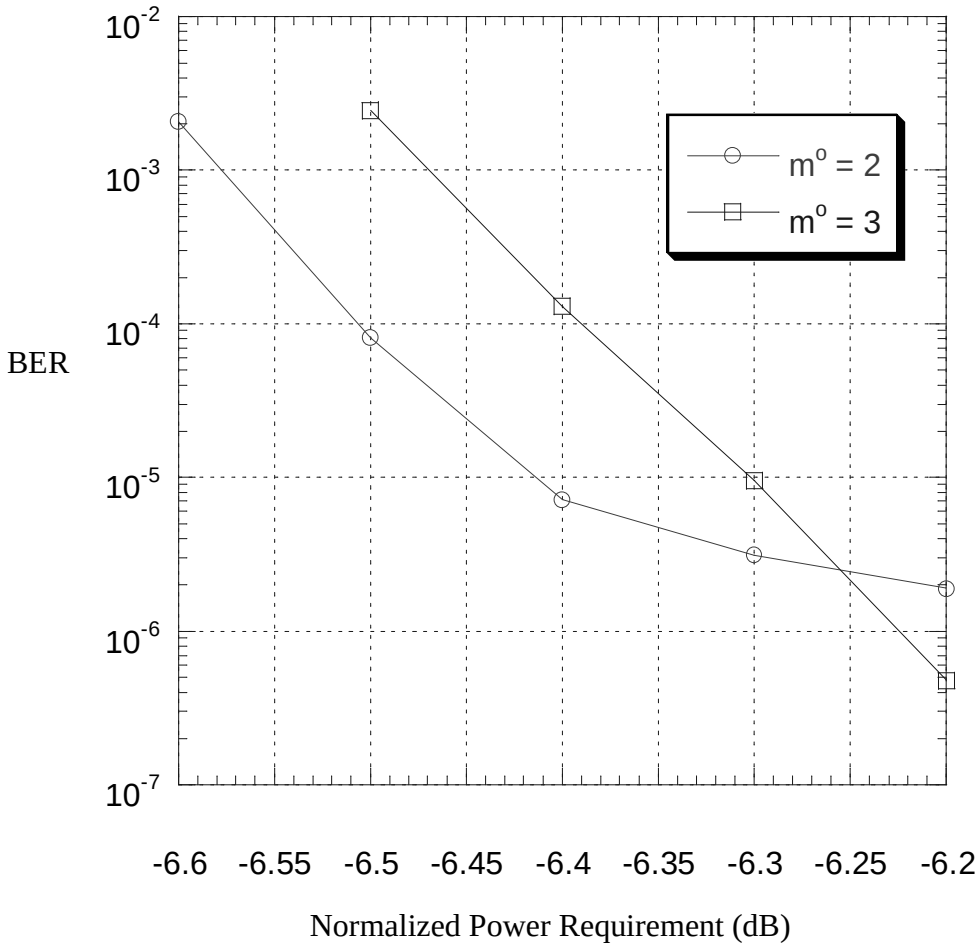

Figure 38. Simulation of SCTCM-8-OPPM. The inner code has 2 states and m^o is the memory of the outer code.

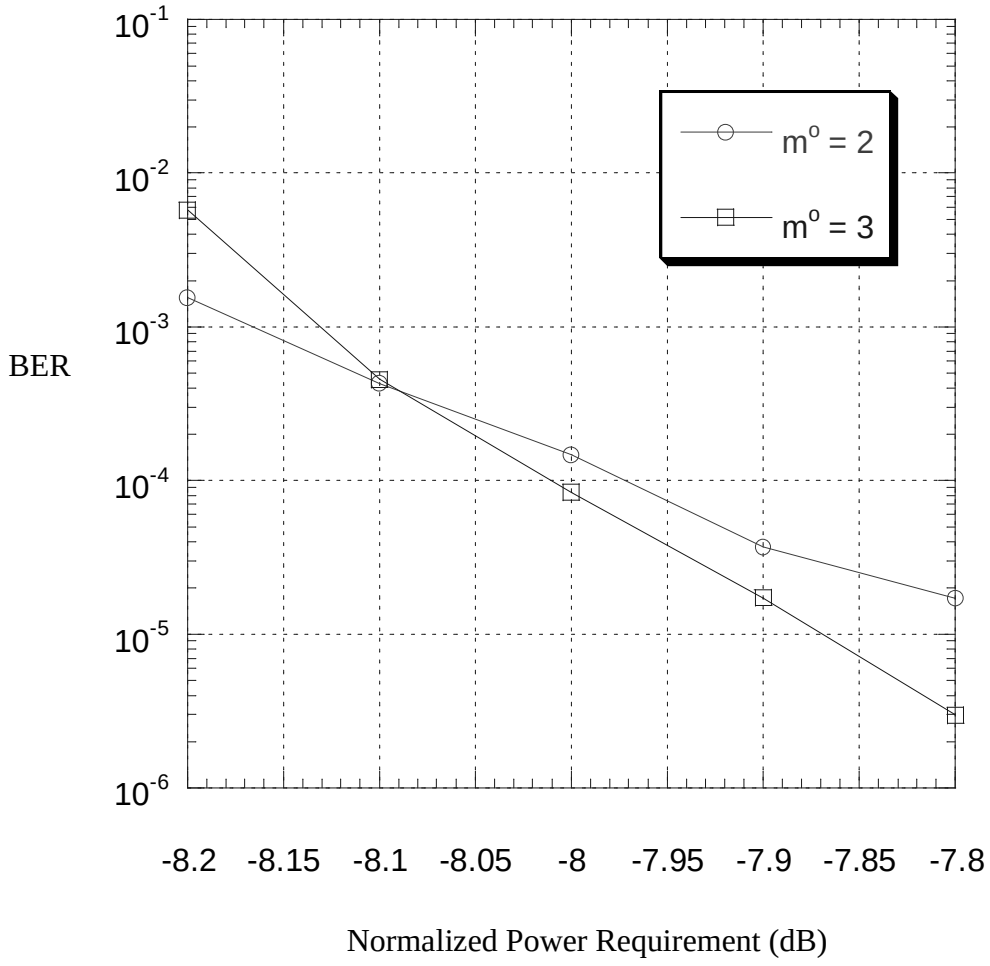

Figure 39. Simulation of SCTCM-64-OPPM. The inner code has 2 states and m^o is the memory of the outer code.

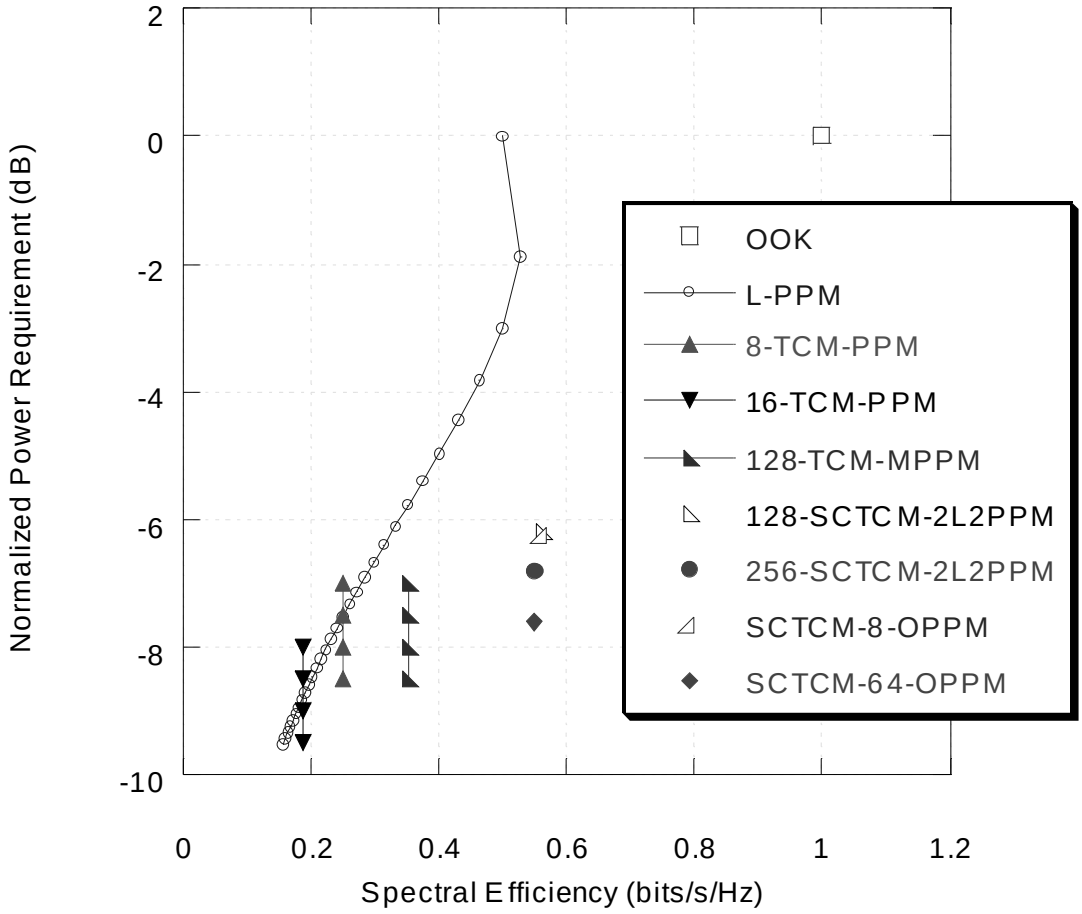

Figure 40. Normalized power requirement versus spectral efficiency of proposed SCTCM-8-OPPM and SCTCM-64-OPPM compared to previous coded modulation schemes for BER = 10^{-6}.

If we consider the total number of edges in the trellises of the inner and outer decoders as the decoding complexity, we can compare the decoding complexity of the proposed SCTCM schemes with the previous SCTCM schemes, which are proposed in chapter 5 in the following table, Table 12. The table shows that we gain up to a 64% decrease in decoding complexity.

Table 12. Decoding Complexity Comparison.

SCTCM scheme	Complexity (trellis-edges/bit)
128-SCTCM-2L2PPM	512
256-SCTCM-2L2PPM	853
SCTCM-8-OPPM	312
SCTCM-64-OPPM	312

6.4 Summary

This chapter proposed a low-complexity SCTCM scheme to achieve high spectral efficiency. In this SCTCM scheme, two cases of OPPM modulation scheme are combined with a rate-1 inner code. Monte Carlo simulations show performance comparable to more complex systems. At spectral efficiency of 0.5 bits/s/Hz, the proposed OPPM-based coded modulation scheme outperforms those of chapter 5 by up to 0.9 dB in the power requirement, while decreasing the decoding complexity by a factor of 64%.

Chapter 7

Concluding Remarks

7.1 Summary of Results

To increase the power and spectral efficiencies of optical communication systems, both modulation and coding are critical. Pulse position modulation and related modulations schemes have been adopted in optical communications because of their high peak-to-average power ratios. Turbo-coded modulation schemes and iterative decoding are found to be effective in spectrally efficient communication systems. This research has explored many aspects of turbo-coded modulation schemes for optical communications. We began, in chapter 2, by providing the necessary background on optical communications. In chapter 3, we reviewed turbo codes, iterative decoding, and several types of turbo-coded modulations for spectral efficient communication systems.

In chapter 4, we introduced a new modulation scheme that is suitable for optical communications. The new modulation is two-level two-pulse position modulation (2L2PPM), which is a combination of MPPM and multilevel modulation techniques. The

uncoded BER performance of this modulation technique is compared with OOK, PPM and MPPM schemes that are already used in this field. We also used the cut-off rate to evaluate the power efficiency of this modulation when combined with coded modulation techniques. These results show that up to 6.7 to 7.1 dB of normalized power requirements and between 0.55 and 0.5 bits/s/Hz spectral efficiencies could be obtained by using 128 and 256 symbols 2L2PPM modulation. At 7.0 dB normalized power requirement, this outperforms a previously proposed scheme [18] by 42% increase in the spectral efficiency.

In chapter 5, we developed a serial-concatenated trellis-coded modulation combined with 2L2PPM modulation. The system was decoded with an iterative decoder. We modified the performance error bounds for serial-concatenated convolutional codes, introduced by Benedetto et al. [1], [2] for the case of TCM inner codes. Assuming large S-random interleavers, convolutional outer and inner codes, and high optical SNRs, we derived the design criteria for the SCTCM encoder. For this case the effective minimum Euclidean distance of the SCTCM is found to be the product of the free Hamming distance of the outer code and the minimum Euclidean distance of the inner code, which is at least double the effective minimum Euclidean distance of SCTCM encoder with just random interleavers. We found that Gray mapping is better than natural mapping, because it minimizes the number bit errors in the inner decoding process.

Then we conducted a random search and used the design criteria to find good inner codes for the two cases of signal mappings for constraint lengths from 2 to 5. The results

of the random search are tabulated. Using Monte Carlo simulation, we found that Gray mapping is better than natural mapping by 0.1 dB for the case of 4 states outer code and 4 states inner code. The improvement increases with increasing the constraint length of the outer code or inner code.

Simulations of the SCTCM encoders with iterative decoding were found. In conclusion, short constraint length outer and inner codes outperform the ones with larger constraint lengths in small and medium optical SNRs. We also employed the performance error bounds to gauge SCTCM's performance at very low BER that is not feasible by Monte Carlo simulations. Finally, a comparison was made between the performance of the proposed SCTCM and some previous trellis-coded modulations in the area of infrared communications. The comparison was done in terms of power efficiency, spectral efficiency, decoding complexity, and distance to the cut-off rates. The proposed SCTCM schemes offer up to a 42% increase in the spectral efficiency for the same range of power requirement and decoding complexity.

Because overlapping pulse position modulation (OPPM) scheme is more bandwidth efficient than multiple PPM scheme, we introduced a new SCTCM based on OPPM. An inner code of rate-one is utilized to increase the spectral efficiency. Two OPPM cases were proposed with this new SCTCM because of their good power efficiency in the required range of spectral efficiency. In the first case, the inner code was combined with one period of symbol duration of 64-OPPM with duty cycle $\alpha = 0.1$. The resultant spectral

efficiency is 0.5 bits/s/Hz. For the second case, we combined the inner code with two symbol durations of 8-OPPM and $\alpha = 0.22$, which produced a spectral efficiency of 0.55 bit/sec./Hz. The inner code in this system does not offer a coding gain by itself, but the Monte Carlo simulations of the resulting SCTCM encoder with iterative decoding indicates that the proposed schemes offer normalized power requirements of 6.3 to 7.7 dB. The general structure of recursive convolutional codes was used for the inner code in this system. Although the minimum Euclidean distance of the inner code can not be increased, we still used the other design criteria, which are introduced in chapter 5, to obtain the polynomials of the inner codes. Simulation results show that these SCTCM schemes outperform the schemes in chapter 5 by up to 0.9 dB and a 64% decrease in the decoding complexity.

7.2 Future Research Recommendations

The following is a list of recommended areas of future work in this field.

- We based our beginning assumptions on designing codes on very long block lengths, S-random interleavers, convolutional codes for both outer and inner codes, and working at high optical SNR range. For short interleavers and for low range SNR some of these design criteria need to be improved or replaced with better ones. For example, if the interleaver is short and the SNR is high, the bit error performance is still decided by the effective minimum Euclidean

distance (MED) of the SCTCM, but the use of S-random interleavers does not guarantee the MED to be the product of the outer code's free Hamming distance and the inner code's minimum Euclidean distance.

- New design criteria have to be found for the low and medium range of optical SNR and for the case of short block lengths.
- Low density parity check (LDPC) codes are the best known codes in approaching the capacity of additive white Gaussian noise channels. Using LDPC codes as component codes in multilevel coding technique should be investigated for good coded modulation schemes.
- The Monte Carlo simulation of SCTCM codes is time consuming, mainly with very long block lengths or large memory constituent codes. Additionally, it is not feasible to use Monte Carlo simulations for very low BER in order of 10^{-9}. Therefore, a need for ways of speeding theses simulation methods is essential. One way to address this issue is to develop importance sampling techniques for turbo codes and turbo-coded modulation systems.
- We have seen that using S-random interleavers increases the effective minimum Euclidean distance of the SCTCM. More advanced S-interleavers, suggested by Fargouli and Wesel [38], could be used to increase the effective minimum Euclidean distance even more. However, one question that remains

to be asked is what is the effect of S-interleavers on the spectrum thickness of SCTCM codes.

References

[1] S. Benedetto, G. Montorsi, D. Divsalar, and F. Pollara, “Serial Concatenation of Interleaved Codes,” in the Telecommunications and Data Acquisition Progress Report 42-126, July-September 1996, pp. 1-26, Jet Propulsion Laboratory, August 1995.

[2] S. Benedetto, D. Divsalar, G. Montorsi, and F. Pollara, “Serial Concatenation of Interleaved Codes: Performance Analysis, Design, and Iterative Decoding,” IEEE Transactions on Information Theory, vol. 44, no. 3, pp. 909-926, May 1998.

[3] S. Benedetto, D. Divsalar, G. Montorsi, and F. Pollara, “Serial Concatenated Trellis Coded Modulation with Iterative Decoding,” International Symposium on Information Theory, pp. 8, June-July 1997.

[4] J. M. Kahn, J. R. Barry, M. D. Audeh, J. B. Carruthers, W. J. Krause, and G. W. Marsh, “Non-Directed Infrared Links for High-Capacity Wireless LANs,” IEEE Personal Communication Magazine, vol. 1, no. 2, pp. 12-25, Spring 1994.

[5] J. R. Barry, Wireless Infrared Communications, Kluwer Academic Publishers, Boston, 1994.

[6] J. M. Kahn and J. R. Barry, “Wireless Infrared Communications,” Proceedings of the IEEE, vol 85, no. 2, February 1997.

[7] F. R. Gfeller and U. H. Bapst, “Wireless In-House Data Communication via Diffuse Infrared Radiation,” Proceedings of IEEE, vol. 67, pp. 1474-1486, November 1979.

[8] J. Gowar, Optical Communication Systems, Prentice Hall International (UK) Ltd., Second Edition, 1993.

[9] G. Lachs, Fiber Optic Communications: Systems, Analysis, and Enhancements, McGraw-Hill, 1998.

[10] J. R. Lesh, J. Katz, H. H. Tan. and D. Zwillinger, “2.5 Bits/Detected Photon Demonstration Program: Description, Analysis, and Phase I Results,” Jet Propulsion Laboratory, Pasadena, Ca, TDA Rep. 42-66, pp. 115-132, December 1981.

[11] X. Sun and F. Davidson, “Direct-Detection Optical Intersatellite link at 220 Mbps Using AlGaAs Laser Diode and Silicon APD with 4-ary PPM signaling,” NASA CR-186380, 1990.

[12] J. M. Budinger, S. D. Kerslake, L. A. Nagy, M. J. Shalkhauser, N. J. Soni, M. A. Cauley, J. H. Mohamed, J. B. Stover, R. R. Romanofsky, P. J. Lizanich, and D. J. Mortensen, “Quaternary Pulse-Position Modulation Electronics for Deep-Space Laser Communications,” NASA Lewis Research Center, NASA Tech. Mem. 104502, September 1991.

[13] J. R. Pierce, “Optical Channel: Practical Limits With Photon Counting,” IEEE Transactions on Communications, vol. 26, no. 12, pp. 1819-1821, December 1978.

[14] H. Sugiyama and K. Nosu, “MPPM: A Method for Improving the Band-Utilization Efficiency in Optical PPM,” Journal of Lightwave Technology, vol. 7. no. 3, pp. 465-472, March 1989.

[15] D. Lee, J. Kahn, and M. Audeh, “Trellis-Coded Pulse Position Modulation for Indoor Wireless Infrared Communications,” IEEE Trans. on Comm. vol. 45, pp. 1080-1087, September 1997.

[16] G. Ungerboeck, “Channel Coding with Multilevel/Phase Signals,” IEEE Transactions on Information Theory, vol. 28, pp. 55-67, January 1982.

[17] H. Park, Coded Modulation and Equalization for Wireless Infrared Communications, Ph.D. thesis, School of Electrical and Computer Engineering, Georgia Institute of Technology, July 1997.

[18] H. Park and J. Barry, “Trellis-Coded Multiple Pulse-Position Modulation for Wireless Infrared Communication,” IEEE Global Communications Conference (Globecom,98), vol. 1, pp. 225-230, Sydney, November 1998.

[19] C. Berrou, A. Glavieux, and P. Thitimajshima, “Near Shannon Limit Error Correcting Coding and Decoding: Turbo Codes,” Proceedings 1993 IEEE International Conference on Communications, pp. 1064-1070, 1993.

[20] S. Benedetto and G. Montorsi, “Average Performance of Parallel Concatenated Block Codes,” Electronics Letters, vol. 31, no. 3, pp. 156-158, February 2, 1995.

[21] S. Benedetto and G. Montorsi, “Design of Parallel Concatenated Codes,” IEEE Transactions on Information Theory, vol. 44, no. 5, pp. 591-600, May 1996.

[22] S. Benedetto and G. Montorsi, “Performance Evaluation of Turbo Codes,” Electronics Letters, vol. 31, pp. 163-165, January 1995.

[23] S. Benedetto and G. Montorsi, “Role of Recursive Convolutional Codes in Turbo Codes,” Electronics Letters, vol. 31, pp. 858-859, May 25, 1995.

[24] S. Benedetto and G. Montorsi, “Unveilling Turbo Codes: Some Results on Parallel Concatenated Coding,” IEEE Transactions on Information Theory, vol. 42, no. 2, pp. 409-428, March 1996.

[25] L. C. Perez, J. Seghers, and D. J. Costello Jr., “A Distance Spectrum Interpretation of Turbo Codes,” IEEE Transactions on Information Theory, vol. 42, no. 6, pp. 1698-1709, November 1996.

[26] P. Robertson, “Illuminating the Structure of Code and Decoder of Parallel Concatenated Recursive Systematic (Turbo) Codes,” Proceedings, GlobeComm 1994, pp. 1298-1303, 1994.

[27] J. Hagenauer, E. Offer, and L. Papke, “Iterative Decoding of Binary Block and Convolutional Codes,” IEEE Transactions on Information Theory, vol. 42, no. 2, pp. 429-445, March 1996.

[28] S. LeGoff, A. Glavieux, and C. Berrou, “Turbo-codes and High Spectral Efficiency Modulation,” Proc. ICC’94, pp. 645-649, May 1994.

[29] P. Robertson and T. Worz, “A Novel Coded Modulation Scheme Employing Turbo Codes,” Proc. URSI & ITG conf ‘Kleinhubacher Tagung’, October 1995.

[30] P. Robertson and T. Worz, “Coded Modulation Scheme Employing Turbo Codes,” Electronics Letters, pp. 1546-1547, August 1995.

[31] P. Robertson and T. Worz, “A Novel Bandwidth Efficient Coding Scheme Employing Turbo Codes,” Proc. of ICC’96, pp. 962-967, June 1996.

[32] P. Robertson and T. Worz, “Bandwidth-Efficient Turbo Trellis-Coded Modulation Using Punctured Component Codes,” IEEE Journal On Selected Areas In Communications, vol.16, no. 2, pp. 206-218, February 1998.

[33] W. J. Blackert, and S. G. Wilson, “Turbo Trellis Coded Modulation,” Proc. of Conf. Info. Sciences, December 1995.

[34] H. Ogiwara and M Yano, “Improvement of Turbo Trellis-Coded Modulation System,” IEICE Transactions on Fundamentals of Electronics Communications and Computer Sciences, E81A: (10), pp. 2040-2046, October 1998.

[35] S. Benedetto, D. Divsalar, G. Montorsi, and F. Pollara, “Bandwidth Efficient Parallel Concatenated Coding Schemes,” Electronics Letters, pp. 2067-2069, November 1995.

[36] S. Benedetto, D. Divsalar, G. Montorsi, and F. Pollara, “Parallel Concatenated Trellis Coded Modulation,” Proc. of ICC’96, pp. 974-978, June 1996.

[37] C. Fragouli and R. D. Wesel, “Symbol Interleaved Parallel Concatenated Trellis Coded Modulation,” IEEE Communications Theory Mini-Conference, pp. 42-46, June 1999.

[38] C. Fargouli and R. D. Wesel, “Turbo-Encoder Design for Symbol-Interleaved Parallel Concatenated Trellis-Coded Modulation,” IEEE Transactions on Communications, vol. 49, no. 3. pp. 425-435.

[39] B. E. Wahlen and C. Y. Mai, “Turbo Coding Applied to Pragmatic Trellis-Coded Modulation,” IEEE Communications Letters, vol. 4, no. 2, pp. 65-67, February 2000.

[40] H. Ogiwara and V. B. Bajo, “Iterative Decoding of Serially Concatenated Punctured Trellis-Coded Modulation,” IEICE Transactions on Fundamentals of Electronics Communications and Computer Sciences, E82A: (10), pp. 2089-2095, October 1999.

[41] H. Park and J. Barry, “Modulation Analysis for Wireless Infrared Communications,” International Conference on Communications, Seattle, vol. 2, pp. 1182-1186, June 1995.

[42] S. G. Wilson, Digital Modulation and Coding, Prentice-Hall, Inc., 1996.

[43] G. D. Forney, Jr., Concatenated Codes, Cambridge, Massachusetts, Massachusetts Institute of Technology, 1996.

[44] L.R. Bahl, J. Cocke, F. Jelinek, and J. Raviv “Optimal Decoding of Linear Codes for Minimizing Symbol Error Rate”, IEEE Transaction on Information Theory, vol. IT-20, page 284-287, March 1974.

[45] S. S. Pietrobon and S. A. Barbulescu, “A simplification of the modified Bahl decoding algorithm for Systematic Convolutional Codes,” Int. Symp. on Inform. Theory and its Applications, pp. 1073-1077, November 1994. Revised 4 January 1996.

[46] S. Benedetto, D. Divsalar, G. Montorsi, F. Pollara, “A Soft-Input Soft-Output APP Module for Iterative Decoding of Concatenated Codes,” IEEE Communication Letters, vol. 1 no. 1, pp. 22-24, January. 1997.

[47] S. Benedetto, G. Montorsi, D. Divsalar, and F. Pollara, “A Soft-Input Soft-Output Maximum a Posteriori (MAP) Module to Decode Parallel and Serial Concatenated Codes,” in The Telecommunications and Data Acquisition Progress Report 42-127, pp. 1-20, Jet Propulsion Laboratory, November 1996.

[48] S. Benedetto, D. Divsalar, G. Montorsi, F. Pollara, “Soft-Output Decoding Algorithm for Continuous Decoding of Parallel Concatenated Convolutional Codes,” Proc. ICC’96, vol.1, pp.112-117, June 1996.

[49] S. Benendetto and G. Montorsi, “Iterative Decoding of Serially Concatenated Convolutional Codes,” Electronics Letters, vol. 32, pp.1186-1187, May 1996.

[50] P. Hoeher, “TCM on Frequency-Selective Fading Channels: A Comparison of Soft Output Probabilistic Equalizers,” Proc. of GlobeComm 1990, pp. 401.4.1-401.4.5, November 1990.

[51] H. Imai and S. Hirakawa, “A New Multilevel Coding Method Using Error Correcting Codes,” IEEE Transactions on Information Theory, vol. IT-23, pp. 371-377, May 1977.

[52] S. I. Sayegh, “A Class of Optimum Block Codes in Signal Space,” IEEE Transactions on Communications, vol. Com. 34, no. 10, pp. 1043-1045, October 1986.

[53] K. Yamaguchi and H. Imai, “Highly Reliable Multilevel Channel Coding System Using Binary Convolutional Codes,” Electronics Letters, vol. 23, no. 18, pp. 939-941, August 1987.

[54] T Woerz and J. Hagenauer, “Multistage Coding and Decoding for a M-PSK System,” Proceedings of GlobeComm’90, pp. 501.1.1-501.1.6, December 1990.

[55] A. R. Calderbank, “Multilevel Codes and Multistage Decoding,” IEEE Transactions on Communications, vol. 37, no. 3, pp. 222-229, March 1989.

[56] G. L. Pottie and D. P. Taylor, “Multilevel Codes Based on Partitioning,” IEEE Transactions on Informations Theory, vol. IT-35, no. 1, pp. 87-98, January 1989.

[57] J. Huber and U. Wachsmann, “Capacities of Equivalent Channels in Multilevel Coding Schemes,” Electronics Letters, vol. 30, pp. 557-558, March 1994.

[58] J. Huber, “Multilevel Codes: Distance Profiles and Channel Capacity,” ITC-Fachbericht 130, Conf. Rec. (Munchen Germany), pp. 305-319, October 1994,

[59] J. Huber and U. Wachsmann, “Design of Multilevel Codes,” Proc. Information Theory Workshop (ITW) (Rydzyna, Poland), pp. 4.6, June 1995.

[60] J. Huber and U. Wachsmann, “On Set Partitioning Strategies for Multilevel Coded Modulation Schemes,” Mediterranean Workshop on Coding and Information Integrity, Palma de Mallorca, Spain, February-March 1996.

[61] Y. Kofman, E. Zehavi, and S. Shamai, “Analysis of a Multilevel Coded Modulation System,” 1990 Bilkent International Conference New Trends in Communications, Control, and Signal Processing, Conf. Rec. (Ankara, Turkey, July 1990), pp. 367-382, 1990.

[62] Y. Kofman, E. Zehavi, and S. Shamai, “Performance Analysis of a Multilevel Coded Modulation System,” IEEE Transactions on Communications, vol. 42, pp. 299-312, 1994.

[63] U. Wachsmann, R. Fischer, and J. Huber, “Multilevel Codes: Theoretical Concepts and Practical Design Rules,” IEEE Transactions on Information Theory, vol. 45, no. 5, pp. 1361-1391.

[64] H. Herzberg, “On the Spectrum of Distances of a Multilevel Code, Decoded by a Multistage Decoder,” IEEE Transactions on Information Theory, vol. 43, no. 5, pp. 1736-1740, September 1997.

[65] U. Wachsmann and J. Huber, “Power and Bandwidth Efficient Digital Communication Using Turbo Codes in Multilevel Codes,” European Transactions on Telecommunications (ETT), vol. 6, no. 5, pp. 557-567, 1995.

[66] J. Huber, U. Wachsmann, and R. Fischer, “Coded Modulation by Multilevel-Codes: Overview and State of the Art,” ITG-Fachbericht, pp. 255-266, March 1998.

[67] H. Herzberg, “Multilevel Turbo Coding with Short Interleavers,” IEEE Journal On Selected Areas In Communications, vol. 16, no. 2, pp. 303-309, February 1998.

[68] F. Amoroso, “The Bandwidth of Digital Data Signals,” IEEE Communications Magazine, Vol. 18, pp. 13-24, November 1980.

[69] W. A. Gardner, Statistical Spectral Analysis: A Non-Probabilistic Theory, Prentice-Hall, 1988.

[70] J. L. Massey, “Coding and Modulation in Digital Communication,” Proc. Int. Zurich Seminar on Digital Communications, Switzerland, E2 1-4, March 1974.

[71] S. Dolinar and D. Divsalar, “Weight Distributions for Turbo Codes Using Random and Nonrandom Permutations,” Jet Propulsion Laboratory (JPL) Progress report pp. 42-122, August 15, 1995.

[72] S. Lin and D. J. Costello, Error Control Coding: Fundamentals and Applications, 1983.

[73] E. Biglieri, D. Divsalar, P. J. McLane and M. K. Simon, Introduction to Trellis-Coded Modulation with Applications, Macmillan Publishing Company, 1991.

[74] J. Du and M. Kasahara, “Improvement of the Information-Bit Error Rate of Trellis Code Modulation Systems,” The Transactions of the IEICE, vol. E72, no. 5, pp. 609-614, May 1989.

[75] J. Du and B. Vucetic, “New M-PSK Trellis Codes for Fading Channels,” Electronics Letters, vol. 26, pp. 1267-1269, August 1989.

[76] Y. Yasuda, K. Kashiki, and Y. Hirata, “High-Rate Punctured Convolutional Codes for Soft Decision Viterbi Decoding,” IEEE Trans. Communications, vol. Com-32, no. 3, pp. 315-319, March 1984.

[77] M. Rouanne and D. J. Costello, Jr., “An Algorithm for computing the distance spectrum of trellis codes,” IEEE Journal of Selected Areas in Communications, Vol. 7, pp. 929-940, August 1989.

[78] G. L. Bechtel and J. W. Modestino, “Pulsewidth-Constrained Signaling and Trellis Coded Modulation on The Direct-Detection Optical Channel,” IEEE Global Telecommunications Conference (Globecom’88), vol. 2, pp. 842-847, 1988.

[79] P. Thitimajshima, “Systematic Recursive Convolutional Codes and their application to Parallel Concatenation,” Ph.D. dissertation, University de Bretagne Occidentale, December 1993.

[80] G. H. Golub and C. F. Van Loan, Matrix Computations, Third Edition, The John Hopkins University Press, 1996.

[81] E. Zehavi and J. K. Wolf, “On the Performance Evaluation of Trellis Codes,” IEEE Transactions on Information Theory, Vol. 82, No. 2, pp. 196-202, March 1987.

[82] S. Benedetto, M. Mondin, and G. Montorsi, “Performance Evaluation of Trellis Coded Modulation Schemes,” Proceedings of IEEE, Vol. 82, No. 6, pp. 833-855, June 1994.

Vita

Abdallah Said Alahmari was born in Dammam, Saudi Arabia on August 31, 1968. He received Bachelor's and Master's degrees in Electrical Engineering in 1991 and 1994, respectively, from King Fahd University of Petroleum & Minerals, Dhahran, Saudi Arabia. He received a Ph.D. in Electrical Engineering in January 2003 from the Georgia Institute of Technology in Atlanta, Georgia. He worked as a graduate assistant and as a lecturer from 1991 to 1994 and from 1994 to 1995, respectively, in King Fahd University of Petroleum & Minerals, Dhahran, Saudi Arabia. His current research interests are in the general area of digital communications systems engineering with emphasis on error correction and modulation coding.